



THE HONG KONG  
POLYTECHNIC UNIVERSITY

香港理工大學

Pao Yue-kong Library

包玉剛圖書館

---

## Copyright Undertaking

This thesis is protected by copyright, with all rights reserved.

**By reading and using the thesis, the reader understands and agrees to the following terms:**

1. The reader will abide by the rules and legal ordinances governing copyright regarding the use of the thesis.
2. The reader will use the thesis for the purpose of research or private study only and not for distribution or further reproduction or any other purpose.
3. The reader agrees to indemnify and hold the University harmless from and against any loss, damage, cost, liability or expenses arising from copyright infringement or unauthorized usage.

### IMPORTANT

If you have reasons to believe that any materials in this thesis are deemed not suitable to be distributed in this form, or a copyright owner having difficulty with the material being included in our database, please contact [lbsys@polyu.edu.hk](mailto:lbsys@polyu.edu.hk) providing details. The Library will look into your claim and consider taking remedial action upon receipt of the written requests.

Pao Yue-kong Library, The Hong Kong Polytechnic University, Hung Hom, Kowloon, Hong Kong

<http://www.lib.polyu.edu.hk>

**DEVELOPMENT OF MICRO INLINE CROSS-  
FLOW TURBINE FOR ENERGY HARVESTING  
FROM URBAN WATER MAINS**

**DU JIYUN**

**PhD**

**THE HONG KONG POLYTECHNIC UNIVERSITY**

**2018**

The Hong Kong Polytechnic University

Department of Building Services Engineering

**Development of Micro Inline Cross-flow Turbine for  
Energy Harvesting from Urban Water Mains**

**DU JIYUN**

A thesis submitted in partial fulfilment of the requirements for  
the degree of Doctor of Philosophy

June 2018

## CERTIFICATE OF ORIGINALITY

I hereby declare that this thesis is my own work and that, to the best of my knowledge and belief, it reproduces no material previously published or written, nor material that has been accepted for the award of any other degree or diploma, except where due acknowledgement has been made in the text.

\_\_\_\_\_ (Signed)

DU Jiyun \_\_\_\_\_ (Name of student)

# ABSTRACT

Abstract of thesis entitled:

Development of Micro Inline Cross-flow Turbine for Energy Harvesting  
from Urban Water Mains

Submitted by: Du Jiyun

For the degree of: Doctor of Philosophy

at The Hong Kong Polytechnic University in June 2018.

Water supply is of vital importance for urban development and the subsistence of urban residents. Due to continually increasing populations and urban development, many cities around the world are facing great challenges in securing a reliable water supply. However, fresh water is often wasted in the delivery process due to leakage or pipe bursting. It is estimated that more than 32 billion m<sup>3</sup> of water from water mains is wasted every year worldwide. In Hong Kong, for instance, nearly 1200 Mm<sup>3</sup> of water is delivered through water pipes to residents annually, and the amount will grow to 1315 Mm<sup>3</sup> in 2030. However, nearly 15% of fresh water was wasted in 2016 due to pipe leakage. Therefore, many kinds of water monitoring sensors, including water flow sensors, pressure sensors, and acoustic leakage sensors, are used along urban water mains for timely detection of water leakage. However, most of the monitoring devices are powered by chemical batteries which need to be replaced frequently. The main objective of this thesis is to develop a micro inline hydropower technology to provide constant and reliable power for the water monitoring system.

Numerical simulations and experimental methods were first used to develop a

novel inline cross-flow turbine. In the design scheme of the inline turbine, a DN100 T-joint is integrated to a part of water main, then a cross-flow runner, which connects a generator via a shaft, is inserted in the pipe through the T-joint to harvest hydropower and transmit power to the generator. Two blocks that are fixed on the pipe inner wall are used to let more water flow through the runner, increasing the velocity of water that passes through the runner and reducing the resistance of water on the returning blades. A prototype with self-adjustable vane was developed by Computational Fluid Dynamics (CFD) method. Relevant lab tests were conducted to study the turbine performance. The test results could not only prove feasibility of the proposed design scheme, but also provide validation for the CFD simulation results. The prototype test results showed that the turbine output power at the design point was 69.1W with 2.62m water head reduced. Besides, over a flow velocity range varying from 1.2m/s to 2.2m/s, the water head loss was always below 5m, so the normal water supply would not be affected.

A novel mathematic design method for the block design was then developed and a theoretical analysis on the working mechanism of the cross-flow runner was performed. The mathematic design method and theoretical analysis could not only provide an understanding of working principle of the inline cross-flow turbine, but also show the effects of different geometrical parameters on turbine performance, which provides inspirations for performance improvement of the inline cross-flow turbine.

Furthermore, numerical studies were conducted to investigate the effects of block geometries on turbine performance. Several turbine models with different block designs were established and simulated. Then output power and water head loss were recorded to compare the performance of different turbine models. After that, analysis of flow velocity and pressure distribution was performed to study the block's effects

on flow inlet angle, flow separation in the blades passages and water head loss through the runner. The analysis could offer an in-depth understanding about the influencing mechanism of blocks on turbine performance and provide guidance for the determination of the optimal block shape in this research.

Moreover, the effects of runner geometries on turbine performance were studied by CFD simulations. In this research, several turbine models with different runner geometries were built and simulated to analyze the output power, water head loss and flow characteristics. Therefore, the optimal runner geometrical parameters (i.e. runner inlet arc angle, blades outer angle, diameter ratio and blades number) of the inline cross-flow turbine can be obtained. Based on the research results, the maximum turbine efficiency could reach 50.9% after block and runner optimization.

Finally, a bidirectional inline cross-flow turbine was newly designed and relevant lab tests were performed to study its performance. The experimental results indicated that when runner rotation speed was 600rpm, the bidirectional turbine reached its best efficiency 17.4% with 190W output power and 4.7m water head reduction, which could meet the design requirement in this case study. The case study indicated that the research presented in this thesis could provide an effective method for the design of inline cross-flow turbine design under different working conditions.

## LIST OF PUBLICATIONS

### Journal papers

- Du, J.,** Shen, Z., & Yang, H. (2018). Effects of different block designs on the performance of inline cross-flow turbines in urban water mains. *Applied Energy*, 228, 97-107.
- Du, J.,** Shen, Z., & Yang, H. (2018). Numerical study on the impact of runner inlet arc angle on the performance of inline cross-flow turbine used in urban water mains. *Energy*, 158, 228-237.
- Du, J.,** Yang, H., Shen, Z., Guo, X. (2018). Development of an inline vertical cross-flow turbine for hydropower harvesting in urban water supply pipes. *Renewable Energy*, 127, 386-397.
- Du, J.,** Yang, H., Shen, Z. (2018). Study on the impact of blades wrap angle on the performance of pumps as turbines used in water supply system of high-rise buildings. *International Journal of Low-Carbon Technologies*, 13(1), 102-108.
- Du, J.,** Yang, H., Shen, Z., Chen, J. (2017). Micro hydro power generation from water supply system in high rise buildings using pump as turbines. *Energy*, 137, 431-440.
- Du, J.,** Shen, Z., & Yang, H. (2018). Performance enhancement of an inline cross-flow hydro turbine for power supply to water leakage monitoring system. *Energy Procedia*, 145, 363-367.
- DU Jiyun,** Shen Zhicheng, Yang Hongxing. Development of a bidirectional inline cross-flow turbine for urban water mains. (Completed for submission)

## **Conference papers**

**Du Jiyun**, Shen Zhicheng, Yang Hongxing. Micro magnetic driven bidirectional turbine used in urban water mains for hydropower generation. TechConnect World Innovation Conference & Expo. Anaheim, California, the USA, 13-16 May, 2018.

**Du Jiyun**, Shen Zhicheng, Yang Hongxing. Performance enhancement of an inline cross-flow hydro turbine for power supply to water leakage monitoring system. Applied Energy Symposium and Forum, REM2017: Renewable Energy Integration with Mini/Microgrid, Tianjin University, China, 18-20 Oct, 2017.

**Du Jiyun**, Shen Zhicheng, Yang Hongxing. Study on the impact of blades curving degree on the performance of pumps as turbines used in water supply system of high rise buildings. The 16th International Conference on Sustainable Energy Technologies (SET 2017), University of Bologna, Italy, 17-20 July, 2017.

**Du Jiyun**, Chen Jian, Shen Zhicheng, Guo Xiaodong, Yang Hongxing. Micro hydro power generation from water supply system in high rise buildings using pump as turbines. The 15th International Conference on Sustainable Energy Technologies (SET 2016), The National University of Singapore, Singapore, 19-22 July, 2016.

## ACKNOWLEDGEMENTS

I hereby express my hearty gratitude to my supervisor, Prof. Yang Hongxing, Department of Building Services Engineering of The Hong Kong Polytechnic University for offering this valuable opportunity to pursue my PhD study. His in-depth knowledge and patient guidance are invaluable for my PhD study and future research. I have benefited a lot from his expertise and wisdom in renewable energy technologies as well as his positive and optimistic attitudes towards life.

Furthermore, I would like to thank Mr. Shen Zhicheng for his assistance in my research. He has done lots of work in test rig setup, prototype manufacture and lab tests. He can always share his idea with me to solve the problems encountered in my research process.

Moreover, I would like to express my thanks to Mr. Guo Xiaodong and Dr. Sun Ke for their professional guidance in the domain of CFD simulation. Their valuable suggestions are really helpful to the progress of my research.

In addition, I would appreciate the financial supports provided by the Innovation and Technology Fund of the Hong Kong Special Administrative Region Government (Grant No.: ITS/032/13) and the help from the Water Supplies Department of the Hong Kong SAR Government.

Besides, I would like to thank all the members in the Renewable Energy Research Group (RERG) for their assistance and company during my three-year PhD study.

Finally, I would like to give my sincere appreciation to my beloved parents, Du Chuanxi and Li Cuiling, my dear fiancée, Cheng Xiaocui, and my brother, Du Jifang. Their unconditional love and encouragement have been a solid pillar of support for me to overcome any challenges that I faced.

# TABLE OF CONTENTS

CERTIFICATE OF ORIGINALITY .....	I
ABSTRACT .....	II
LIST OF PUBLICATIONS .....	V
ACKNOWLEDGEMENTS .....	VII
TABLE OF CONTENTS .....	VIII
LIST OF FIGURES .....	XV
LIST OF TABLES .....	XXII
NOMENCLATURE.....	XXIII
CHAPTER 1 INTRODUCTION .....	1
1.1 Background .....	1
1.2 Requirement of micro hydropower generation in water pipes.....	5
1.3 Aims and objectives .....	6
1.4 Organization of this thesis.....	7
CHAPTER 2 LITERATURE REVIEW AND RESEARCH METHODOLOGY...	10
2.1 Micro hydro turbine technologies .....	10
2.1.1 Impulse turbines .....	11
2.1.2 Reaction turbines.....	13

2.1.3	Turbine selection criteria.....	16
2.2	Micro hydropower from water supply pipes.....	18
2.2.1	Inline Francis turbines.....	18
2.2.2	Inline cross-flow turbines.....	21
2.2.3	PAT for inline application.....	22
2.2.4	Lift-type turbine .....	26
2.2.5	Other inline turbines.....	27
2.3	Research on cross-flow turbines .....	29
2.3.1	Effects of nozzle shape.....	31
2.3.2	Effects of runner inlet arc angle.....	35
2.3.3	Effects of attack angle and blades outer angle .....	37
2.3.4	Effects of blades inner angle.....	38
2.3.5	Effects of runner diameter ratio .....	39
2.3.6	Effects of blades number.....	40
2.4	Review of research methodology.....	41
2.4.1	Theoretical analysis.....	42
2.4.2	Experimental method .....	43
2.4.3	Numerical method.....	44
2.5	Research gap and methodology .....	48

## CHAPTER 3 DEVELOPMENT OF A NOVEL INLINE CROSS-FLOW TURBINE

BY NUMERICAL AND EXPERIMENTAL METHODS.....	51
3.1 Scheme of the inline cross-flow turbine.....	51
3.2 Research methodology for turbine development .....	53
3.2.1 Geometrical parameters .....	54
3.2.2 CFD setting .....	55
3.2.3 Experimental setup.....	58
3.2.4 Data analysis .....	61
3.3 Numerical results and analysis.....	63
3.3.1 Design of block shape .....	63
3.3.2 Effects of tip clearance.....	69
3.3.3 Design of self-adjustable vane .....	72
3.4 Experimental results and analysis .....	75
3.4.1 Validation of the numerical results .....	76
3.4.2 Experimental performance of the turbine .....	79
3.5 Summary .....	80
CHAPTER 4 DEVELOPMENT OF THE BLOCK DESIGN METHOD AND THEORETICAL ANALYSIS ON THE CROSS-FLOW RUNNER .....	82
4.1 Mathematic design method for the blocks .....	82
4.1.1 Introduction and assumptions .....	82
4.1.2 Design procedure .....	84

4.1.3	Implications for block optimization .....	88
4.2	Theoretical analysis of the cross-flow runner .....	89
4.2.1	Derivation of turbine fundamental equations.....	89
4.2.2	Fundamental equations of cross-flow turbine .....	92
4.2.3	Implications for runner optimization .....	95
4.3	Main geometrical parameters of the blades .....	96
4.4	Summary .....	97
CHAPTER 5 NUMERICAL STUDY ON THE EFFECTS OF GUIDE BLOCK ORIENTATION ANGLE ON THE PERFORMANCE OF INLINE CROSS-FLOW TURBINE .....		99
5.1	Physical turbine models with different guide block orientation angles .....	100
5.2	Meshing and numerical setup.....	101
5.3	Data analysis .....	103
5.4	Results analysis and discussion.....	104
5.4.1	Output power and efficiency of the turbine .....	104
5.4.2	Analysis of flow characteristics .....	105
5.4.3	Analysis of pressure distribution.....	109
5.4.4	Water head reduction .....	112
5.5	Summary .....	113
CHAPTER 6 NUMERICAL STUDY ON THE EFFECTS OF RUNNER INLET		

ARC ANGLE ON THE PERFORMANCE OF INLINE CROSS-FLOW TURBINE..

..... 115

6.1 Physical turbine models with different runner inlet arc angles..... 116

6.2 Results analysis and discussion..... 116

6.2.1 Numerical turbine performance ..... 116

6.2.2 The function of the conversion block ..... 119

6.2.3 Flow velocity characteristics..... 120

6.2.4 Pressure distribution..... 122

6.2.5 Torque of each blade and stage..... 125

6.3 Summary ..... 127

CHAPTER 7 INVESTIGATION OF THE EFFECTS OF RUNNER AND BLADES GEOMETRIES ON THE PERFORMANCE OF INLINE CROSS-FLOW TURBINE

..... 129

7.1 Study on effects of blades outer angle ..... 129

7.1.1 The optimal range of blades outer angle ..... 129

7.1.2 Turbine performance ..... 131

7.1.3 Torque output of each runner stage..... 133

7.2 Study on effects of runner diameter ratio..... 135

7.2.1 Turbine performance ..... 135

7.2.2 Torque output of each runner stage..... 138

7.3	Study on effects of blades number .....	139
7.3.1	Turbine performance .....	139
7.3.2	Torque output of each runner stage.....	141
7.4	Summary .....	142
CHAPTER 8 DEVELOPMENT OF A MAGNETIC DRIVEN BIDIRECTIONAL INLINE CROSS-FLOW TURBINE: A CASE STUDY .....		144
8.1	Design process .....	144
8.1.1	Design of the blocks.....	145
8.1.2	Geometries of the runner.....	146
8.1.3	Application of magnetic coupling.....	147
8.1.4	Mechanical structure of the turbine.....	149
8.2	Prototype and experimental setup .....	150
8.3	Results and discussion .....	152
8.3.1	Turbine performance at different rotation speed.....	152
8.3.2	Effects of the distance between block and runner on turbine performance .....	154
8.4	Summary .....	157
CHAPTER 9 CONCLUSIONS AND RECOMMENDATIONS FOR FUTURE WORK .....		159
9.1	Experimental study on the preliminary turbine prototype .....	159

9.2	Theoretical analysis on the inline cross-flow turbine .....	160
9.3	Effects of block geometries on the turbine performance .....	161
9.4	Effects of runner geometries on the turbine performance.....	161
9.5	Case study about the development of bidirectional inline cross-flow turbine.. .....	162
9.6	Limitations and recommendations for future work.....	163
	REFERENCES.....	165

## LIST OF FIGURES

Fig.1.1 Working principle of Water Intelligent Network .....	2
Fig.1.2 Schematic diagram of DMA and PMA .....	2
Fig.1.3 The structure and working principle of the PRV .....	4
Fig.2.1 The classification of micro hydropower turbines .....	10
Fig.2.2 The typical structure of Pelton turbine .....	11
Fig.2.3 The runner and working principle of Turgo turbines .....	12
Fig.2.4 The structure of cross-flow turbine.....	13
Fig.2.5 The structure of Francis turbine.....	14
Fig.2.6 The runner and working principle of Propeller turbines.....	15
Fig.2.7 The structure of pumps as turbines .....	15
Fig.2.8 The various turbines in terms of head and flow rate.....	17
Fig.2.9 Part flow efficiencies of different turbines .....	18
Fig.2.10 On-site product of the Francis turbine developed by Tanaka.....	19
Fig.2.11 Working principle of the Francis turbine developed by Tanaka .....	19
Fig.2.12 Micro Francis turbine developed by Hitachi .....	20
Fig.2.13 Micro cross-flow turbine for water pipes .....	21
Fig.2.14 Micro cross-flow turbine developed by Vincenzo Sammartano .....	22

Fig.2.15 PAT installation in the pumping station at Breech, Germany .....	23
Fig.2.16 Sketch of locations of PATs in water distribution system.....	24
Fig.2.17 Installation scheme of PAT and valves.....	25
Fig.2.18 Lift-type turbine developed by Lucid Energy.....	26
Fig.2.19 DN100 inline hydropower generator unit.....	27
Fig.2.20 Radial-flux energy harvester.....	28
Fig.2.21 Battery-free smart flowmeter.....	28
Fig.2.22 Main geometrical parameters of the traditional cross-flow turbine.....	29
Fig.2.23 Nozzle shape design method developed by Sammartano V: (a) Geometrical profile; (b) Principle of the design method .....	31
Fig.2.24 Nozzle shape design method developed by Adhikari et al. ....	32
Fig.2.25 Numerical study on effects of nozzle shape on turbine performance by Acharya et al. ....	33
Fig.2.26 Cross-flow tidal turbine developed by Prasad et al. ....	34
Fig.2.27 Dual-nozzle cross-flow turbine developed by Elbatran et al. ....	35
Fig.2.28 2D model of cross-flow turbine in the research of Chen, et al. ....	36
Fig.2.29 Effects of blades inner angle on power output of each runner stage .....	39
Fig.2.30 Effects of diameter ratio on power output of each runner stage .....	40
Fig.2.31 A hydraulic test rig developed by Pereira et al. ....	43
Fig.2.32 Flow chart of the methodology .....	49

Fig.3.1 The turbine design scheme .....	52
Fig.3.2 The research flow chart.....	53
Fig.3.3 The main geometrical parameters of the cross-flow runner .....	54
Fig.3.4 The dependence of shaft power on the grid number.....	56
Fig.3.5The final meshing scheme .....	56
Fig.3.6 The hydraulic test rig at the MOSWTW .....	59
Fig.3.7 Schematic diagram of the controller .....	60
Fig.3.8 Control effect of the controller .....	61
Fig.3.9 The electricity control and storage system .....	61
Fig.3.10 Different block models .....	63
Fig.3.11 The output power of four cases with different TSR .....	65
Fig.3.12 The water head loss of four cases with different TSR.....	65
Fig.3.13 The velocity vectors of different cases .....	67
Fig.3.14 The output power of four cases on off-design points .....	68
Fig.3.15 The water head loss of four cases on off-design points.....	69
Fig.3.16 Tip clearance of the inline cross-flow turbine .....	69
Fig.3.17 The output power of models with different tip clearance .....	70
Fig.3.18 The water head loss of models with different tip clearance .....	70
Fig.3.19 The pressure contours of models with different tip clearance .....	71
Fig.3.20 The schematic diagram of the self-adjustable vane .....	73

Fig.3.21 The water head loss of models with and without self-adjustable vane.....	74
Fig.3.22 The output power of models with and without self-adjustable vane .....	74
Fig.3.23 The off-design performance of turbine model with self-adjustable vane....	75
Fig.3.24 The inline cross-flow turbine prototype.....	76
Fig.3.25 The comparison between experimental and numerical output power .....	76
Fig.3.26 The comparison between experimental and simulation water head loss .....	77
Fig.3.27 The turbine performance in one typical day .....	79
Fig.3.28 Daily electricity generation.....	80
Fig.4.1 Design scheme of the inline turbine (a) Main structure of the turbine (b) Diagram of cross section at the conversion block inlet.....	83
Fig.4.2 Micro fluid stream in the blades passage.....	90
Fig.4.3 Flow streamline through the cross-flow runner.....	92
Fig.4.4 Flow velocity triangle at the runner inlet.....	95
Fig.4.5 Blades geometrical parameters of the cross-flow runner.....	96
Fig.5.1 Turbine models with different guide block orientation angles .....	100
Fig.5.2 Grid independence test results .....	101
Fig.5.3 Final meshing scheme: (a) Meshing of the whole computational domain; (b) Meshing of the turbine body; (c) Zoomed view of the blades meshing .....	102
Fig.5.4 Output power of inline turbines with different blocks.....	105
Fig.5.5 Efficiency of inline turbines with different blocks .....	105

Fig.5.6 Flow velocity vectors of the three models at a TSR of 0.7.....	106
Fig.5.7 Computed and designed flow velocity along the runner inlet arc .....	107
Fig.5.8 Computed flow inlet angle along the runner inlet arc .....	109
Fig.5.9 Pressure contours of the three models at a TSR of 0.7 .....	110
Fig.5.10 Torque output of each blade at the first and second stage .....	111
Fig.5.11 Torque output of different stages.....	111
Fig.5.12 Water head reduction of the three models .....	113
Fig.5.13 Water head reduction caused by the conversion block.....	113
Fig.6.1 Physical models of the inline cross-flow turbine (a) Case 1: $\lambda=90^\circ$ (b) Case 2: $\lambda=105^\circ$ (c) Case 3: $\lambda=120^\circ$ (d) Case 4: $\lambda=135^\circ$ .....	116
Fig.6.2 Output power of different cases.....	117
Fig.6.3 Water head reduction of different cases .....	118
Fig.6.4 Efficiency of different cases .....	118
Fig.6.5 water head reduction through conversion block.....	119
Fig.6.6 Velocity vectors showing water flow through the inline cross-flow turbine (a) Case 1: $\lambda=90^\circ$ (b) Case 2: $\lambda=105^\circ$ (c) Case 3: $\lambda=120^\circ$ (d) Case 4: $\lambda=135^\circ$ .....	120
Fig.6.7 Flow velocity distribution along the runner inlet arc.....	122
Fig.6.8 Pressure distribution through the inline cross-flow turbine: (a) Case 1: $\lambda=90^\circ$ ; (b) Case 2: $\lambda=105^\circ$ ; (c) Case 3: $\lambda=120^\circ$ ; (d) Case 4: $\lambda=135^\circ$ .....	123
Fig.6.9 Water head distribution along the runner inlet arc .....	124

Fig.6.10 Torque output of each blade at the first runner stage .....	125
Fig.6.11 Torque output of each blade at the second runner stage.....	125
Fig.6.12 Torque output of each runner stage .....	126
Fig.7.1 The variation of flow inlet angle along the runner inlet arc .....	130
Fig.7.2 The influence of blades outer angle on turbine output power .....	132
Fig.7.3 The influence of blades outer angle on water head reduction .....	132
Fig.7.4 The influence of blades outer angle on turbine efficiency.....	133
Fig.7.5 The influence of blades outer angle on torque output of each blade .....	134
Fig.7.6 The influence of blades outer angle on torque output of each runner stage	134
Fig.7.7 The influence of runner diameter ratio on turbine output power.....	136
Fig.7.8 The influence of runner diameter ratio on water head reduction.....	136
Fig.7.9 The influence of runner diameter ratio on turbine efficiency .....	137
Fig.7.10 The influence of runner diameter ratio on torque output of each blade ....	138
Fig.7.11 The influence of runner diameter ratio on torque output of each runner stage .....	139
Fig.7.12 The influence of blades number on turbine output power .....	140
Fig.7.13 The influence of blades number on turbine water head reduction.....	140
Fig.7.14 The influence of blades number on turbine efficiency .....	141
Fig.7.15 The influence of blades number on torque output of each runner stage....	142
Fig.8.1 Block shape of the bidirectional cross-flow turbine .....	145

Fig.8.2 Physical model of the runner and blade.....	147
Fig.8.3 Structure and working principle of magnetic coupling .....	148
Fig.8.4 The prototype of magnetic coupling: (a) Internal coupling half; (b) Containment shroud (c) External coupling half.....	149
Fig.8.5 The structure of bidirectional inline cross-flow turbine .....	149
Fig.8.6 Prototype of the bidirectional turbine .....	150
Fig.8.7 Hydraulic test rig for the bidirectional turbine .....	150
Fig.8.8 Dynamic torque meter system for the bidirectional turbine .....	151
Fig.8.9 Turbine power and water head reduction under different rotation speed....	152
Fig.8.10 Turbine efficiency under different rotation speed .....	153
Fig.8.11 Output power of the bidirectional turbine.....	154
Fig.8.12 Water head reduction of the bidirectional turbine .....	155
Fig.8.13 Efficiency of the bidirectional turbine .....	155

## LIST OF TABLES

Table 2.1 Definition of different geometrical parameters.....	30
Table 2.2 Summary of experimental studies on cross-flow turbines.....	44
Table 2.3 Summary of numerical studies on cross-flow turbines.....	46
Table 3.1 The values of runner main geometrical parameters.....	54
Table 3.2 Simulated results of four cases on the design point.....	64
Table 3.3 Comparison between computed and measured results.....	78
Table 7.1 The main runner geometrical parameters with different $\beta_1$ .....	130
Table 7.2 The main runner geometrical parameters with different $D_2/D_1$ .....	135
Table 8.1 The main geometrical parameters of runner and blade.....	146

# NOMENCLATURE

## Abbreviations

BEP	Best efficiency point
CFD	Computational Fluid Dynamics
DMA	District Metering Area
MOSWTW	Ma On Shan Water Treatment Works
PAT	Pump as turbine
PMA	Pressure Management Area
PRV	Pressure reducing valve
RANS	Reynolds averaged Navier–Stokes
SST	Shear stress turbulence
TSR	Tip speed ratio
WIN	Water Intelligent Network
WSD	Water Supplies Department
WSS	Water supply system

## Symbols

$A_{in}$	Inlet area of the conversion block calculated by fluid continuity
$A'_{in}$	Inlet area of the conversion block calculated by definite integration
$A_{\theta}$	Area of the cross section through runner central axis and $R_{\theta}$ calculated by fluid continuity
$A'_{\theta}$	Area of the cross section through runner central axis and $R_{\theta}$ calculated by definite integration

$a$	Length of long axes of the pipe cross-section ellipse
$b$	Length of short axes of the pipe cross-section ellipse
$B$	Nozzle width
$C$	Allowable deviation of inlet area of the conversion block
$C(\psi)$	Bernoulli constant
$D_1$	Runner outer diameter
$D_2$	Runner inner diameter
$D_2/D_1$	Runner diameter ratio
$e_1$	Total energy of the micro fluid stream at blades passage inlet
$e_2$	Total energy of the micro fluid stream at blades passage outlet
$\Delta e$	Energy from micro fluid stream that captured by blades
$H$	Pressure head across the turbine
$H_{in}$	Water head at inlet boundary
$H_{out}$	Water head at outlet boundary
$\Delta H$	Water head reduction through the turbine
$L$	Runner length
$n$	Rotation speed of turbine
$N_b$	Blades number
$p$	Fluid pressure
$P_{in}$	Input power of the turbine
$P_s$	Actual simulation power output
$P_{shaft}$	Turbine shaft power

$dP_t$	Theoretical power from the micro flow stream
$P_t$	Theoretical power output of first runner stage
$P_{tcft}$	Theoretical power of cross-flow turbine
$Q$	Total flow rate through the runner
$Q_{in}$	Flow rate at the inlet of conversion block
$r$	Runner outer radius
$R_0$	Distance from runner central axis to the inlet of conversion block
$R_b$	Blades Radius
$R_{pipe}$	Radius of the water pipe
$R_\theta$	Distance from runner central axis to conversion block at different azimuthal angle
$S_0$	Nozzle throat width
$T$	Turbine shaft torque
$t_1, t_2$	Substitution parameters
$u$	Fluid velocity
$u_i'$	Fluctuating velocity due to turbulence
$U$	Time-averaged velocity
$U_x$	Velocities of the rotating reference system
$V_x$	Absolute flow velocities
$V$	Flow velocity at runner inle
$V_0$	Water flow velocity in the pipe
$V_{in}$	Flow velocity at the inlet of conversion block

$W_x$  Relative flow velocities

### Greek Symbols

$\alpha$  Attack angle

$\beta_1$  Blades outer angle

$\beta_2$  Blades inner angle

$\eta_{me}$  Overall mechanical efficiency

$\eta_g$  Conversion efficiency of generator

$\omega$  Runner rotation speed

$\gamma$  Orientation entry angle of the conversion block

$\theta_0$  Orientation angle of the guide block

$\lambda$  Runner inlet arc angle

$\alpha_x$  Angle between relative flow velocities and velocities of the rotating reference system

$\beta_x$  Angle between absolute flow velocities and velocities of the rotating reference system

$\rho$  Density of water

$\nu$  Kinematic viscosity of fluid

$\eta_{t\text{eft}}$  Theoretical turbine efficiency

$\eta_{t\text{max}}$  Maximum turbine efficiency

$\eta$  Turbine efficiency

# CHAPTER 1 INTRODUCTION

## 1.1 Background

Water supply is not only of vital importance for urban development, but also essential to the subsistence of urban residents. Usually, the water treatment and pump stations for urban water supply are located in suburb areas, so long water supply pipes are needed to delivery fresh water to every user. Besides, water head in urban water supply pipelines is usually very high to ensure consistent water supply throughout the urban area [1]. Taking Hong Kong for instance, more than 8000 km water mains are laid underground to supply water for over 7 million populations, and due to the hilly topography and long pipes, the water head could reach 80m [2]. Similar to most of the developed countries, water loss along the water supply pipes in Hong Kong is also a perennial problem as a considerable length of water mains has approached the end of their service life in the 1990s and the deterioration of water mains may result in severe water leakage. Although water leakage can be significantly reduced through the replacement and rehabilitation of aged water mains, it is estimated that there is still nearly 15% of fresh water wasted in 2016 due to pipe leakage [2].

However, the deterioration of water mains cannot be stopped. Although replacing and rehabilitating aged water mains is an effective way to reduce water leakage, it is also time-consuming, costly and will cause inconvenience to residents' living. With the technology development of sensors, telemetry, data analysis software in recent years, the Water Intelligent Network (WIN) has been a promising method to maintain the healthiness of water supply pipes. The WIN is essentially a continuous monitoring system which achieves its function using a lot of monitoring and sensing equipment,

including flow meters and pressure sensors. The working principle of the WIN is shown in Fig.1.1. To apply the WIN, the water distribution network is divided into a lot of District Metering Areas (DMAs) and associated Pressure Management Areas (PMAs). The schematic diagram of DMA and PMA is shown in Fig.1.2. In each DMA and PMA, high-technology monitoring and sensing equipment are installed to support the WIN. By processing data from different sensors, the WIN can fully analyze the pipes' condition and determine the most cost-effective means to maintain their healthiness.

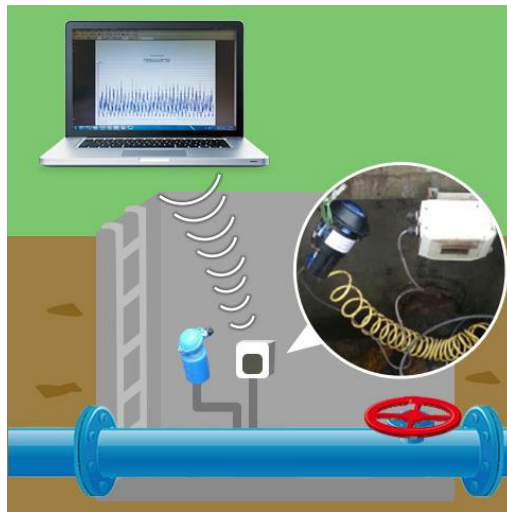


Fig.1.1 Working principle of Water Intelligent Network

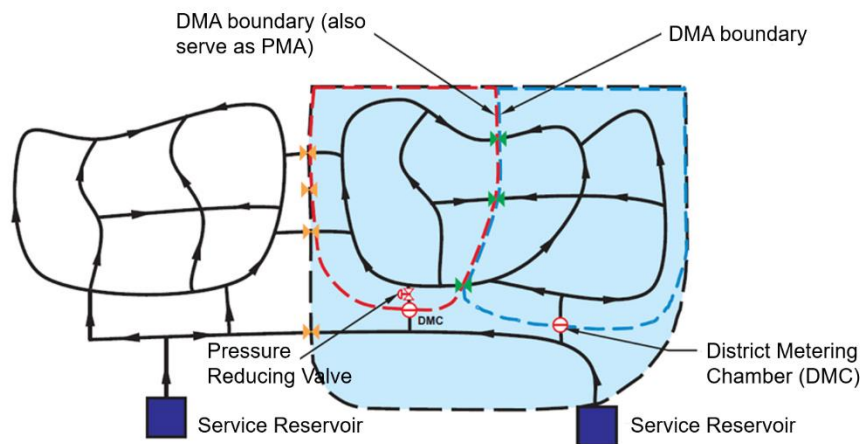


Fig.1.2 Schematic diagram of DMA and PMA

The WIN mainly has four functions when applied in the water supply systems.

1) Active leakage detection and control using monitoring and sensing equipment installed in the network.

2) Pressure management to reduce pressure without affecting the minimum supply pressure to sustain normal supply.

3) Quality and speedy repairs to water main leaks and bursts

4) Asset management by re-provisioning of aged water mains which are beyond economic repair.

However, the monitoring and sensing equipment in the WIN are mainly powered by traditional chemical batteries which usually have limited lifespans even with efficient energy conserving mechanisms [3]. Once the batteries ran out, the WIN would stop functioning, so the batteries need to be replaced frequently, resulting in a high cost and a huge demand for labor [4]. It has been an important issue for urban water supply industry to find an alternative power source for the WIN. Instead of chemical batteries, many researchers investigated renewable energies to supply power to water monitoring sensors.

It has been proved in the current research that renewable energy sources including vibration, solar energy and wind energy can be adopted to provide power for water monitoring system [5][6][7]. However, there are several drawbacks of these renewable sources. Firstly, these power sources are uncontrollable and not steadily available, so they cannot be harvested whenever wanted [8]. On the other hand, their energy harvesters are usually bulky and therefore need more space to install. But most of the water monitoring sensors and meters are usually located underground or limited spaces

that surrounded by trees or buildings in the urban areas, which significantly restricts the application of these renewable sources. In fact, the pressure inside the water supply pipes are usually excess to ensure sufficient water supply through the urban area, however, the excess water head also possesses a threat to pipe healthiness. As can be seen in Fig.1.2, in the water distribution network in Hong Kong, pressure reducing valves (PRVs) are installed at the entrance of the PMAs for pressure reduction without affecting the minimum supply pressure to sustain normal supply. As shown in Fig.1.3 is the structure of the PRV. A PRV is a kind of throttling control element with local resistance, by changing its throttling area, the flow rate and kinetic energy of fluid that flows through the PRV could be changed, resulting in different pressure reduction of the fluid. However, the PRV reduces the overall water pressure in pipeline by decreasing throttling area to increase water head losses, which means the excess energy is wasted and the whole energy efficiency in water supply system (WSS) would be adversely affected. Instead of reducing the excess water pressure, this part of water head can be harvested by micro turbines for power supply to the WIN.

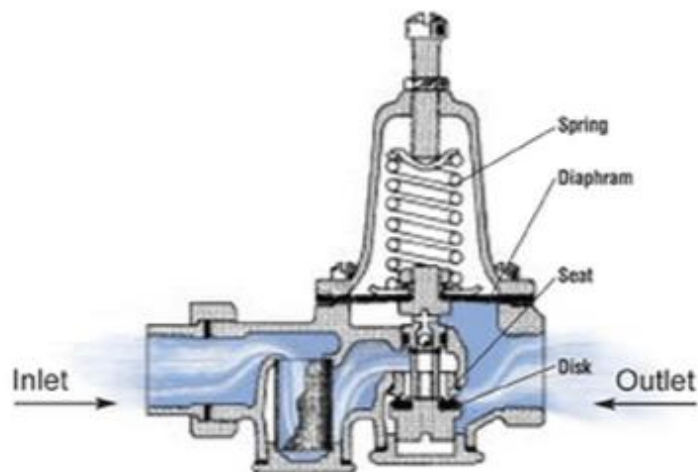


Fig.1.3 The structure and working principle of the PRV

## **1.2 Requirement of micro hydropower generation in water pipes**

In the past decades, micro hydropower technologies in the domains of remote power supply, pumped storage power plant and industrial hydropower recovery have been very mature, but micro hydropower generation in water supply pipes has been less studied and is still at the developmental stage [9][10]. The main challenge of hydropower generation in water supply pipes is the selection or design of proper turbines that can meet the requirements of water supply. The requirements are as follows:

1) Compared to rivers, sewage water or other sources for micro hydropower, fresh water in the water distribution networks is more fluctuant due to the water demand variation over time. Based on the data from the Water Supplies Department (WSD) in Hong Kong, the range of flow velocity inside water supply mains is from 1-2m/s.

2) Although there exists some excess water head in the water pipes, the turbine cannot consume too much water head. To avoid negative effects on the normal water supply through the whole urban area, the consumed water head cannot exceed 5m water.

3) The generated electricity should meet the power demand of water monitoring system, but too much power may possess a huge load on the energy control and storage system. Based on the data provided by the WSD of Hong Kong, 40-100W power is sufficient for nearly any water monitoring system.

4) As most of the urban water pipes are laid underground, the installation space is very limited and the modification of the pipes should be as slight as possible.

5) The most important thing is that the application of water turbine cannot have

bad impact on the water quality, which possesses a high requirement for the material, sealing and lubrication of the water turbines.

Considering the above requirements, suitable off-the-shelf turbine is not available in the market. To harvest hydropower from water supply pipelines, it is necessary to design and manufacture a turbine according to the working conditions.

### **1.3 Aims and objectives**

This research will focus on the development of technologies that can be applied in the water supply mains of the water distribution network in Hong Kong. For hydropower harvesting from water mains, the hydro turbine is the key equipment that transfer the kinetic energy of water flow into electricity. Besides, it is of vital importance to manage and store the generated power. The detailed aims and objectives of this research are summarized as follows:

- 1) To determine the design scheme of the inline turbine that could be used in the water distribution network for hydropower harvesting. Based on the expected working conditions and the optimal water head and flow rate of different turbines, the scheme will be determined. After that, the feasibility of the proposed scheme will be verified using numerical and experimental methods.

- 2) To propose a design method for the inline turbine to be used in water mains for hydropower harvesting. There have been mature design methods for traditional water turbines, however, the inline turbine to be used in water pipes has no mathematic method for design or optimization, it is necessary to develop a mathematic method to provide guidance for inline turbine design.

- 3) To investigate the influencing factors on the performance of inline turbine.

Many geometrical parameters of the turbine will have impacts on turbine performance. In this study, a series of turbine models with different geometrical parameters will be developed with the proposed mathematic method. Then, by using the CFD methods, the influencing mechanism of different parameters will be investigated by analyzing the pressure and velocity distribution inside the turbine and the results can provide guidance for performance enhancement of the inline turbine.

4) To perform a systematic study to determine the optimal geometrical parameters of the inline cross-flow turbines. Based on the numerical analysis, the optimal values of different geometrical parameters can be obtained.

5) A case study will be conducted to verify the proposed design method and the research results presented in the thesis. In the case study, a novel inline turbine will be developed. Besides, a hydraulic test rig will be built and the performance of the developed turbine will be fully investigated.

## **1.4 Organization of this thesis**

This thesis consists of nine chapters. The first chapter presents a brief introduction of the research background. Besides, the research objectives of the thesis are proposed at the end of this chapter.

Chapter 2 gives a comprehensive literature review of current research. Firstly, a review of the existing micro hydropower technologies and the corresponding turbines is conducted to choose a proper turbine for this project. By comparing the working conditions of different turbines and the requirement of this project, the cross-flow turbine is considered an acceptable choice for the research. After that, current researches on design and optimization of cross-flow turbine by numerical and experimental methods is analyzed and the research gap is identified. Finally, a research

flowchart is presented to indicate the research process in this thesis.

Chapter 3 develops a novel inline cross-flow turbine by numerical and experimental methods. Firstly, a design scheme of the inline turbine which consists two blocks integrated to the pipe inner wall is proposed. Then, the detailed numerical method including meshing scheme, solver setup and boundaries setup, experimental method and data analysis method are described. After that, the development of a preliminary prototype is introduced. The real performance of the designed prototype is investigated in the test rig and a duration test is also conducted. The experimental results can not only prove feasibility of the proposed design scheme, but also provide validation for the CFD simulation results

In Chapter 4, a design method for the block is proposed based on fluid continuity. After that, the working principle of the runner is analyzed based on Bernoulli's equation. Then the theoretical equation about turbine efficiency related to geometrical parameters of the runner is derived to determine the influencing factors of the turbine performance.

Chapter 5 and Chapter 6 investigate the impacts of different block shapes on the performance of inline cross-flow turbine. Based on the proposed design method, the profile of the block is determined, the numerical investigations are carried out to verify the proposed method and study the effects of different block designs on turbine performance. The flow velocity, pressure distribution, the numerical output power and water head reduction are analyzed, then the optimal block shape is determined.

Chapter 7 investigates the influence of different runner parameters on the turbine performance. Specifically, models with different blades outer angle, runner diameter ratio and blades number are developed and simulated. By analyzing the flow velocity,

flow inlet angle, pressure distribution, and numerical performance of the turbine, the optimal parameters of the runner are obtained.

In Chapter 8, a magnetic driven bidirectional inline turbine is developed and manufactured using the proposed method and the suggested optimal parameters in this research. After that, the prototype is tested in a lab test rig to study its performance including power output, water head reduction and efficiency.

Finally, Chapter 9 summarizes the main conclusions and contributions of this thesis Besides, some limitations and recommendations for the future work are also given in this chapter.

## CHAPTER 2 LITERATURE REVIEW AND RESEARCH METHODOLOGY

The micro hydropower has obtained sufficient development in the past decades and many kinds of water turbines that suitable for different working conditions have been developed. Besides, a lot of novel turbines used in water pipes were also designed. To enhance the performance of micro hydro turbines, large amounts of research has been conducted by theoretical, numerical and experimental methods over the past few years. A comprehensive review is provided in this chapter.

### 2.1 Micro hydro turbine technologies

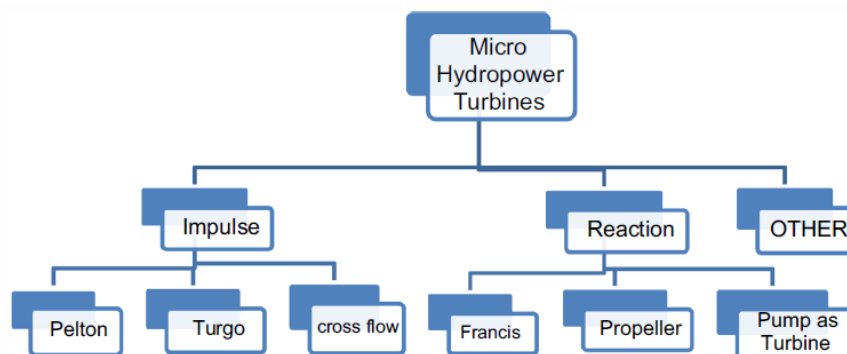


Fig.2.1 The classification of micro hydropower turbines [11]

Micro hydropower generation is one branch of hydropower, this technology is mainly used in remote or mountainous areas where national grid could not research for electricity generation [12]. Correspondingly, micro hydro turbines which generate very reliable power though with very simple designs and fabrications have gained a rapid growth in the power generation field [13]. Micro hydro turbines can be mainly divided into two types based on their working principle: impulse turbine and reaction

turbine. Fig.2.1 shows the detailed category of micro hydro turbines.

### 2.1.1 Impulse turbines

In impulse turbines, hydraulic energy is first converted into kinetic energy in form of free water jet by nozzles. The water jet impacts the runner blades and due to change of momentum of the jet, a force is created on the runner blades that makes the turbine rotate.

#### (1) Pelton turbine

Fig.2.2 shows the detailed structural scheme of Pelton turbine. The runner of Pelton turbine is surrounded by several cups, which converts the momentum of water from the jet into the kinetic energy of the runner. Generally, Pelton turbine is widely used in the micro hydropower sites with high water head and low flow rate [14]. In micro hydro power projects, Pelton turbine is usually designed with a single jet and the maximum efficiency could reach 70-90% [10]. However, in order to keep the wheel clear of flow, the Pelton turbine must be located above the water level of tailrace, which results in a huge water head reduction [10]. Besides, Pelton turbines are not preferred under low head conditions.

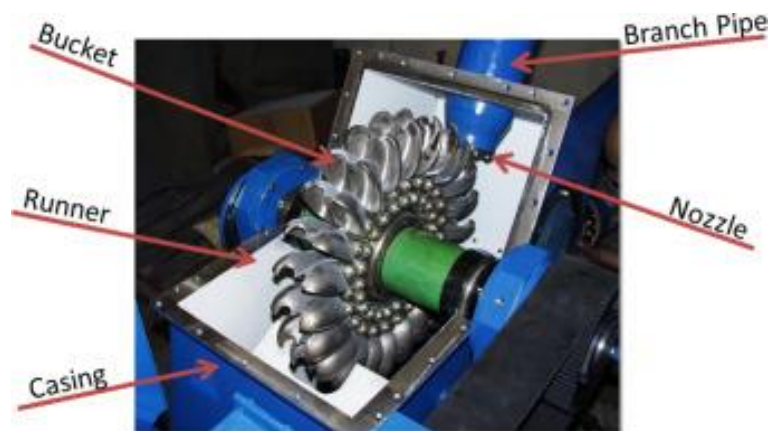


Fig.2.2 The typical structure of Pelton turbine [15]

## (2) Turgo turbines

The working principle of Turgo turbines (as shown in Fig.2.3) is similar with that of Pelton turbine. For micro hydropower applications, Turgo turbines can be used in a wide head range (3-150m) [17]. The efficiency of Turgo turbines depends significantly on the jet position, jet inclined angle and speed ratio, in the research of Williamson et al., the maximum efficiency is about 90% [17]. However, Turgo turbines are seldom put into use in micro hydropower engineering, and the reason why it is preferred by very few companies may partly because of the complexity of the runner that makes it difficult to manufacture and to some extent, the cost is relatively high [16].

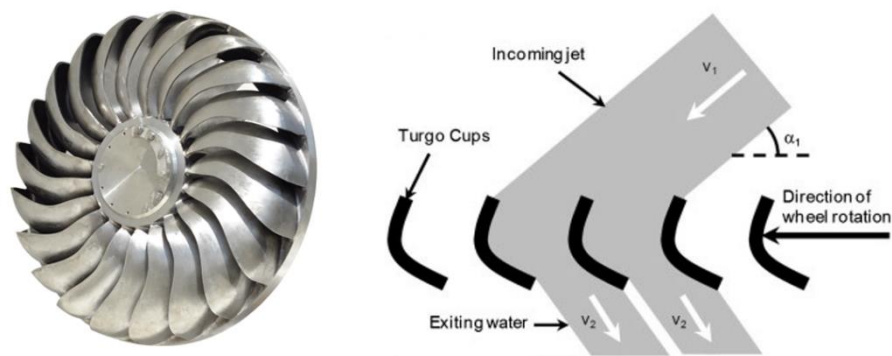


Fig.2.3 The runner and working principle of Turgo turbines [17][18]

## (3) Cross-flow turbine

The cross-flow turbine is another typical impulse turbine, and it is widely used for micro hydropower projects in some developing countries because that it is almost the simplest turbines to be designed and manufactured [19].

The cross-flow turbine can be installed in either horizontal or vertical configuration and can be applied at high flow rate and low water head. The average efficiency of cross-flow turbines is usually 80% for small and micro-power outputs; but can reach up to 86% in the case of medium and large units [20].

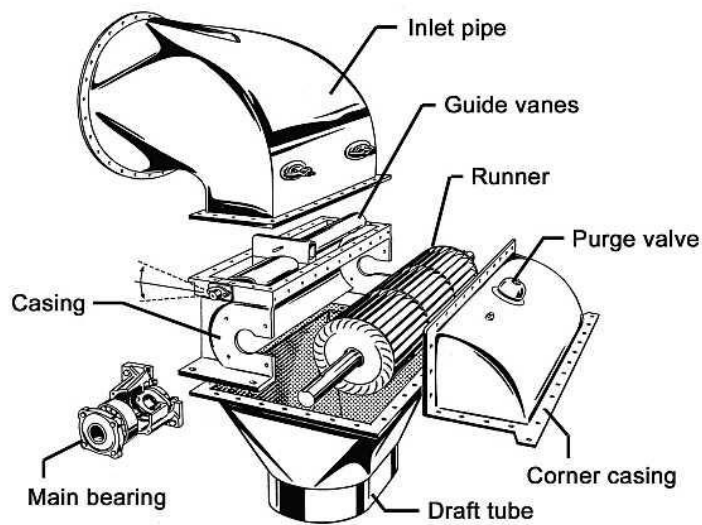


Fig.2.4 The structure of cross-flow turbine [21]

### 2.1.2 Reaction turbines

In reaction turbines, the water head and flow velocity change when water flows through the machine, meanwhile, the change of water pressure and velocity create a reaction on the blades, which makes the runner to rotate. Because the pressure is the basic condition of energy conversion, the wheel part of a reaction turbine must always be full of water. Typical types of reaction turbines applied in micro hydropower technology are Francis turbine, Propeller turbine and Pump-as-turbine. These turbines will be described in detail in the following paragraphs.

#### (1) Francis turbine

Francis turbine is basically a radial flow machine, where water enters the runner through the outer periphery in the radial direction and leaves in the axial direction (as shown in Fig.2.5) A Francis turbine is currently the most widely used turbine at hydropower stations. It is estimated that the working head range of a Francis turbine is between 1m to 900m, so this kind of turbine can be used in micro, medium or large

hydropower projects [22]. As for velocity of flow, Francis turbine can be used within 0.4 to 20 m<sup>3</sup>/s [22]. The Francis turbine may have a poor performance under part flow conditions, it is reported that vibration and mechanical shock may occur when the Francis turbine works below 40% of its rated flow rate [23].

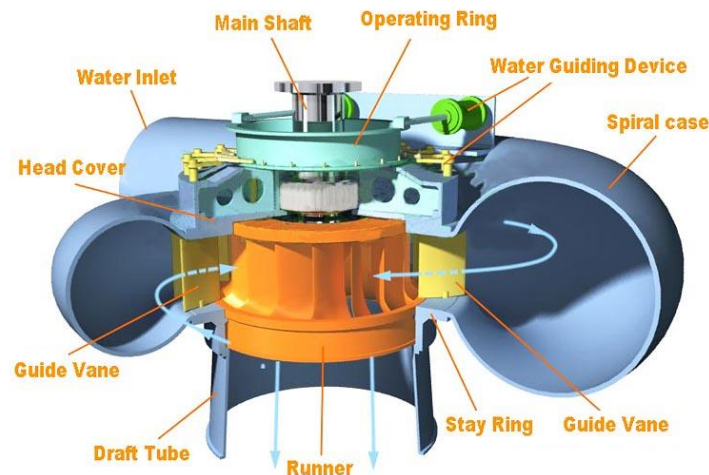


Fig.2.5 The structure of Francis turbine [24]

## (2) Propeller turbines

The Propeller turbine is a special kind of Kaplan turbine, which is a type of axial turbine. For the Kaplan turbine, the runner blades and guide vanes can be made adjustable (seen in Fig.2.6(a)) and the flow direction in the turbine is parallel to the draft when working (seen in Fig.2.6(b)). In the micro hydropower projects, the blades of Kaplan turbine are often made fixed, so in this case, the Kaplan turbine is also called Propeller turbine. The Propeller turbine can work optimally between 30% and 100% of the maximum design flow [23] and are mostly used in small head hydropower plants. For micro hydropower projects, the fixed-blade propeller can simply be encased in a section of the penstock. The propeller turbines used in hydropower projects can have up to 6 blades [25].

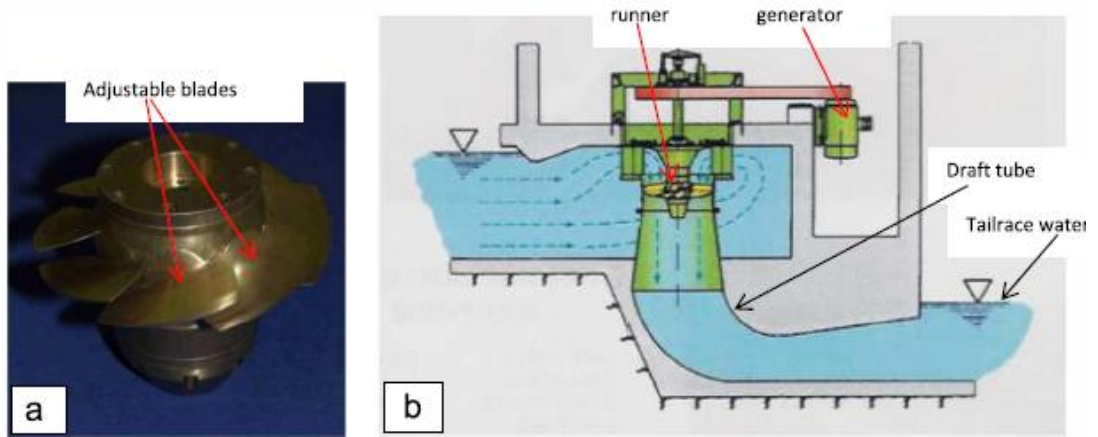
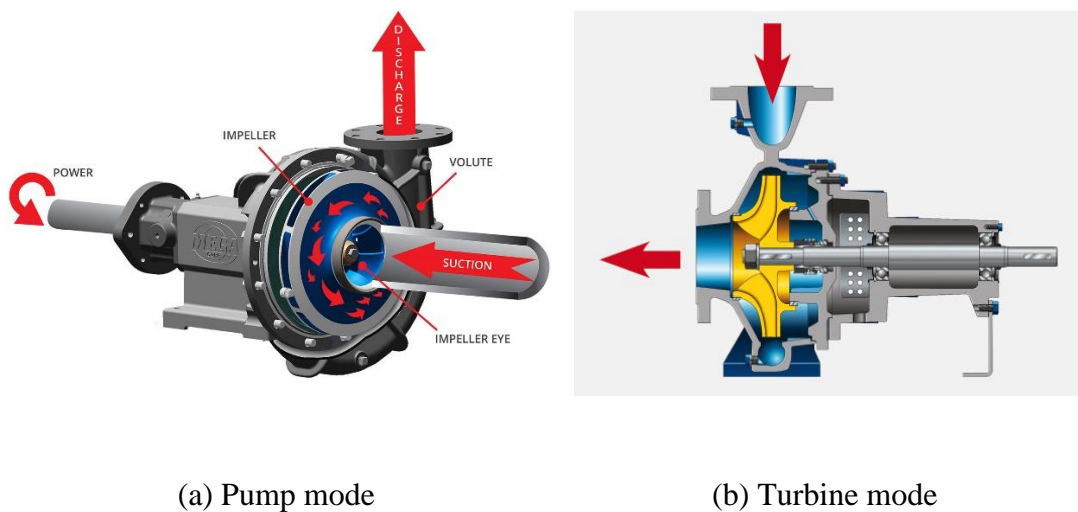


Fig.2.6 The runner and working principle of Propeller turbines [23]

### (3) Pump as turbines

Generally, pump as turbine (PAT) means a pump operated in reverse as a turbine for power generations. When a pump operating in pump mode, as shown in Fig.2.7(a), power transfers from the shaft to the impeller and water is sucked into the pump and leaving the pump with pressure and kinetic energy. However, when a pump operating in reverse as a turbine, as shown in Fig.2.7(b), water with pressure and kinetic energy flow into the pump in the outlet and push the impeller to rotate, power transfers from the impeller to the shaft.



(a) Pump mode

(b) Turbine mode

Fig.2.7 The structure of pumps as turbines [26]

The ability for pumps to operate efficiently in reverse as turbines was first established by Thoma in 1931 while mapping the full operating characteristic of a centrifugal pump [27]. In 1950s and 1960s, PATs were used in pumped storage power plants in developed countries to satisfy the peak power demands. In later years, chemical industries became another area for the application of PATs for energy recovery [28]. It has been proved by experiments that when a pump operates in a turbine mode, its mechanical operation is smooth and quiet; its peak efficiency is same as in pump mode; head and flow at the best efficiency point (BEP) are higher than that in pump mode and the power output is higher than that the pump input power at its best efficiency [29].

### **2.1.3 Turbine selection criteria**

Many factors must be considered in the process of hydro turbine selection, such as various ranges of the head, flow rate, shaft speed and specific speed [30]. Besides, the performance and cost effectiveness should also be considered when choosing a turbine [31].

Water head and flow rate are the key elements when selecting a turbine because these two parameters determine the classification of turbine type. As analyzed in above parts, the Pelton turbine and Turgo turbine are suitable for high water head and low flow rate, while the Propeller turbine and cross-flow turbine may have a good performance under high water flow rate with low water head. The turbine performance is determined on the basis of water head and flow rate, Fig.2.8 shows the operating range of different turbines for a given head and flow rate. The figure can also be used as a reference for selecting the most suitable micro-hydropower turbine type if a certain power output is required.

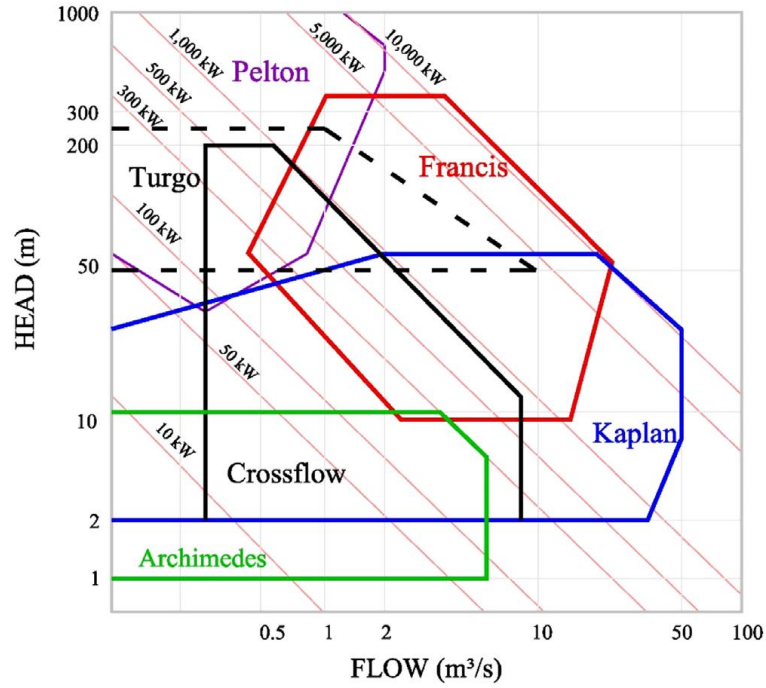


Fig.2.8 The various turbines in terms of head and flow rate [32]

In addition, the performance of a turbine also relies on the ‘specific speed’, which is a dimensionless parameter. The specific speed is determined by the output power of turbine, the rotation speed and water head across it, as in the followed equation [33].

$$N_s = \frac{nP_{shaft}^{0.5}}{H^{1.25}} \quad (2.1)$$

where  $n$  is the rotation speed of turbine, rpm;  $P_{shaft}$  is the shaft power, kW; and  $H$  is the pressure head across the turbine, m.

In this research, the turbine type is determined based on the performance curves of different turbines in Fig.2.8. Based on the above description of commonly used micro turbines and the working conditions inside the water mains, the cross-flow turbine is likely to be a promising device for the followed reasons:

- 1) The cross-flow turbine can operate in a wide range of flow velocity. It can be

seen that in Fig.2.8, the cross-flow turbine works under the flow rate from about  $0.3\text{m}^3/\text{s}$  to  $9\text{m}^3/\text{s}$ . As the water flow rate in urban water mains fluctuates all the time, it is necessary that the inline turbine can operate under a wide flow range.

2) The cross-flow turbine has a stable efficiency in the operating range of flow rate. Fig.2.9 indicates the part flow efficiencies of different turbines. Compared to other types of turbine, the cross-flow turbine has a smaller starting flow rate and its efficiency keeps stable around 80% at the operating flow range.

3) The simple construction of the cross-flow turbine. Most of the water mains are laid underground and it is difficult to maintain the turbines. For application in urban water mains, cross-flow turbine is a promising device because its simple construction, low cost and easy maintenance.

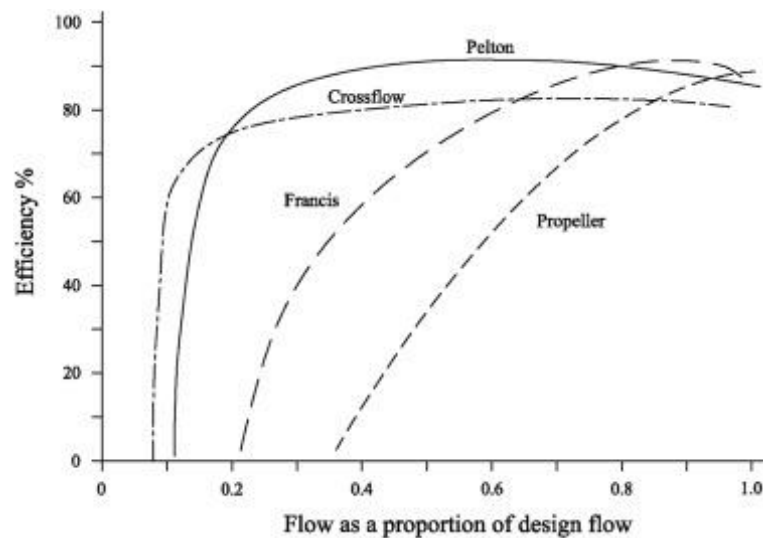


Fig.2.9 Part flow efficiencies of different turbines [32]

## 2.2 Micro hydropower from water supply pipes

### 2.2.1 Inline Francis turbines

Actually, the hydropower potential in water supply pipeline has been noticed for

a long time, but it has not been deeply explored worldwide, the main obstacle to the implementation of the traditional micro hydropower technologies in the water supply mains is the high implementation cost [34]. Some research groups or commercial companies developed hydro turbines that suitable for the water supply pipes.



Fig.2.10 On-site product of the Francis turbine developed by Tanaka[35]

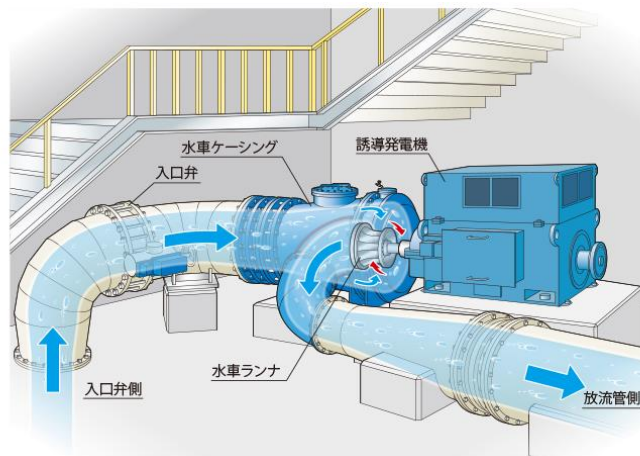


Fig.2.11 Working principle of the Francis turbine developed by Tanaka [35]

In 2005, Tanaka Hydropower Co., LTD in Japan developed an inline Francis turbine which is showed in Fig.2.10 and Fig.2.11. The working ranges of water head and flow rate are 10-80m and 0.15-0.5m<sup>3</sup>/s, separately. And its maximum installation capacity is 200kW [35]. As can be seen in Fig.2.10, this Francis turbine is designed as

pipe insertion type, which makes it easy to be installed and there is no need to change the flow path in water pipes. Fig.2.11 shows the working principle of the inline Francis turbine, which is little different from the traditional Francis turbine. The volute is integrated to the water pipe, water in the pipe is directed by the draft tube and can flow through the runner directly. The structure of this novel Francis turbine is very complex, and a huge space is needed for its installation.

Two micro Francis turbines were developed by Hitachi Industrial Equipment Systems Co., Ltd, as shown in Fig.2.12. The field tests showed that the output power of this micro Francis turbine could be between 2-9kW, the effective water head is 25-40m while the working flow rate is 0.02-0.05 m<sup>3</sup>/s, after calculation, the efficiency is about 40%. These two turbines are similar to traditional Francis turbine and they can be applied in water pipes with small diameters. However, the diameters of urban water mains are usually very large, so these kinds of turbine are not suitable for this project. Besides, due to the small size of the runner and volute, the water head loss through it may be high [36].



(a) 9kW prototype



(b) 3kW prototype

Fig.2.12 Micro Francis turbine developed by Hitachi [37]

### 2.2.2 Inline cross-flow turbines

Except for Francis turbine, the cross-flow turbine also draws attention on power generation in the WSS. In 2007, a micro cross-turbine was designed by SINFONIA Technology Co., Ltd [38] which is shown in Fig.2.13. This turbine is a very compact cross-flow turbine integrated with a permanent magnet generator with the output of about 1 kW, its working water head is between 0.5-10m, working flow rate is about  $0.004\text{-}0.01\text{m}^3/\text{s}$  and the expected output power is 10-1000W. However, this kind of turbine is not available for this project either. Firstly, to use the cross-flow turbine, the flow path in water pipe has to be changed, which increases the installation cost significantly. Secondly, this cross-flow turbine is preferable to be installed in open environment and the output water flow may have no more water head, which is not allowed in the water mains.

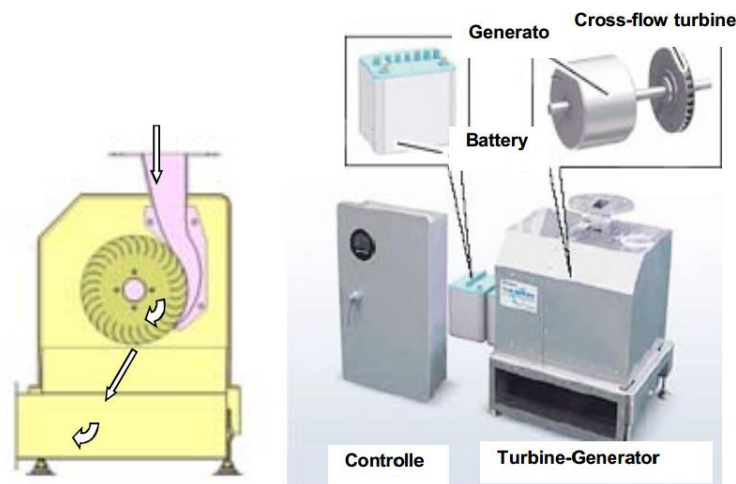
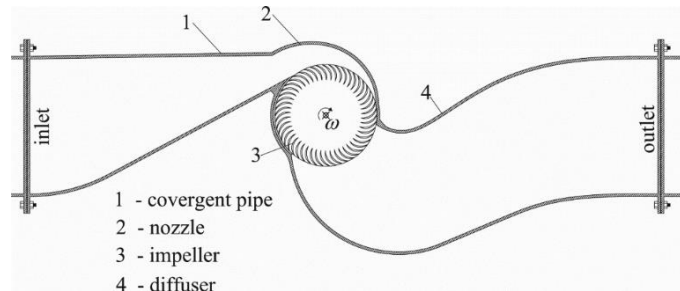


Fig.2.13 Micro cross-flow turbine for water pipes [38]

A novel cross-flow turbine which has a simple geometry and stable efficiency in a wide flow rate range was developed by Vincenzo Sammartano by experimental method [39]. In this cross-flow turbine, rotational velocity adaptation is used to improve the turbine efficiency under off-design conditions. The experimental results

showed that the efficiency of the developed turbine is more than 65% at the flow rate from 32-144m<sup>3</sup>/h. However, the water head reduction through the turbine is far beyond the requirement of this project. For example, at the flow rate of 144 m<sup>3</sup>/h, the water head loss is more than 20m.



(a) Working principle



(b) Prototype

Fig.2.14 Micro cross-flow turbine developed by Vincenzo Sammartano [39]

### 2.2.3 PAT for inline application

As introduced before, traditional centrifugal pump can be used inverse to operate as turbine. Due to the easy access and relative low investment costs, The PATs present advantages for using in micro hydropower plants (5–100kW) either as pump or as turbine [40]. Furthermore, based on the research of Ramosetal [41], it is possible to use pumps as turbines with relatively higher efficiency (up to 85%). So, hydropower generation using the PATs in the WSS has attracted increasing attention in the past

decades.

Garcia et al suggested that in the main pipe of WSS, the maximum installation capacity could reach 100kW by using PATs [42]. At Breech in Germany, eight pumps are employed in the electricity recovery system to reduce the pipeline pressure along with generation of electricity (Fig.2.15), as these pumps are simultaneously used as turbines for energy recovery [26]. The total installed capacity was 300 kW and the electricity was fed into the grid of the local energy provider by the Regional Water Association. In 1996, a PAT was installed in the water supply system of Blackpool in England [43], the PAT caused 30m water head drop and generated 3.5 kW electricity. The installation of PAT was carried out by tapping into the main pipeline without draining the system. This added the cost, but avoided an interruption of water supply to consumers. Even so, the cost of the plant, approximately \$30,000, was much less than the proposed connection to the regional electricity company's supply, and represents a worthwhile investment for the water company.



Fig.2.15 PAT installation in the pumping station at Breech, Germany [26]

Fontana et al. investigated the water distribution system in one district of Naples to assess the energy potential of hydropower generation using the PATs (as shown in

Fig.2.16) [44]. In this research, a numerical model based on genetic algorithms was firstly developed to determine the optimal PRVs locations in the water distribution system for better water pressure control. After that, all or some of the PRVs were replaced by the PATs for power generation, results showed that although do not have a fine regulation of water head, the PATs did achieve a good balance between hydropower recovery and water head reduction. In the three cases of this research, all the PATs have better performance in loss reduction than that of PRVs. Besides, the generated power of the PATs could be as high as about 2000kWh/day totally, which proved that the application of PATs in the WSS is a promising way for electricity generation as well as water head reduction.

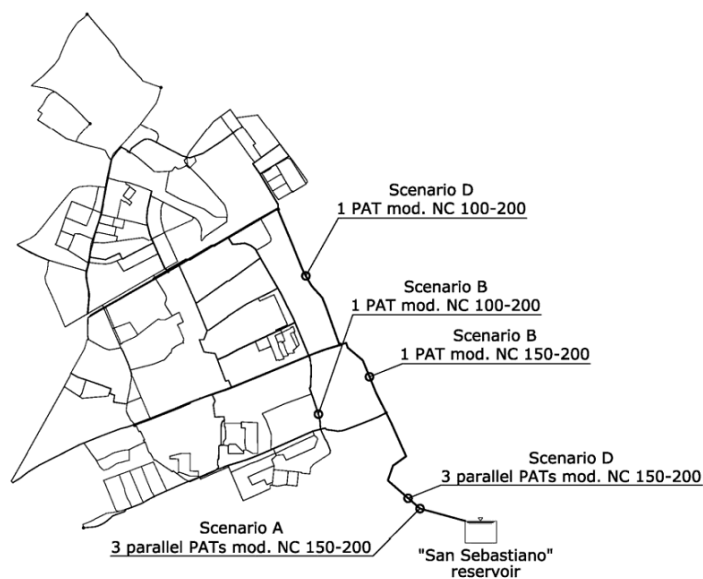


Fig.2.16 Sketch of locations of PATs in water distribution system [44]

In the research of Fecarotta et al., a multistage pump for WSS application was studied in numerical and experimental ways [45]. The results showed that the performance of a PAT was very different from that of a PRV. For a PRV, the water head reduction could be adjusted by changing its opening degree. As to a PAT, due to the fixed geometrical characteristics and inner flow space, its performance on water

pressure reduction was easily affected by the variation of flow rates. In order to solve this problem, A. Carravetta et al designed a PAT installation scheme, in which a bypass and two regulating valves were adopted to cooperate with the PAT to adjust the water head and flow rate through the PAT (As shown in Fig.2.17) [46]. If the regulation is performed only by valves, the series valve dissipates the surplus head while the valve in the parallel branch can bypass a part of the discharge, in order to move the available operating flow rates and water head reductions onto the characteristic curve of the PAT. For an available head higher than the head-drop deliverable by the machine, the valve in series (A) dissipates the excess pressure. Instead, when the discharge is larger, the PAT would produce a head-drop higher than the available head: in this case the bypass (B valve) is opened to reduce the discharge flowing in the PAT. Conversely, if the PAT is regulated only by the inverter, the rotational speed is modified to move the characteristic curve of the machine, matching the required values of discharge and head. In this way the working condition of PAT could stay around its best efficiency point and the water pressure reduction was also ensured. Relevant cost-benefit analysis of this PAT installation scheme was tested on a water pipe network, results showed that the proposed installation scheme was economically acceptable and had little impact on the reliability of pipe networks [47].

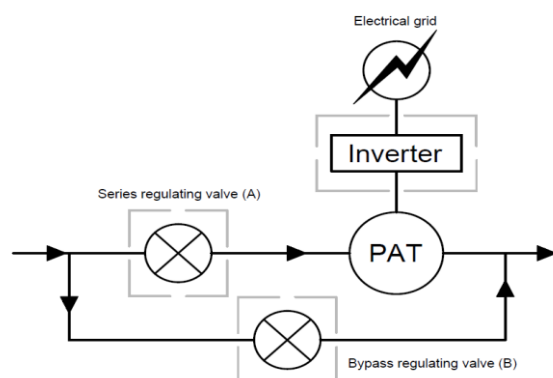


Fig.2.17 Installation scheme of PAT and valves [45]

However, Alatorre-Frenk reported that, in the domain of pumps where impulse principle does not work, very low specific speeds can only be achieved by using multistage pumps. They can be used as turbines, but their cost advantage over impulse turbines may be offset by the high cost of multistage pumps compared to that of single-stage pumps. Also, multistage pumps might be costlier compared with small Pelton, Turgo and cross-flow turbines, which can be fabricated in local workshops. Moreover, multistage pumps have higher maintenance costs especially for bearings and seals than Pelton turbines [48].

#### **2.2.4 Lift-type turbine**

A novel lift-type water turbine was developed by Lucid Energy for application in water mains. Fig.2.18 shows the main structure of the lift-type turbine which has been installed in the water pipes of Portland. It is reported that the newly developed energy harvesting system can supply power to an individual building like a school or a library [49]. However, this system is only developed for the pipelines which is bigger than 600mm.

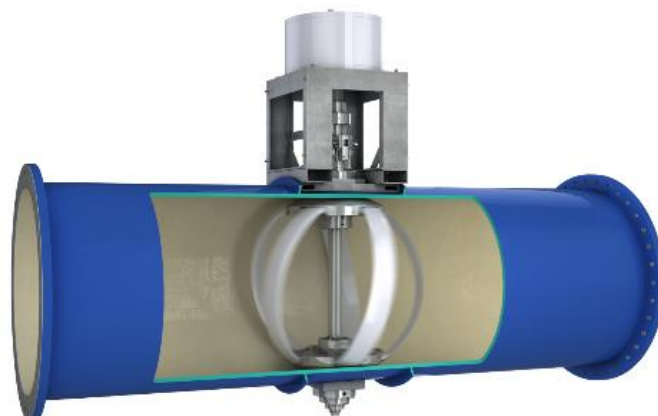


Fig.2.18 Lift-type turbine developed by Lucid Energy [50]

### 2.2.5 Other inline turbines

Regardless of traditional water turbines, some researchers focus their attention on the development of novel turbines. Chen et al. [51] designed a novel vertical axis water turbine for hydropower harvesting in DN100 water pipelines in numerical and experimental ways. The inline hydroelectric generator unit is developed under the demand that the turbine should be inserted in the conduit. The physical diagram is shown in Fig.2.19. This kind of turbine has the advantage of easy installation and less occupancy. But it can only be used in water pipes with small diameter.

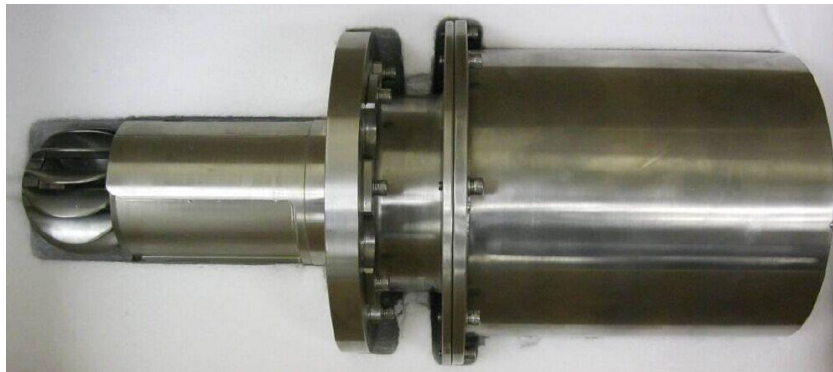


Fig.2.19 DN100 inline hydropower generator unit

Hoffmann [52] developed a radial-flux energy harvester incorporating a three-phase generator for converting energy from water flow in domestic water pipelines, as shown in Fig.2.20. The energy harvester together with a power management circuit and energy storage is used to power a smart metering system installed underground making it independent from external power supplies or depleting batteries. The energy harvester is able to generate up to 720 mW when using a flow rate of 20 l/min (fully opened water tap). A minimum flow rate of 3 l/min is required to get the harvester started. In this case a power output of 2 mW is achievable.

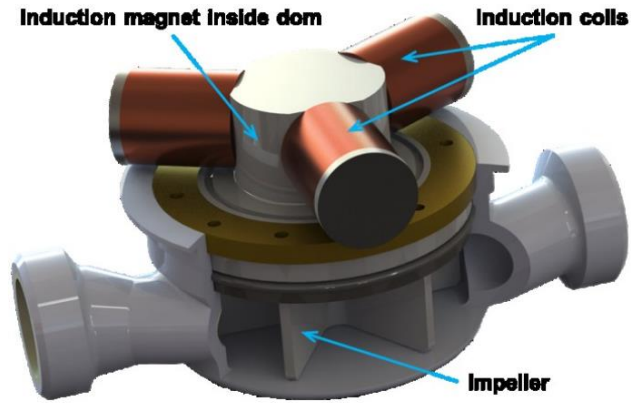


Fig.2.20 Radial-flux energy harvester

Hao et al. [53]. developed a self-powered smart flow meter cooperated with a novel water turbine and it is indicated in Fig.2.21. In this system, a new attempt and simple approach was developed to successfully extract a portion of the kinetic energy from the fluid/air, store it in a capacitor and used it efficiently. Feasibility was demonstrated through repeated experiments: for air flowing in an 11mm diameter pipe, 18 s of energy harvesting at 10 revolution-per-second turbine speeds generated enough power for the flowmeter to operate for 720 s with a flowrate of 20 revolution-per-second, without battery or any external power.

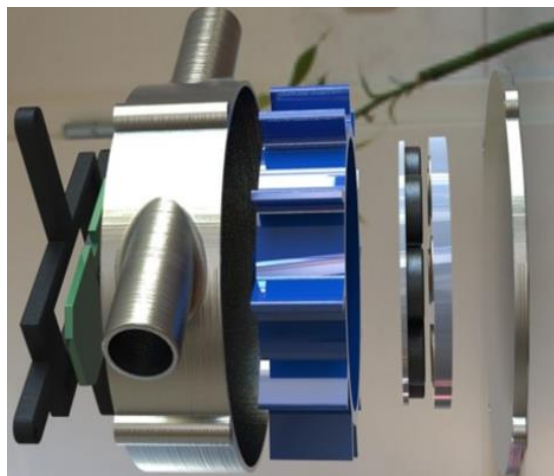


Fig.2.21 Battery-free smart flowmeter

These two super-micro hydro turbines are designed integrates with generator and flow meters, so they are very compact. However, this kind of turbine is too small to be used in water supply pipeline, which usually has a relatively large diameter.

### 2.3 Research on cross-flow turbines

Cross-flow turbine is a kind of impulse turbine which was first invented by Michell in 1904 [54]. Since then, lots of research has been done for the design method and performance enhancement of cross-flow turbine. As research on the cross-flow turbine used in water pipes is still rare, there has not been a systematic design method for inline cross-flow turbine yet. The literature review of conventional cross-flow turbine research will provide inspiration for this research. The performance of cross-flow turbine is significantly affected by its geometry and many researchers investigated the influence of different geometrical parameter on turbine performance by numerical and experimental methods. In this part, a literature review of the research about the effects of different geometrical parameters on the performance of cross-flow turbine is presented.

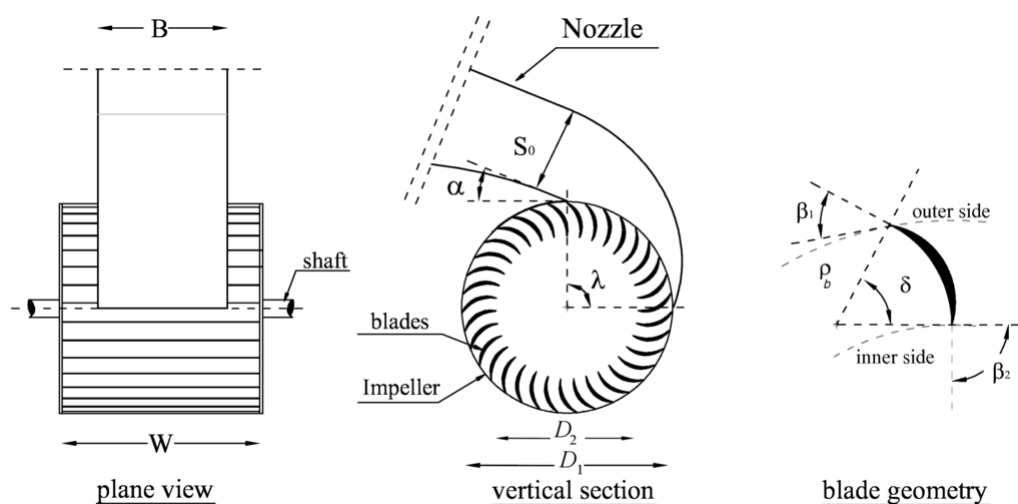


Fig.2.22 Main geometrical parameters of the traditional cross-flow turbine [55]

Table 2.1 Definition of different geometrical parameters

Components	Symbol	Definition
Nozzle	$B$	Nozzle width
	$S_0$	Nozzle throat width
Impeller	$W$	Impeller Width
	$\alpha$	Attack angle
	$\lambda$	Impeller inlet arc angle
	$D_1$	Impeller outer diameter
	$D_2$	Impeller inner diameter
Blades	$\beta_1$	Blades outer angle
	$\beta_2$	Blades inner angle
	$\rho_b$	Blades Radius
	$\delta$	Blades curve angle

Cross-flow turbines are widely used in micro hydropower projects due to their simple structure and easy maintenance. Fig.2.22 shows the main geometrical parameters of the traditional cross-flow turbine while Table 2.1 indicates the definition of different symbols. Among them, the attack angle  $\alpha$  means the angle between the flow attack direction and the tangent direction of the impeller at the impeller inlet. Blades outer angle  $\beta_1$  is the angle between the flow direction and the tangent direction of impeller outer diameter while blades inner angle  $\beta_2$  means the angle between the flow direction and the tangent direction of impeller inner diameter. Impeller inlet arc angle  $\lambda$  means the available discharge arc along the impeller outer diameter.

### 2.3.1 Effects of nozzle shape

In conventional cross-flow turbine, a nozzle is often located on the upstream side of the runner to accelerate the water flow and direct it to the runner. Large amount of research has been done by numerical or experimental methods for nozzle design and optimization to improve the overall turbine performance.

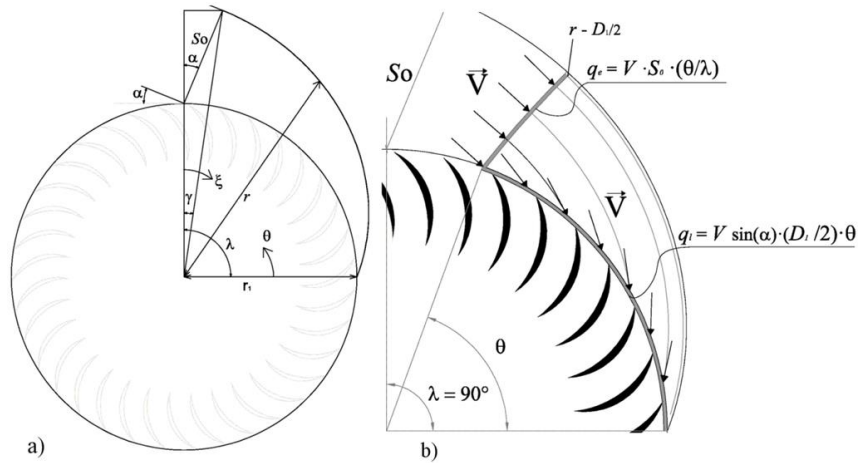


Fig.2.23 Nozzle shape design method developed by Sammartano V: (a) Geometrical profile; (b) Principle of the design method [54]

Sammartano et al. [54] proposed a nozzle design method by assuming a linear variation of the nozzle inner wall radius  $r$  with the angle  $\theta$  (as shown in Fig.2.23 (a)) to obtain an approximately constant attack angle along the impeller inlet. As shown in Fig.2.23 (b), the aim of this design method is to ensure that the mass flow rate through a cross-section of the nozzle is equal to mass flow rate entering the impeller through the inlet arc that from the cross-section to the terminal of the impeller inlet, that is

$$q_l = q_e = (V \sin \alpha) \frac{D_1}{2} \theta = V_r \frac{D_1}{2} \theta \quad (2.2)$$

where  $q_l$  is the mass flow rate through the cross-section of the nozzle,  $\text{m}^3/\text{s}$ ;  $q_e$  is the

mass flow rate entering the impeller through the inlet arc,  $m^3/s$ ;  $V$  is the flow velocity which is assumed constant in the nozzle,  $m/s$ ;  $V_r$  is the radial velocity,  $m/s$ .

Numerical results indicated that the attack angle and velocity inside the nozzle can keep stable along the impeller inlet arc angle, which means the proposed could achieve the design aim very well.

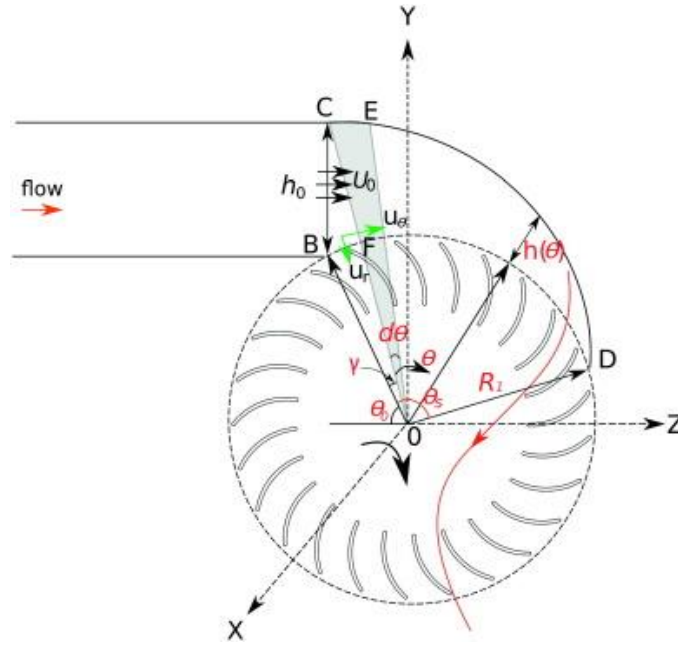


Fig.2.24 Nozzle shape design method developed by Adhikari et al. [56]

Adhikari et al. [56] developed a two-dimensional analytical model for the nozzle design of cross-flow turbines by theoretical and numerical methods. The analytical model is proposed based on fluid continuity and energy conservation. As shown in Fig.2.24,  $u_r$  and  $u_\theta$  are the radial and tangential velocities, respectively. According to fluid continuity, the variation of mass flow rate in radial direction should be equal to that in tangential direction:

$$r u_r d\theta = -h(\theta + d\theta) u_\theta(\theta + d\theta) + h(\theta) u_\theta(\theta) \quad (2.3)$$

where  $u_r$  is the radial velocity at the runner inlet,  $m/s$ ;  $u_\theta$  is the tangential velocity at

the runner inlet, m/s;  $h(\theta)$  means the width between the nozzle and impeller inlet arc, m.

By Integrating Eq.2.3, the expression of  $h(\theta)$  can be obtained. With the proposed analytical model, the authors re-designed one existing 7kW cross-turbine and studied the turbine's performance using numerical method. The results showed that the maximum efficiency increased from 69% to 87% only by redesigning the nozzle shape.

In addition to theoretical method for nozzle design, many researchers studied the effects of nozzle geometry on turbine performance by numerical methods. By varying the nozzle geometries, different models can be obtained and simulated to determine the optimal model. Acharya et al. [57] investigated the performance of seven cross-flow turbines with different nozzle shape (as shown in Fig.2.25) numerically. The results indicated that turbine efficiency increase from 63.67% to 67.26% by varying the nozzle edge radius.

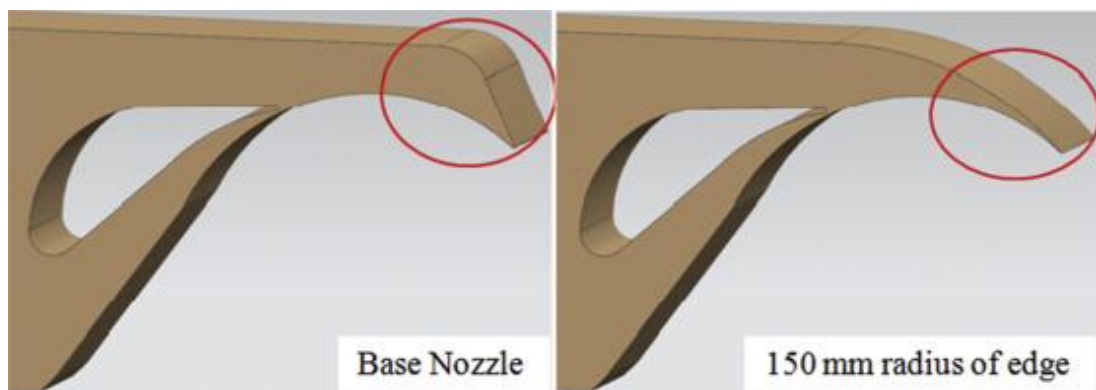


Fig.2.25 Numerical study on effects of nozzle shape on turbine performance by Acharya et al. [57]

Although research on cross-flow turbine used in water pipes is still rare, some cross-flow turbines are developed for application in water tunnels, in which the working situation is similar to that in water pipes. When applied in water pipes or water

tunnels, the configuration of cross-flow turbine must be modified as the turbine is used submerged and the water flow will exert negative torque on the returning blades, resulting in a bad influence on the turbine performance [58]. Many investigators enhanced the performance of submerged cross-flow turbines in water tunnel by placing ducted or augmented elements around the impeller to increase flow velocity and pressure difference and shield the flow towards the returning blades. Prasad et al. [59] investigated the performance characteristics of a cross-flow tidal turbine by numerical and experimental methods. Fig.2.26 shows the developed cross-flow turbine and its test rig. The flow characteristics and power output of the turbine was studied in a numerical water tank, and the maximum efficiency is recorded 55% with 14W power generated.

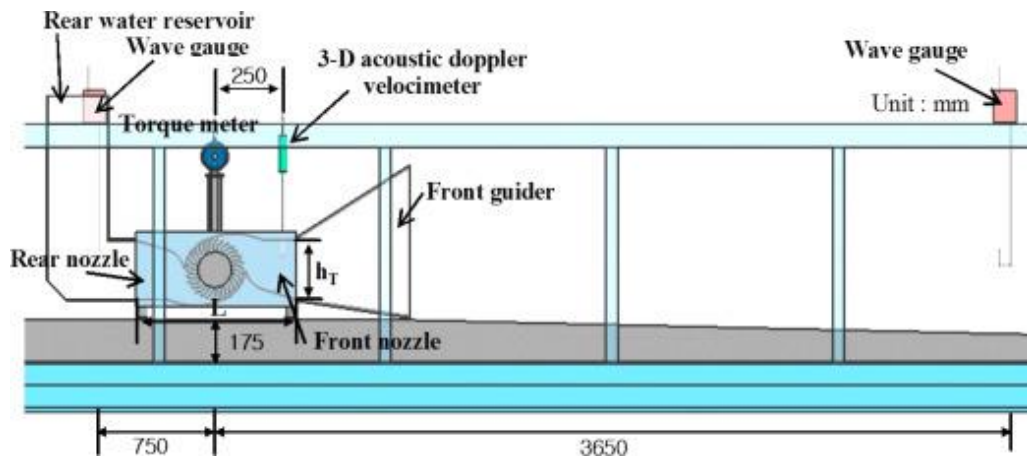


Fig.2.26 Cross-flow tidal turbine developed by Prasad et al. [59]

Elbatran et al. [60] designed a cross-flow turbine with dual directed nozzles used in channels. Fig.2.27 indicates the main structure of the developed turbine which contains two parallel cross-flow runners surrounded by dual directed nozzles. The simulation results indicated that the nozzles can increase flow velocity inside the channel and the turbine has a maximum efficiency of 52%.

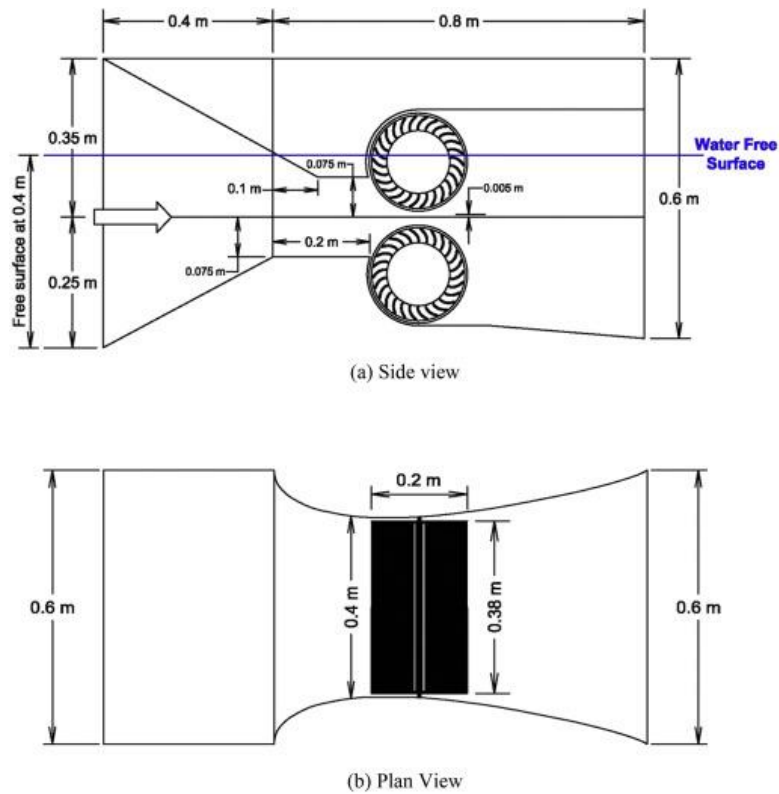


Fig.2.27 Dual-nozzle cross-flow turbine developed by Elbatran et al. [60]

In conclusion, when the cross-flow turbine is used submerged, the nozzle has two main functions. Firstly, the nozzle is used to direct more water to flow through the impeller and increase flow velocity. Besides, the nozzle is also used to cover the returning blades so that the water flow will not exert negative torque on them.

### 2.3.2 Effects of runner inlet arc angle

The influence of runner inlet arc angle on the efficiency of cross-flow turbine has been investigated by many investigators. In the research of Fukutomi et al. [61], four models with runner inlet arc angles of  $30^\circ$ ,  $60^\circ$ ,  $90^\circ$  and  $120^\circ$  were studied using experimental methods. The results showed that a bigger runner inlet arc angle can lead to a higher value of pressure distribution along the runner inlet arc. The experimental study of Fiuzat and Akerkar [62] indicated a cross-flow turbine with  $90^\circ$  runner inlet arc angle has a better performance than that with  $120^\circ$  runner inlet arc angle because

more cross-flow exists in the runner of  $90^\circ$  runner inlet arc angle, which leads to a higher efficiency. Besides, the  $90^\circ$  runner inlet arc angle can improve the power output of the runner second stage. Based on the experimental results, the second stage of turbine with  $90^\circ$  runner inlet arc angle contributes 45% of its total output power, but for turbine with  $120^\circ$  runner inlet arc angle, the ratio is 41%. In the research of Chen et al. [63], a two-dimensional model of cross-flow turbine (as shown in Fig.2.28) was built and simulated to study the effects of runner inlet arc angle on turbine efficiency flow velocity in draft tube. The results inferred that the flow velocity increases with the reduction of runner inlet arc angle. The maximum efficiency occurs when the runner inlet arc angle is  $93^\circ$ . Besides, the research of Chen Z, et al. also indicated that when runner inlet arc angle reduces, the output power at Stages 1 and 2 increases, which is similar to the research results of Fiuzat and Akerkar [62]. In the research of Khosrowpanah et al. [64], experimental study was done to compare the performance of cross-flow turbine when the runner inlet arc angle increases from  $58^\circ$  to  $90^\circ$ , results indicated that a smaller runner inlet arc angle results in a higher head at the nozzle tip but a lower efficiency of the turbine. The recorded maximum turbine efficiency of the investigation is 80% when the runner inlet arc angle equals to  $90^\circ$ .

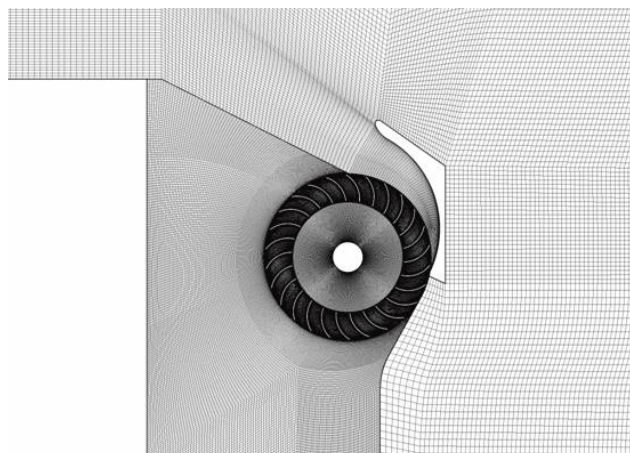


Fig.2.28 2D model of cross-flow turbine in the research of Chen, et al. [63]

### 2.3.3 Effects of attack angle and blades outer angle

The attack angle is a key geometrical parameter that affecting the cross-flow turbine performance. A suitable attack angle can reduce flow separation in blades passages and decrease hydraulic loss at runner inlet arc, thus improve the total performance of the cross-flow turbine [20]. Mockmore and Merryfield [65] investigated the efficiency of cross-flow turbine theoretically and suggested the relationship of attack angle and blades outer angle as:

$$\tan \beta_1 = 2 \tan \alpha \quad (2.4)$$

where  $\beta_1$  is the blades outer angle and  $\alpha$  is the attack angle.

To achieve the highest mechanical efficiency, Mockmore and Merryfield [65] suggested that the attack angle should be  $16^\circ$  and the corresponding blades outer angle is about  $30^\circ$ . An experimental and numerical study was conducted by Katayama et al. [66], four prototypes with different blades outer angle were manufactured and tested. The blades outer angles of the four prototypes are  $21^\circ$ ,  $24^\circ$ ,  $27^\circ$  and  $30^\circ$ , respectively. The experimental results indicated that when blades outer angle equals to  $30^\circ$ , the turbine has the maximum efficiency. After that, numerical study was performed to investigate the effects of blades outer angle on turbine power output. It was found that with the increase of blades outer angle, the output power ratio of the runner first stage increases while that of the runner second stage reduces. It is reported in the thesis of Desai [67] that the maximum efficiency of the cross-flow turbine increases with the decrease of attack angle in the range from  $22^\circ$  to  $32^\circ$  and it is recommended the attack angle is  $22^\circ$ . Similar results were obtained from the research of Totapally and Aziz

[68]. Choi et al. investigated the impact of blades shape on the performance and inner flow characteristics of cross-flow turbine by using CFD method [69]. The results showed that when the attack angle decrease from  $35^\circ$  to  $25^\circ$ , the maximum turbine efficiency increases from 60% to 80%. In the domain of cross-flow turbine design, an attack angle value of  $22^\circ$  is widely accepted [54] [70], the corresponding blades outer angle according to Eq.2.3 is  $39^\circ$ .

#### **2.3.4 Effects of blades inner angle**

The blades inner angle is exit flow angle on the runner first stage but also the inlet flow angle on the runner second stage. Mockmore and Merryfield [65] suggested that the optimal value of blades inner angle is  $90^\circ$  so that the shock loss between runner first and second stage can be reduced. When blades inner angle equals to  $90^\circ$ , water flow leaves the runner first stage in radial direction to relative outlet velocity inside the impeller at the inner diameter, so only the energy of the rotating system left to the fluid and the energy can be recovered in the runner second stage [54].

In the research of Adhikari [20], the author compared the performance of two cross-flow turbines with blades inner angle equals to  $90^\circ$  and  $85^\circ$  respectively by numerical method. It was observed that when blades inner angle reduced from  $90^\circ$  to  $85^\circ$ , the turbine efficiency decreased from 88% to 83%. Fig.2.29 shows the effects of blades inner angle on power output of each runner stage obtained by Adhikari [20]. It can be seen in Fig.2.29 that the blades inner angle has little influence on the performance of runner first stage, however, the power production of runner second stage decreases significantly when the blades inner angle reduces. The main reason for this phenomenon is that the flow direction is misaligned with the blades at the inlet of

runner second stage. As suggested by many researchers,  $90^\circ$  is nearly the optimal value of blades inner angle [20][54][65].

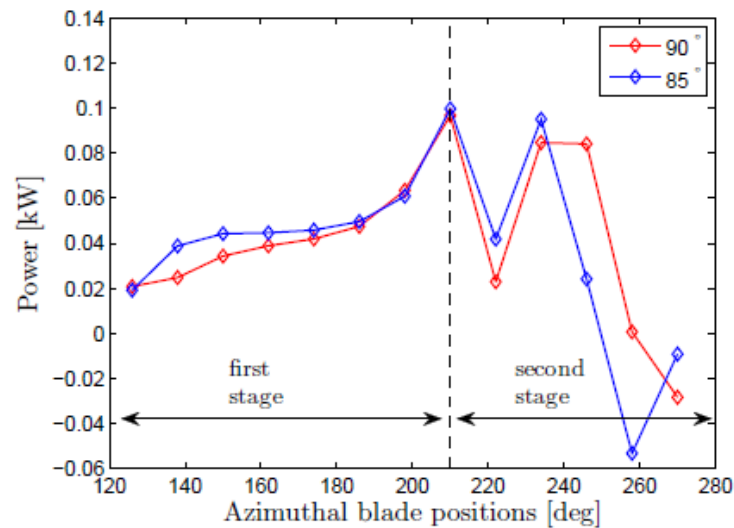


Fig.2.29 Effects of blades inner angle on power output of each runner stage [20]

### 2.3.5 Effects of runner diameter ratio

The ratio between runner inner and out diameter, that is  $D_2/D_1$ , also has an impact on the turbine performance. A bigger runner diameter ratio means a shorter blades length and a bigger curvature of the blades because the blades angle must shift from  $\beta_1$  to  $\beta_2$ , resulting in stronger turbulence. However, a smaller runner diameter ratio corresponds to a longer blades length but a smaller cross-flow region in the runner.

Akerkar [71] considered second stage losses and proposed a value of 0.68 for the diameter ratio. Aziz and Desai [72] examined the effect of diameter ratio experimentally and concluded that a diameter ratio of 0.68 is better than either of the ratios 0.75 and 0.60. Adhikari [20] studied the influencing mechanism of runner diameter ratio on cross-flow turbine performance by numerical method. In the research, three models with runner diameter ratio of 0.64, 0.68 and 0.72 were built and simulated. The results indicated that the maximum efficiency of models with runner diameter

ratio of 0.68 and 0.72 is 88% and 83%, respectively, however, when the ratio reduced from 0.68 to 0.64, the efficiency difference was very slight. Fig.2.30 shows the effects of runner diameter ratio on power output of each runner stage obtained by Adhikari [20]. When runner diameter ratio decreases from 0.72 to 0.68, power output of first runner stage reduces significantly, although the second stage produces more power, the overall turbine efficiency reduces. The power output of model with  $D_2/D_1=0.64$  is similar to that of the model with  $D_2/D_1=0.68$ , which indicate that the optimal value of runner diameter ratio exists between 0.64 and 0.68, but the efficiency variation in the range is very small. Considering the former research,  $D_2/D_1=0.68$  is suggested as the optimal value for runner diameter ratio.

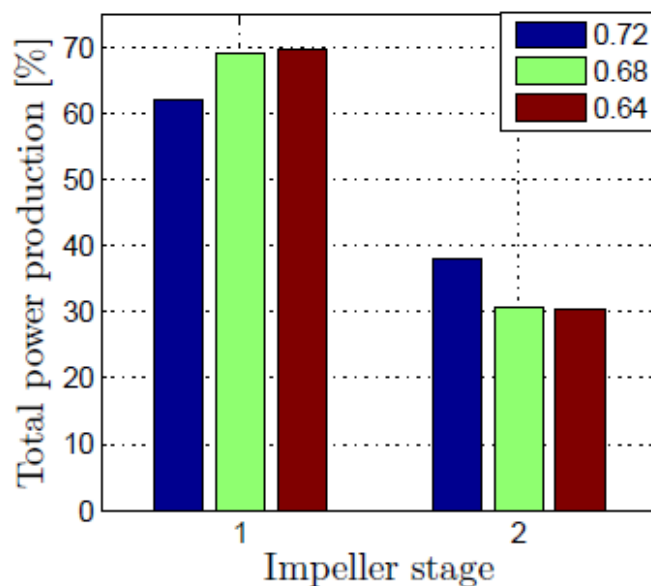


Fig.2.30 Effects of diameter ratio on power output of each runner stage [20]

### 2.3.6 Effects of blades number

The number of blades ( $N_b$ ) is another factor affecting the fluid dynamics, flow separation and power extraction inside the runner. Sammartano [54] numerically studied the effects of blades number on the performance of a 5kW cross-flow turbine

and found the optimal blades number is 35. In the research of Acharya et al. [57], the blades number of a 7kW cross-flow turbine model is varied from 16 to 32, the recorded maximum efficiency is 76.6% when blades number equals to 22. In the research of Khosrowpanah et al. [64], the performance of several models with blades number of 10, 15 and 20 were obtained using experimental method. The experimental results showed that the maximum efficiency was observed 70% when blades number was 15. Besides, with the increase of blades number, the water head loss through the turbine also increases. In the research of Choi et al. [69], a maximum efficiency around 66% was obtained in the case of a model with 26 blades. Adhikari [20] conducted an in-depth numerical study on the influence of blades number on cross-flow turbine performance. It was found that with the increase of blades number, flow separations in blades passages were reduced and more power was produced. However, when the blades number exceeded the optimal value, the growth of boundary layer thickness may cause blockage in the blades passages, resulting in turbine efficiency reduction. It was observed that for the studied 0.53kW cross-flow turbine, the maximum efficiency could reach about 90% when  $N_b=35$ .

Usually, for different working conditions, the geometrical parameters of cross-flow turbine such as nozzle shape, attack angle, blades outer angle, etc. are determined mainly based on available experimental or numerical results. However, due to the large range of possible operating conditions, it is still far away to have a standard design method for cross-flow turbines.

## **2.4 Review of research methodology**

In the previous studies on cross-flow turbine, three main methods were adopted: theoretical analysis, experimental methods and numerical methods. This part presents

a brief review of the methods to provide guidance for the current research.

#### 2.4.1 Theoretical analysis

The main aim of theoretical analysis is to obtain an expression of the turbine efficiency and thus derive the effects of different parameters on the turbine efficiency. Mockmore and Merryfield [65] deduced an equation of the cross-flow efficiency assuming no losses written as:

$$\eta = 4 \frac{u_1}{V_1} \left( \cos \alpha - \frac{u_1}{V_1} \right) \quad (2.5)$$

where  $u_1$  is the peripheral velocity at runner inlet;  $V_1$  is the absolute flow velocity and  $\alpha$  is the flow attack angle.

Furthermore, the maximum efficiency of cross-flow turbine was derived as:

$$\eta_{\max} = 0.5C^2(1+\psi)\cos^2 \alpha \quad (2.6)$$

where  $C$  is the coefficient dependent on the nozzle,  $\psi$  is ratio of the relative velocities at the runner first stage inlet and second stage exit.

Assuming  $C=0.98$  and  $\psi=0.98$ , the maximum efficiency obtained from the research of Mockmore and Merryfield is 87.8%. Other researchers also used theoretical analysis method to redesign the nozzle shape for turbine performance improvement, and this part of research has been described in Part 2.3.1.

## 2.4.2 Experimental method

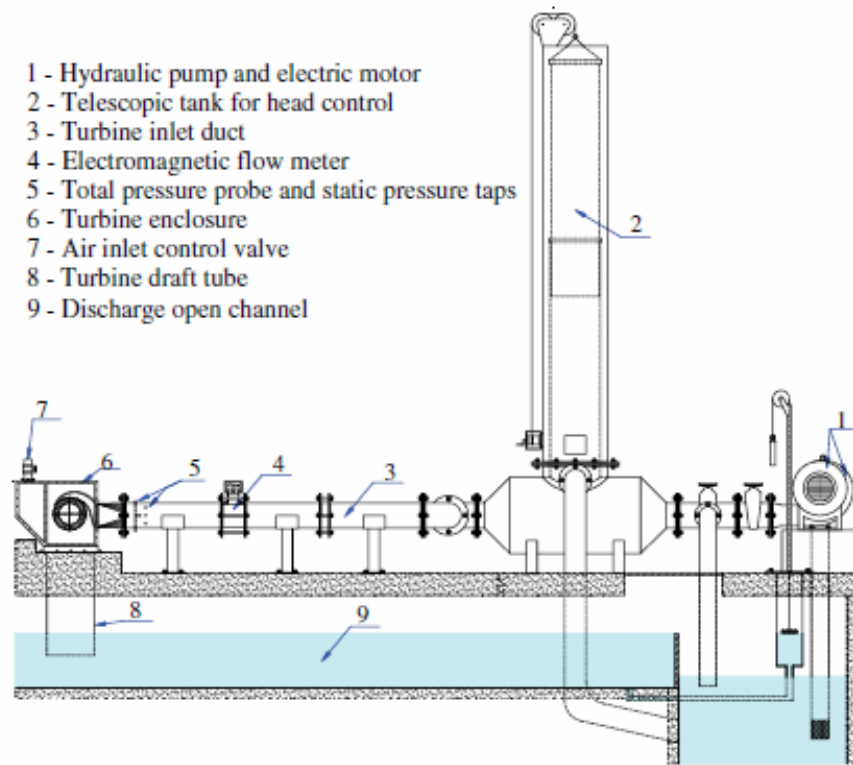


Fig.2.31 A hydraulic test rig developed by Pereira et al. [73]

Experimental research of cross-flow turbine mainly focused on the effects of geometrical parameters, working conditions and runner speed on turbine efficiency, but no information about experimental measurements about the internal flow characteristics is available in the current literatures. Fig.2.31 shows a typical hydraulic test rig developed by Pereira et al. [73] for experimental study of cross-flow turbine. A hydraulic pump is used to provide water flow to the test rig and a telescope tank is used for water head control, in this way the turbine prototype can be tested under its working conditions. Meanwhile, the electromagnetic flow meter and pressure probe are used for the measure of flow rate and water head, respectively. The main setup and turbine parameters of previous experimental research are summarized in Table 2.2.

Table 2.2 Summary of experimental studies on cross-flow turbines

Researcher	$\lambda$	$\alpha$	$\beta_1$	$\beta_2$	$D_2/D_1$	$N_b$	$\eta_{max}$
Macmore and Merryeld [65]	N/A	16°	30°	90°	0.66	20	68%
Sammartano et al. [39]	N/A	15°	N/A	90°	0.75	40	74.6%
Totapally and Aziz [68]	55°	22°	39°	90°	0.68	35	90%
Khosrowpanah et al. [65]	90°	16°	39°	90°	0.68	15	80%
Pereira and Borges [73]	80°	13°	15°	90°	0.67	30	84.8%
Sammartano [74]	90°	22°	39°	90°	0.68	35	82.1%
Hothersall [75]	N/A	16°	N/A	N/A	0.66	21	75%
Desai [67]	90°	22°	39°	90°	0.68	30	90%

### 2.4.3 Numerical method

Although the experimental method can be used to directly measure the power output and water head loss of cross-flow turbine with different geometrical parameters, it is very expensive to measure the internal flow characteristics of the turbine. With the development of computing technologies, the numerical simulation methods have been widely used as powerful and promising tools to investigate the influence of different geometrical parameters on internal flow characteristics, so an in-depth understanding of the influencing mechanism can be obtained. Previous numerical studies on cross-flow turbine are mainly CFD simulations adopting Reynolds averaged Navier–Stokes (RANS) equations with appropriate turbulence models for turbine performance prediction and flow analysis. In the simulation process, the mesh type,

turbulence model, boundary conditions, solver setup can have effects on the results. Therefore, it is necessary to review the previous numerical research for guidance to the current study. The main setup and findings of previous numerical research are summarized in Table 2.3.

Table 2.3 Summary of numerical studies on cross-flow turbines

Researcher	Model type	Mesh type	Mesh number	Turbulence model	Boundary conditions	Findings
Choi et al. [69]	2D	Hexahedral grids	2 million	$k-\omega$ SST	Pressure inlet; Outflow outlet;	The nozzle shape, blades outer angle and blades number have significant effects on the performance and flow characteristics of cross-flow turbine. Among these parameters, the nozzle has the largest effect.
Sammartano et al. [54]	2D	Tetrahedral prismatic grids	0.1 million	$k-\varepsilon$	Pressure inlet; Pressure outlet; Transient rotor stator interface	A linear nozzle can ensure almost uniform flow velocity and attack angle in the nozzle. Besides, the effects of blades number and diameter ratio on turbine performance is little.
	3D	Tetrahedral prismatic grids	3.3 million	$k-\varepsilon$		The 3D simulation indicated that the optimal ratio runner width and nozzle width is 1.
Chen et al. [51]	2D	Hexahedral grids	0.45 million	$k-\omega$ SST	Velocity inlet; Velocity outlet; No-slip wall; Transient rotor stator interface	Firstly, the improvement of nozzle shape in this research leads to an efficiency increase of 12.5%. Besides, the guide nozzle can suppress the negative torque. Thirdly, an improvement of nozzle inlet shape can reduce flow separation in the nozzle.
Adhikari et al. [56]	3D	Unstructured tetrahedral grids	5.4 million	$k-\omega$ SST	Pressure inlet; Velocity outlet; general grid interface;	The improvement of the nozzle shape can convert more water head into kinetic energy and reduce flow separation in the blades passages at runner first stage.
Kim et al. [76]	3D	Hexahedral grids	5.2 million	$k-\omega$ SST	Velocity inlet; Pressure outlet; No-slip wall	The research is about an improvement of a cross-flow turbine used in water channel for tidal power generation. It was found that by using a larger channel area of the turbine, the flow velocity through the runner increases.

Researcher	Model type	Mesh type	Mesh number	Turbulence model	Boundary conditions	Findings
De Andrade et al. [77]	3D	Unstructured tetrahedral grids	2.6 million	$k-\varepsilon$	Velocity inlet; pressure outlet; No-slip wall	The flow attack angle along the runner inlet arc varies from $23^\circ$ to $7^\circ$ . The simulation indicated that nearly 68.5% of the total power is produced by the first runner stage.
Acharya et al. [57]	3D	Unstructured tetrahedral grids	5.1 million	$k-\omega$ SST	Pressure inlet; Outflow outlet	The results indicated that the nozzle shape, guide vane opening degree and blades number have effects on the cross-flow turbine performance. The optimal opening degree of guide vane is $7^\circ$ while the optimal blades number is 22. The simulated maximum efficiency of the cross-flow turbine is 76.6%.
Popescu et al. [78]	2D	N/A	N/A	$k-\omega$ SST	Velocity inlet; pressure outlet;	The uncontrolled flow domain in the internal region of the runner may results in turbine efficiency decrease. It is suggested to adopt internal guiding device to reduce the recirculation phenomena and eliminate shock losses caused by the uncontrolled flow.
Dragomirescu & Schiaua [79]	2D	Structured and quadrilateral unstructured grids	0.8 million	Reynolds Stress Model	Velocity inlet; pressure outlet; Sliding mesh	When the water head drops sharply, the flow attack angle is high, resulting in air pockets behind the blades at the first runner stage. With the increase of runner speed, the air packets size also increases, which reduces the power production at the first runner stage. In this study, the best turbine efficiency is about 55%.

## 2.5 Research gap and methodology

The literature review has indicated that the cross-flow turbine is a promising solution for micro hydropower generation in urban water mains because of its simple structure, easy maintenance and low costs. However, this is a lack of systematic study on the design and optimization of inline cross-flow turbine. The research gaps based on the literature review are shown as follows:

1. There are still few researches on the development of cross-flow turbine used in water pipes. Although several experimental studies are about energy harvesting from water pipes using cross-flow turbines, application of these turbines needs a significant modification on the water pipes and huge installation space. A new cross-flow turbine concept which is more compact and needs slight modification on the water pipe should be proposed for hydropower generation from water pipes.

2. Research on the design method for ducted elements of inline cross-flow turbine is still lack. Like traditional cross-flow turbines, the ducted elements are of vital importance for the turbine performance. Previous researches have proposed several theoretical methods for nozzle design of cross-flow turbine, however, due to the special working conditions of water mains, the methods are not suitable for inline cross-flow turbine design. A theoretical design method for the ducted elements of inline cross-flow turbine should be proposed to provide guidance for such special application.

3. Researches on the effects of ducted elements shape on the performance of inline cross-flow turbine are still lack. Previous researches have demonstrated that the nozzle shape does have impact on turbine performance, it is necessary to study the performance of inline cross-flow turbines with different ducted elements shape hence

the optimal shape can be determined.

4. There is no research on the effects of runner parameters on the performance of inline cross-flow turbine. Runner is the key component for torque harvesting and transmission in cross-turbine and its geometrical parameters, such as attack angle, blades outer angle and diameter ratio, can significantly affect the turbine performance. Previous researches have suggested the optimal geometrical parameters of the runner by numerical or experimental methods. However, due to the different operating conditions in water mains, studies are still needed to determine the optimal runner geometries.

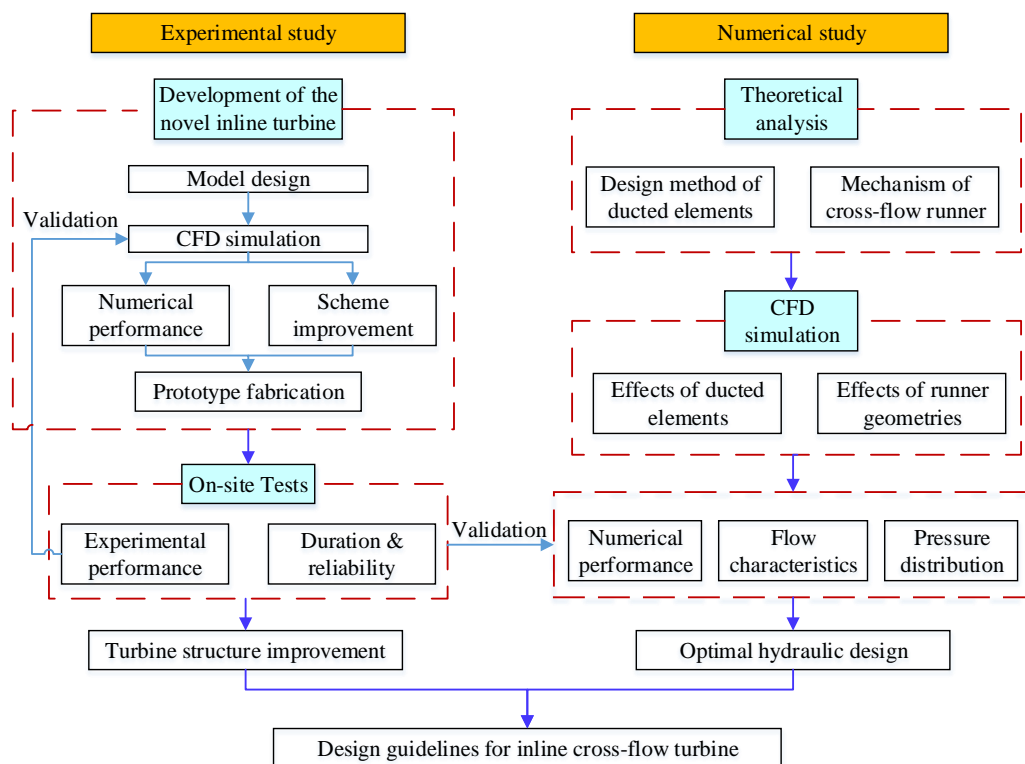


Fig.2.32 Flow chart of the methodology

Based on the literature review, this thesis aims to propose a systematic design method for inline cross-flow turbine used in urban water mains for hydropower harvesting. The flowchart of the research methodology is shown in Fig.2.32.

The thesis can be divided into two main part: experimental study and numerical study. The experimental study starts from the development of a novel configuration of inline cross-flow turbine. In this process, CFD simulation is used to predict turbine performance and provide guidance for scheme improvement. After that, the prototype is fabricated and tested in the hydraulic test rig. There are two objectives of the on-site tests. Firstly, the turbine performance can be obtained through the on-site tests and the results can provide validation for the CFD simulation. Besides, a long-term test is performed to study the durability and reliability of the developed turbine. The results of the long-term tests are helpful for turbine structure improvement.

In the numerical study, a theoretical design method of the ducted elements is proposed and theoretical analysis is performed to investigate the working mechanism of the cross-flow runner. After that, CFD simulation is used to investigate the effects of ducted elements and runner geometries by analyzing the turbine performance, flow characteristics and pressure distribution inside the turbine. Based on the experimental and numerical study, a design guideline can be provided for inline cross-flow turbine design.

# **CHAPTER 3 DEVELOPMENT OF A NOVEL INLINE CROSS-FLOW TURBINE BY NUMERICAL AND EXPERIMENTAL METHODS**

The previous chapter presented a comprehensive literature review of the micro hydro turbines and identified the research gap. In this chapter, the development of one preliminary inline cross-flow turbine prototype and its experimental study are presented. Firstly, the scheme of an inline vertical cross-flow turbine is proposed and several turbine models are established. After that, CFD simulations are carried out to determine the optimal model and to investigate the effects of tip clearance. Besides, a self-adjustable vane is designed to avoid excess water head loss and its function is validated by CFD simulation. Finally, the turbine prototype is fabricated and tested on a lab test rig to study its real performance and durability. The on-site tests can not only provide data for validation of CFD simulation, but also offer guidance for turbine structure improvement.

## **3.1 Scheme of the inline cross-flow turbine**

The main challenge of hydropower generation in water supply pipes is the selection or design of proper turbines that can meet the requirement of water supply. The requirements are as following:

- 1) The generated electricity should meet the power demand of water monitoring system, but too much power may possess a huge load on the energy control and storage system. Based on the data provided by the Water Supplies Department of Hong Kong,

40-100W power is sufficient for nearly any water monitoring system.

2) Although there exists some excess water head in the water pipes, the turbine cannot consume too much water head. To avoid negative effects on the normal water supply through the whole urban area, the consumed water head cannot exceed 5m water.

3) As most urban water pipes are laid underground, the installation space is very limited and the modification of the pipes should be as slight as possible.

4) The most important thing is that the application of water turbine cannot have bad impact on the water quality.

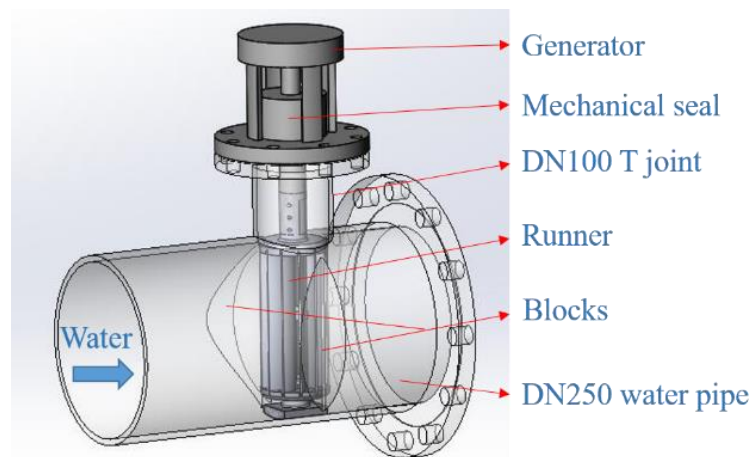


Fig.3.1 The turbine design scheme

To satisfy the requirements mentioned above, a turbine design scheme as shown in Fig.3.1 is proposed. The main idea of this scheme is to integrate a DN100 T-joint to the DN250 pipe, then a cross-flow runner, which connects with a generator via a shaft, is inserted in the pipe through the T-joint to harvest hydropower and transfer the power to the generator. After that, the generated electricity will be stored in chargeable batteries after rectification. As suggested in previous research, ducted elements are

also needed for inline cross-flow turbines. In this research, two blocks that fixed on the pipe inner wall are used to let more water flow through the runner, increasing the velocity of water that passes through the runner and reducing the resistance of water on the returning blades [51].

### 3.2 Research methodology for turbine development

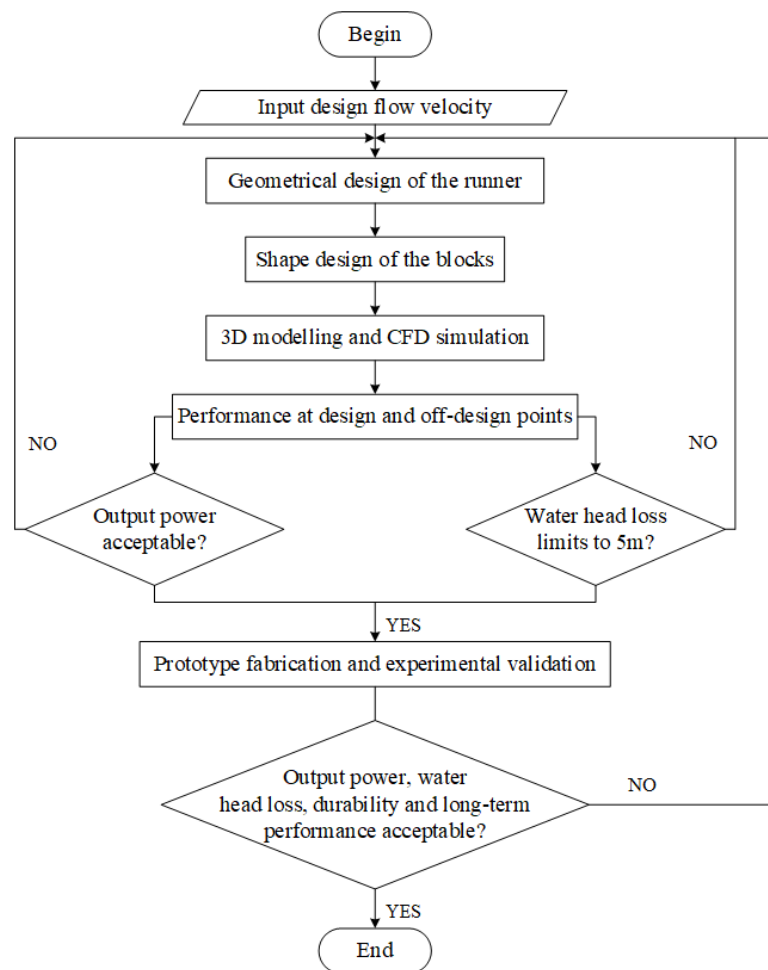


Fig.3.2 The research flow chart

The entire research flow chart is indicated in Fig.3.2. The flow velocity inside the urban water mains is about 1.2-2.0m/s and the average velocity is about 1.5m/s [51]. Thus, the design flow velocity on the design point is set as 1.5 m/s. As shown in Fig.3.2, the turbine design starts with the calculation of the runner geometrical parameters and

the shape design of the blocks. After that, the 3D models of different design will be built and the optimal model is obtained by CFD simulations. Finally, the prototype is fabricated and on-site tests are conducted to validate the numerical results and study the turbine performance. The design process would be repeated if the numerical or experimental results do not satisfy the design requirements.

### 3.2.1 Geometrical parameters

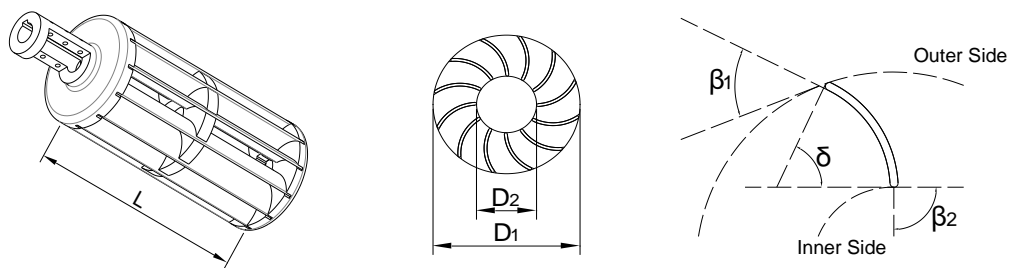


Fig.3.3 The main geometrical parameters of the cross-flow runner

Table 3.1 The values of runner main geometrical parameters

Geometrical Parameters	Symbol	Values
Blades outer angle	$\beta_1$	42°
Blades inner angle	$\beta_2$	90°
Outer diameter	$D_1$	98mm
Inner diameter	$D_2$	45mm
Runner length	$L$	215mm

The key part of the cross-flow turbine is the runner and its main geometrical parameters are indicated in Fig.3.3. Among these parameters, the length  $L$  and the

outer diameter of the runner  $D_1$  are determined by the diameters of water pipe and T joint respectively. Besides, the runner inner diameter  $D_2$ , the blade outer angles  $\beta_1$  and inner angle  $\beta_2$  are determined based on the optimal values suggested by Vincenzo Sammartano [55], and the geometrical parameters are listed in Table 3.1. In the present thesis, the shape of blocks is designed mainly by CFD simulation.

### **3.2.2 CFD setting**

In recent years, the CFD methods have been widely used as powerful and promising tools in turbomachinery design and optimization. In the present research, the CFD method is used to study the effect of different block shapes on the turbine performance and the inside flow field characteristics.

#### **3.2.2.1 Meshing**

The physical model of the turbine, which is composed of four main parts: inlet extension part, turbine body, runner and outlet extension part, was built in SolidWorks 2014, a three-dimensional modeling computer-aided design software. As the computational domain can be regarded as symmetric, only half of the model was built to reduce the computing time. Then the physical model was imported into Ansys ICEM 14.5 for unstructured tetrahedral grids generation. The whole computational domain was separated into two main domains: stationary domain and rotary domain. Inlet extension part, turbine body and outlet extension part belong to the stationary domain while runner is the rotary domain. For simulation, the sliding-mesh interface method was adopted to allow for the mesh motion between static and rotating parts. In the meshing process, the “tetra mesh” was employed to generate grids in the domains far from boundaries, while the “prism mesh” was used for grid generation in the domains near boundaries, i.e. the pipe wall and blades. Such strategy could achieve a good

balance between calculation time and accuracy. To minimize the numerical uncertainty in the solution, a grid independence test was conducted. Six meshing schemes were tested and their grid numbers are 0.63, 1.09, 1.5, 1.91, 3.78 and 9.6 million, respectively. Fig.3.4 shows the dependence of shaft power on the grid number, according to the results, the total grid number of 1.91 million was taken for the next study. The final computational mesh is showed in Fig.3.5.

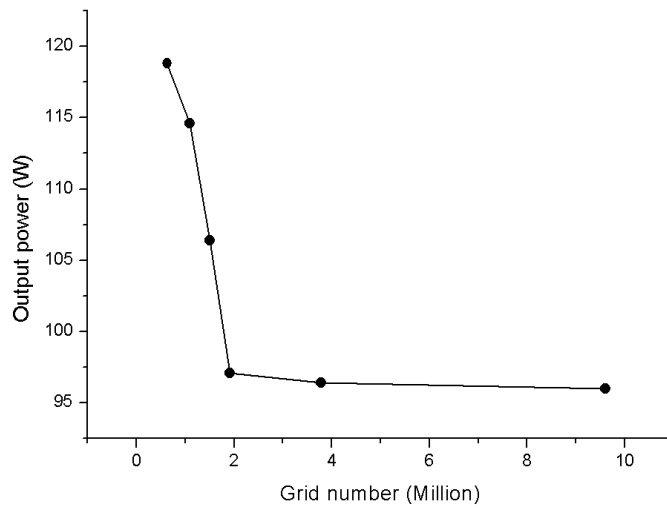


Fig.3.4 The dependence of shaft power on the grid number

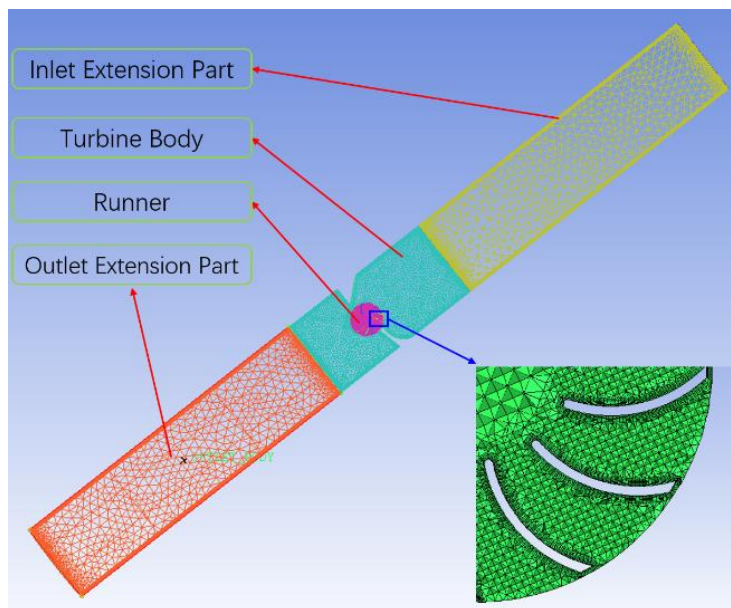


Fig.3.5The final meshing scheme

### 3.2.2.2 Solver setup

The incompressible isothermal flow through a turbomachine is fully described by the continuity and momentum equations, which are called the Navier-Stokes equations and written as:

$$\frac{\partial u_i}{\partial x_i} = 0 \quad (3.1)$$

$$\frac{\partial u_i}{\partial t} + u_j \frac{\partial u_i}{\partial x_j} = -\frac{1}{\rho} \frac{\partial p}{\partial x_i} + \nu \frac{\partial^2 u_i}{\partial x_i \partial x_j} \quad (3.2)$$

where  $u$  is the velocity,  $p$  is the pressure,  $\nu$  is the kinematic viscosity of fluid,  $\rho$  is the density of fluid.

Since solving the Navier-Stokes equations is computationally expensive for high Reynolds number flows in complex geometries, the Reynolds averaged Navier–Stokes (RANS) equations are generally solved to determine the mean velocity field. RANS equations are obtained by time-averaging the Navier-Stokes equations for the mean values of the flow variables over a sufficiently long period compared to the frequencies of turbulent fluctuations, and are written as:

$$\frac{\partial U_i}{\partial x_i} = 0 \quad (3.3)$$

$$\frac{\partial U_i}{\partial t} + U_j \frac{\partial U_i}{\partial x_j} = -\frac{1}{\rho} \frac{\partial P}{\partial x_i} + \frac{\partial}{\partial x_j} \left[ \nu \left( \frac{\partial U_j}{\partial x_i} + \frac{\partial U_i}{\partial x_j} \right) - \overline{\rho u'_i u'_j} \right] \quad (3.4)$$

where  $U$  is the time-averaged velocity,  $u'_i$  is the fluctuating velocity due to turbulence

and  $-\rho\overline{u'_i u'_j}$  is the Reynolds shear stress.

RANS simulations with appropriate turbulence models have been widely used for turbomachinery design analyses due to their low computational cost and satisfactory predictive capability for average device performance [80] [81]. In this study, the SST  $k-\omega$  model is used because the SST  $k-\omega$  model combines the standard  $k-\omega$  model and standard  $k-\varepsilon$  model, it takes the effects of turbulence shear stress into consideration in the definition of the turbulence viscosity and could capture the micro flow in the viscous layer.

The simulations were conducted in ANSYS Fluent 14.5 using a second-order-accurate finite-volume discretization scheme and the maximum residual is set to  $10^{-5}$ . The inlet velocity is considered as the inlet boundary condition of the inlet face while the outlet boundary condition is set as pressure outlet with the pressure equal to atmospheric pressure. The boundary condition of turbine wall and blades is set as non-slip smooth wall. Besides, the boundary condition of symmetric plane is set as symmetry.

### **3.2.3 Experimental setup**

#### **3.2.3.1 Hydraulic test rig**

After a series of simulations, the main structure and components were determined and a prototype was fabricated. The turbine prototype was installed in a hydraulic test rig built based on a carbon contact chamber at Ma On Shan Water Treatment Works (MOSWTW) of Hong Kong to test its performance. Fig.3.6 indicates the diagram of the hydraulic test rig, which is mainly composed of two parallel submersible pumps, DN250 water pipes, the water turbine, two pressure meters, an electromagnetic flow

meter, an adjustable ball valve and a frequency converter controller. The submersible pumps can provide 80m water head at 530m<sup>3</sup>/h (3m/s in DN250 water pipes) to analogize the real flow conditions inside the urban water supply pipes. The working load of the submersible pumps is controlled by the frequency converter controller, by adjusting the working frequency of the submersible pumps and the opening degree of the ball valve, different flow velocity and water head can be achieved in the test rig. A 24V three-phase permanent magnet alternating generator with low starting torque is chose to translate shaft power of the turbine into electric energy. Besides, two pressure meters are used to examine the pressure drop between the upstream and downstream of the water turbine. In the described test rig, the electromagnetic flow meter has a precision of  $\pm 0.5\%$  full scale while the precision of pressure meter is  $\pm 0.25\%$  full scale. Using the prescribed methods for uncertainty estimation [82], the composite errors for water head loss and efficiency measurement are  $\pm 0.25\%$  and  $\pm 0.56\%$ , respectively.

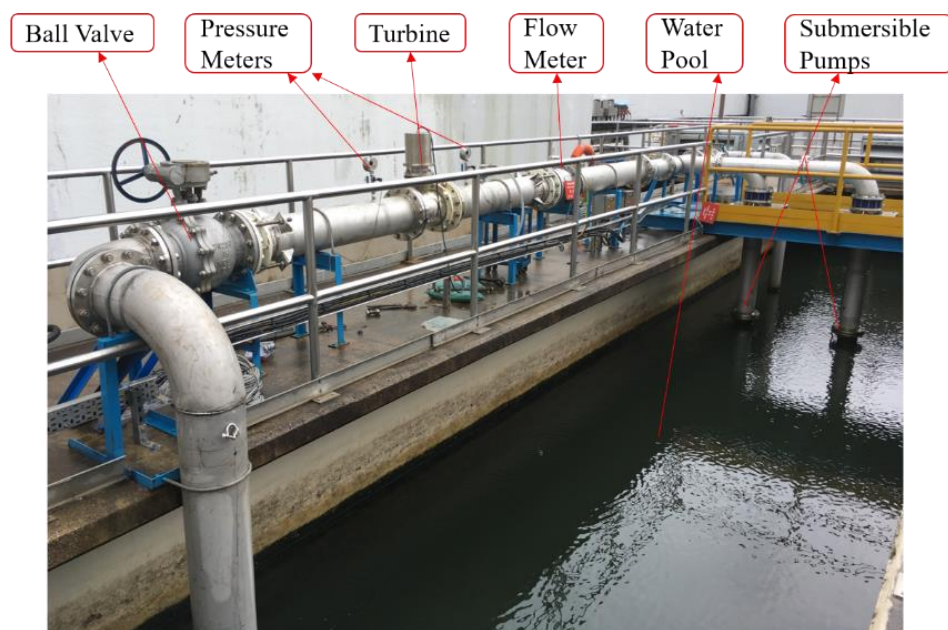


Fig.3.6 The hydraulic test rig at the MOSWTW

### 3.2.3.2 Controller design

One of the significant challenges for micro hydropower harvesting from urban water mains is power management and storage. To solve this problem, a 24V controller is developed. As shown in Fig.3.7 is the control system for micro hydropower generation in urban water mains. The control system consists of rectifier bridge, master controller, lead-acid battery storage module and dummy load module. The rectifier bridge is used to transfer the alternating current to direct current. The master controller consists of one mainboard, one remote communication module, several circuit breakers and relays. And main function of the master controller is to manage the power and send data to the remote computers. Lead-acid battery storage module is used for energy storage while the dummy load module is used for power dissipation. Due to the unstable flow velocity in the urban mains, the output voltage of micro-hydro generator usually fluctuates with time. Once the output voltage is too high, the power will be dissipated by the dummy load to avoid damage on the lead-acid batteries. Fig.3.8 shows the control effect of the controller, it is clear that the controller can keep the battery voltage in an acceptable range.

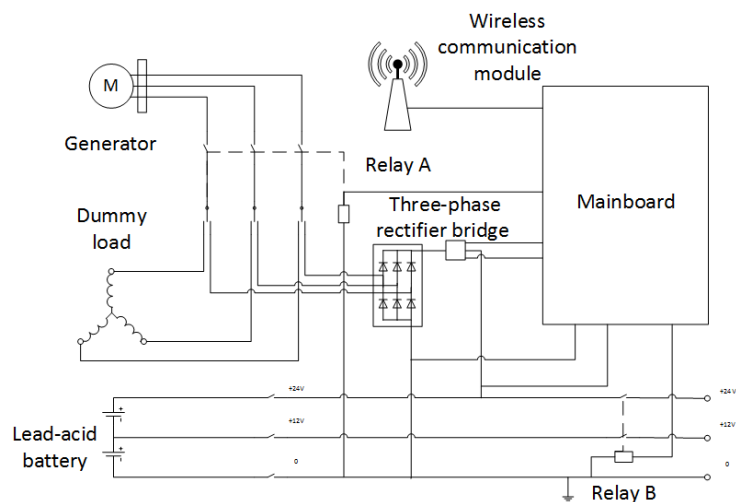


Fig.3.7 Schematic diagram of the controller

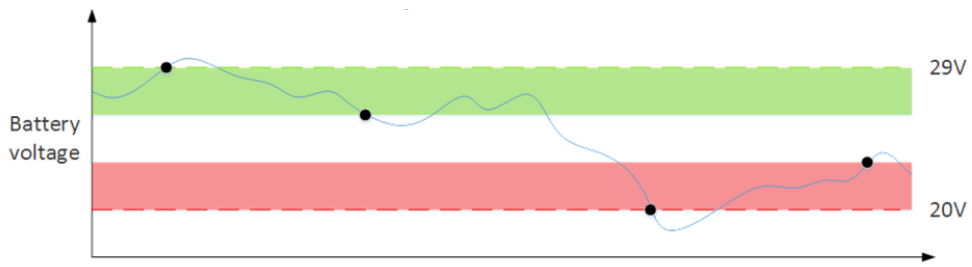


Fig.3.8 Control effect of the controller

As shown in Fig.3.9 is the electricity control and storage system which is mainly composed of controller, two 12V chargeable batteries, dump load and computer. Electricity generated by the permanent magnet alternating generator is rectified in the controller then stored in the chargeable batteries. Once the charging voltage is higher than the bearable voltage of batteries, the dummy load will be used to consume excess electricity. The flow velocities, output power, charging current and voltage and the pressure difference can be monitored and recorded in the computer.

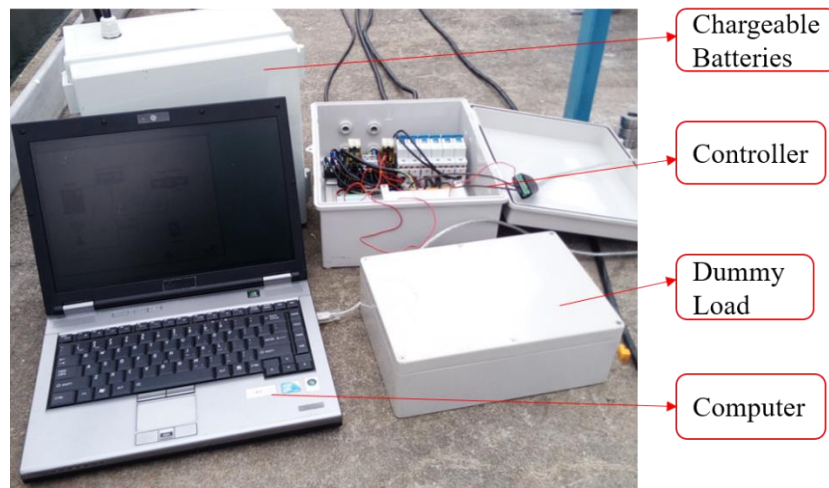


Fig.3.9 The electricity control and storage system

### 3.2.4 Data analysis

To assess the turbine performance, both the numerical and experimental output power and water head loss should be monitored. The experimental results can be

obtained directly based on the data collected in the remote monitoring computer, but some calculation is needed to get the numerical results. In the CFD simulation, the output torque of the runner is recorded and the shaft power of the turbine is calculated by Eq.3.5. For the calculation of actual output power, mechanical loss and generator conversion efficiency must be considered as energy loss is inevitable in energy conversion process, as shown in Eq.3.6.

$$P_{shaft} = T\omega \quad (3.5)$$

$$P_s = \eta_{me}\eta_g P_{shaft} \quad (3.6)$$

where  $P_{shaft}$  is the shaft power, W;  $\omega$  is the rotation speed, rad/s;  $T$  is the shaft torque, N·m;  $P_s$  is the actual simulation power output, W;  $\eta_{me}$  is the overall mechanical efficiency, and  $\eta_g$  is the conversion efficiency of generator. In this study, the mechanical efficiency and generator conversion efficiency are determined based on the data provided by parts suppliers.

The CFD simulations were conducted to study the turbine performance on the design points and off-design points. For performance study on the design points, the tip speed ratio (TSR) was introduced. The TSR means the ratio of the peripheral speed of the turbine runner and the flow velocity and it can be calculated using Eq.3.7. By varying the values of  $\omega$ , different TSRs can be obtained. Correspondingly, by changing the rotation speed in the simulation setup, different output power and water head loss for different TSRs can be acquired. Finally, by changing the inlet velocity of simulation setup, the turbine performance at off-design points were obtained.

$$TSR = \frac{r\omega}{V} \quad (3.7)$$

where  $r$  is the runner radius, m;  $V$  is the flow velocity at runner inlet, m/s.

In the experimental process, the flow velocity, charging voltage and current, water head of upstream and downstream can be transmitted to the controller and recorded in the monitoring computer, so the experimental results can be finally acquired by simple calculations.

### 3.3 Numerical results and analysis

As mentioned before, two blocks are used on the inlet side of the runner decrease the water resistance which exerts on the returning blades, thus the performance of cross-flow turbine can be improved. In this research, the CFD simulations were conducted to investigate the effects of different blocks on the performance of inline cross-flow turbine and further find the optimal block model.

#### 3.3.1 Design of block shape

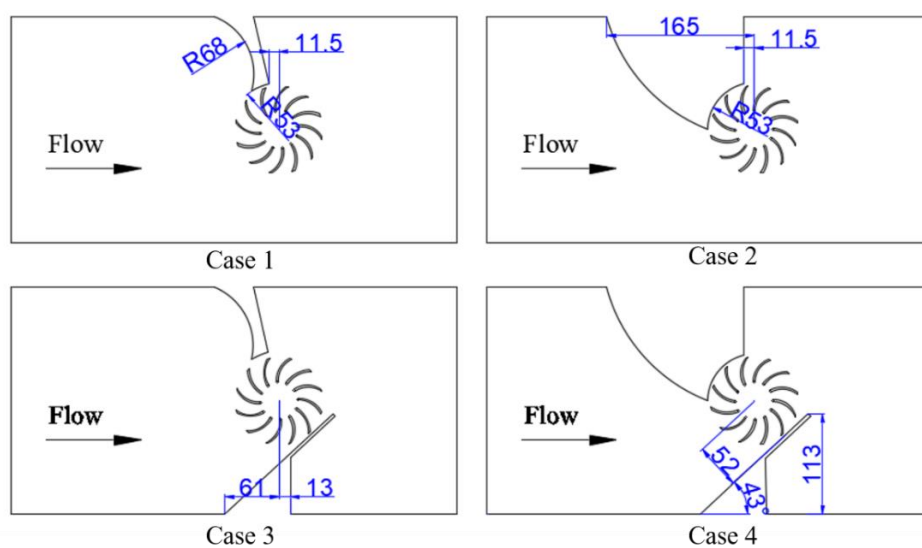


Fig.3.10 Different block models

Four block models with different geometrical design (as shown in Fig.3.10) were built and simulated to study the impact of different block shapes on the turbine performance. In Case 1, one block with concave surface is integrated in the pipe inner wall on the upstream side while one block with convex surface is placed on the same location in Case 2. Compared to Case 1 and 2, one block with plane surface is added in Case 3 and 4, respectively.

Table 3.2 Simulated results of four cases on the design point

No.	Description	Max. power (W)	Water head loss (m)	TSR
Case 1	Upstream concave block	11.2	0.62	0.9
Case 2	Upstream convex block	15.7	0.67	1.1
Case 3	Upstream concave block and downstream plane block	71.8	3.74	1.2
Case 4	Upstream convex block and downstream plane block	125.2	3.3	1.2

The output power and water head loss of the turbine on design point and off-design points are recorded to obtain the characteristics of turbine performance. Fig.3.11 and Fig.3.12 illustrate the output power and water head loss through the turbine for different TSR on the design point. As shown in Fig.3.11, the output powers of Case 1 and Case 2 increase with the increment of TSR until reach maximum values, then decrease. The maximum output power of Case 1 and Case 2 occurs where the TSR is 0.9 and 1.1, respectively. The output power of both Case 3 and Case 4 also increases with the increment of TSR, but the increase trend of Case 4 is more obvious

than that of Case 3. For water head loss through the turbine, all the four cases experience a slight growth with the TSR and all the values are lower than 5m water, which means that all the cases can meet the requirement from the aspect of water head loss at the design point. Table 3.2 compares the maximum output power and the corresponding TSR and water head loss of the four cases.

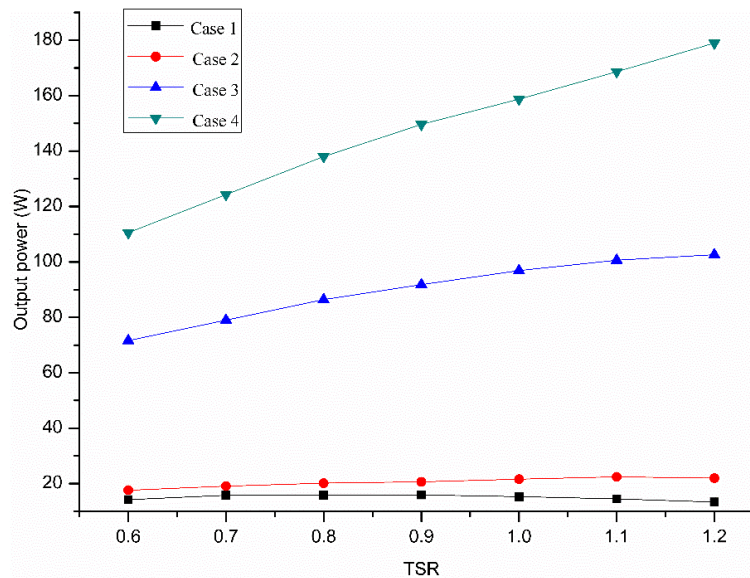


Fig.3.11 The output power of four cases with different TSR

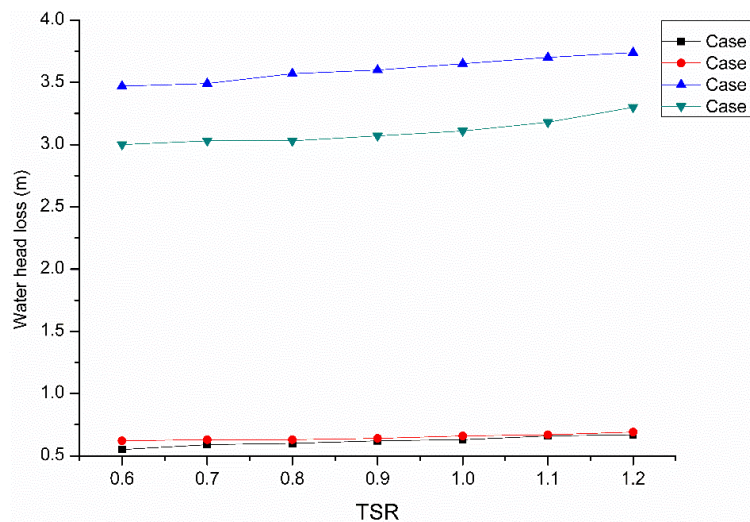


Fig.3.12 The water head loss of four cases with different TSR

Case 1 and Case 2 indicate poor performance in comparison with other two cases, the main reason for the poor performance can be explained by the velocity vectors as shown in Fig.3.13. It can be seen that although the upstream block can modify the flow path and force more water to flow through the runner, most of the water flows away without doing any work on the blades due to the absence of downstream block. By adding downstream blocks in Case 3 and Case 4, the upstream and downstream blocks can act as convergence nozzles while the downstream pipe can function as a diffuser. As indicated in the velocity vectors of Case 3 and Case 4, the highest velocity regions are observed in the domain of runner and the velocity behind the runner is reduced, therefore the total harvested power from water flow raises significantly. Both the Case 3 and Case 4 possess a good performance, but compared to Case 3, Case 4 indicates a good performance in terms of output power. This is mainly due to the smaller inlet discharge area and bigger cover area on the returning blades in Case 4. A small inlet discharge area usually corresponds to a higher flow velocity towards the advancing blades, so more energy can be harnessed by the runner. On the other hand, a bigger cover area on the returning blades can reduce the influence of negative torque on the turbine performance. It can be observed in Fig.3.12 that the water head loss of Case 3 is the highest among all the cases. This is because that the upstream block with concave surface in Case 3 changes the flow direction sharply, which may cause severe hydraulic loss. Furthermore, it can be seen in the Fig.3.13 that water leakage occurs in the tip clearance between the blades and the upstream block. The water leakage would not only increase friction losses, but also produce negative torque on the blades, leading to significant performance degradation. The optimal tip clearance as determined in the following part.

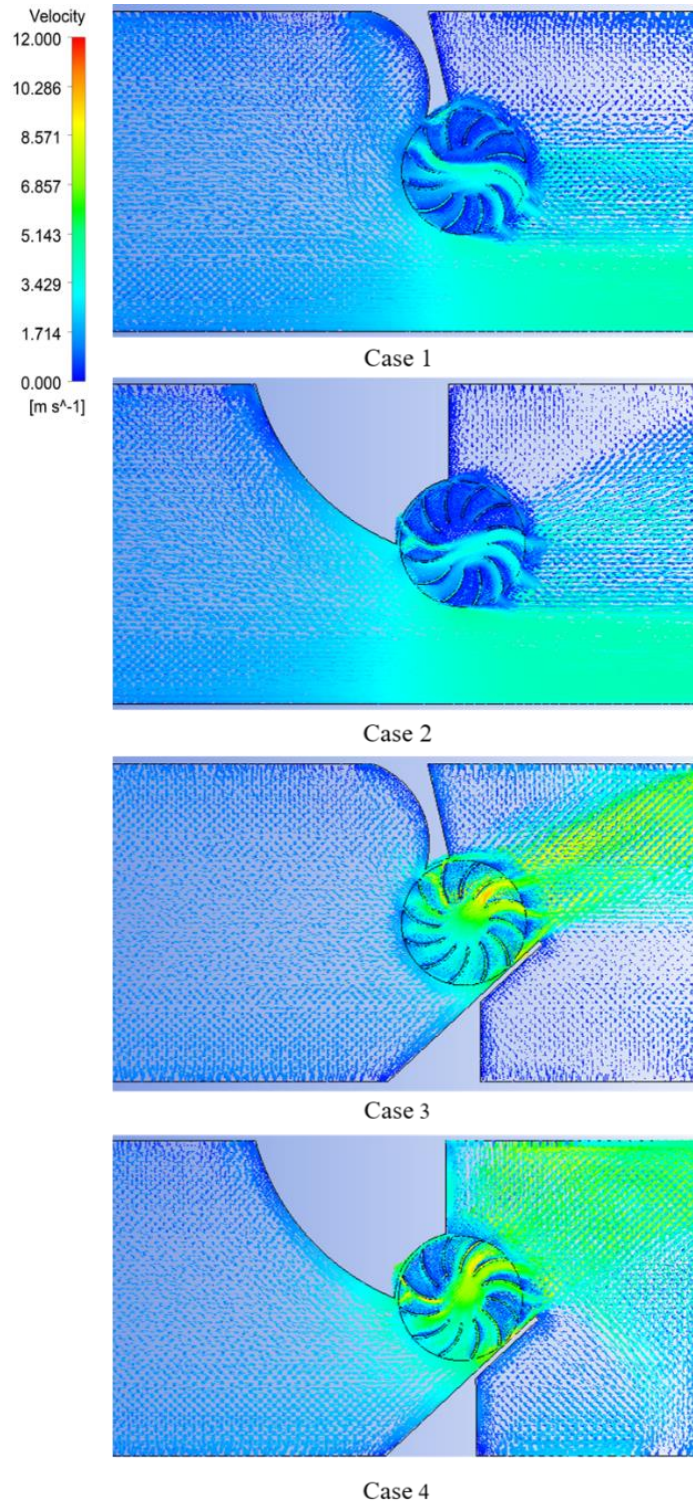


Fig.3.13 The velocity vectors of different cases

Fig.3.14 and Fig.3.15 show the variation of output power and water head loss with respect of flow velocities on the off-design points. It is noticed that the output

power and water head loss of all the cases experience an increase with the increase of flow velocities. However, the performance of Case 1 and Case 2 is still very poor even at a high flow velocity, so these two cases are abandoned in the project. Case 4 indicates the highest output power among all the cases, but its output power at high flow velocities (1.7m/s and above) is so high that may exceed the tolerance of the 24V controller, which is used to rectify and store the generated electricity and to monitor the working conditions of the turbine. By contrast, Case 3 possesses a modest increase with the flow velocities and its output power at 2m/s is about 135W, which meets the security requirement of the controller very well. From the aspect of water head loss, both the Case 3 and Case 4 exceed 5m water head at high flow velocities, this problem can be solved by introducing a self-adjustable vane, which will be studied in the following parts. To sum up, although the output power of Case 4 is better than that of Case 3, it is not the most suitable configuration for this project and the Case 3 will be selected as the optimal model for next step of research.

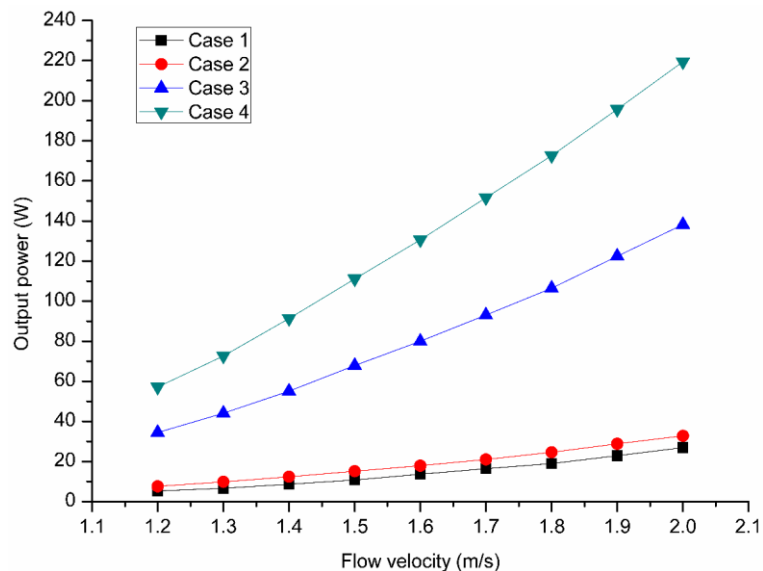


Fig.3.14 The output power of four cases on off-design points

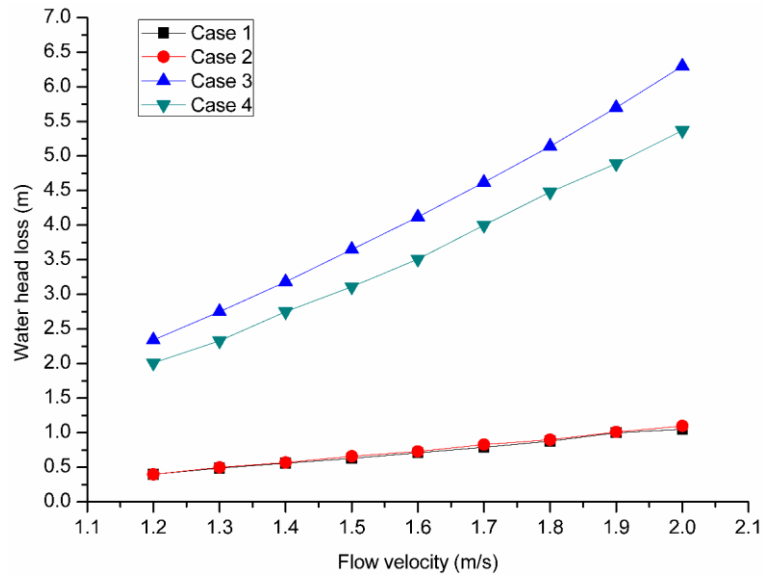


Fig.3.15 The water head loss of four cases on off-design points

### 3.3.2 Effects of tip clearance

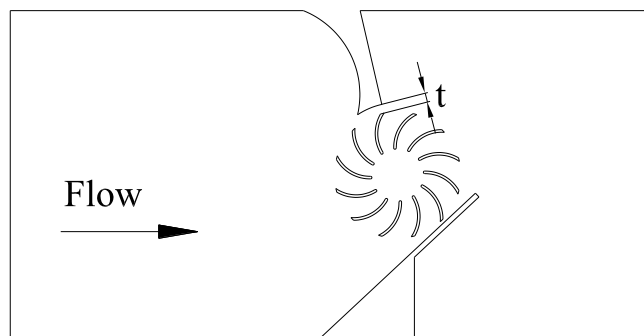


Fig.3.16 Tip clearance of the inline cross-flow turbine

As analyzed in the above part, the blocks can direct and concentrate the water flow to the advancing blades and cover the flow towards the returning blades. Therefore, the positive torque generated by the advancing blades can be enhanced while the negative torque of returning blades can be reduces. However, due to the tip clearance existing between the upstream block and the runner (as shown in Fig.3.16), the tip leakage may have a reverse impact on the turbine performance. In this part, three models with different tip clearances (i.e. 10mm, 8mm and 5mm, respectively)

were simulated for different TSR at the design point to study the effects of tip clearance on the turbine performance.

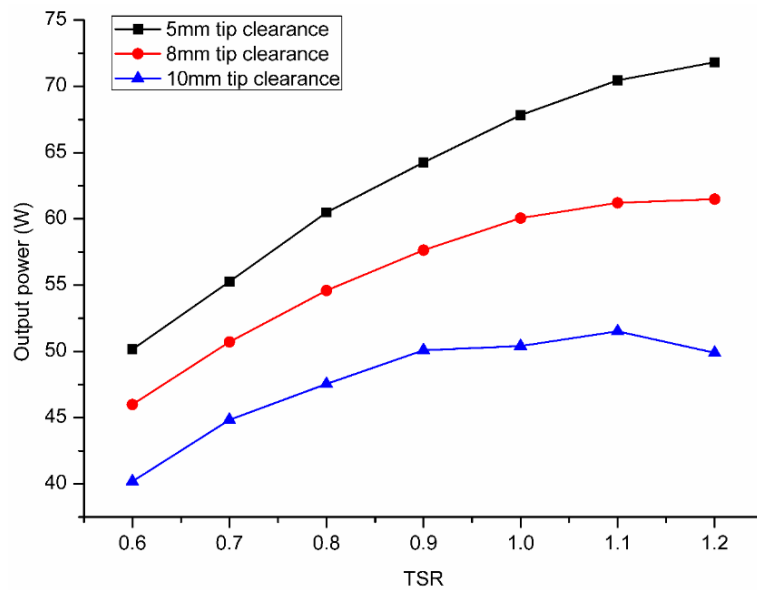


Fig.3.17 The output power of models with different tip clearance

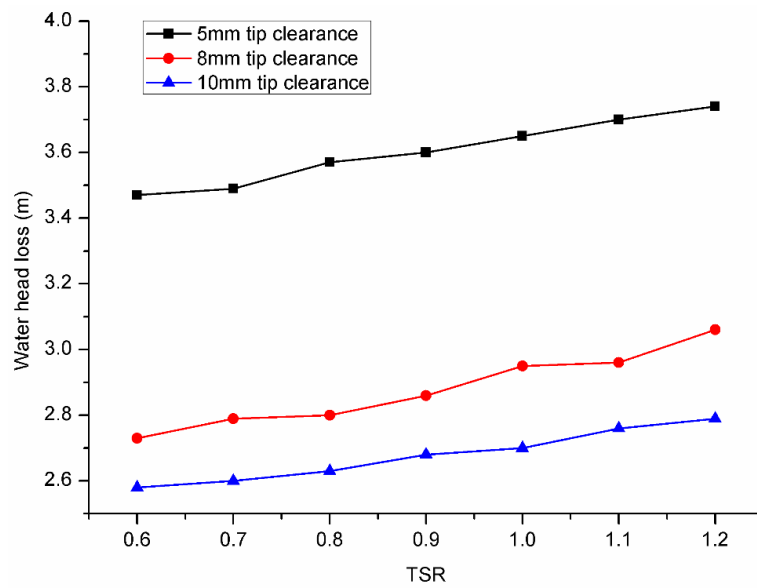


Fig.3.18 The water head loss of models with different tip clearance

The comparisons of output power and water head loss of models with different tip clearance obtained for different TSR are indicated in Fig.3.17 and Fig.3.18. It can be observed that the output power variation of models with different tip clearances is

relatively large. For example, on the design point, the maximum output power of model with 10mm tip clearance is only about 52W while that of the 5mm tip clearance model is more than 70W. On the other hand, although the water head losses of all models encounter a slight variation with the TSR, the head loss of 5mm tip clearance model is much larger than that of the other two models.

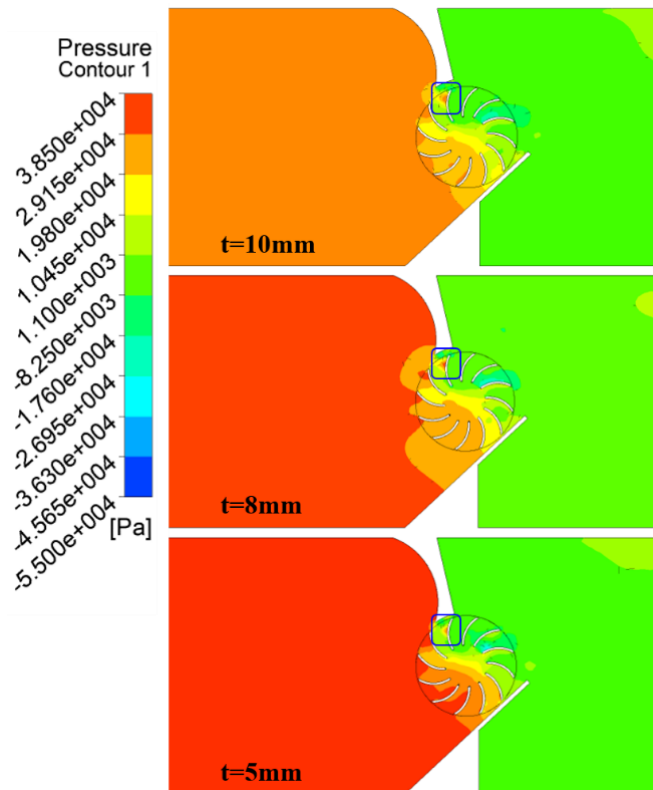


Fig.3.19 The pressure contours of models with different tip clearance

Fig.3.19 shows the pressure contour through the models with different tip clearance. It indicates that a high-pressure region caused by the tip leakage exists on the back of returning blades, resulting in a negative torque on the runner. But by comparing the pressure contours, it is further seen that the smaller the tip clearance is, the lower pressure behind the returning blades will be. Besides, it is found that for a smaller tip clearance, the indicated pressure at the runner inlet side is larger. As a result, the pressure difference between the upstream side and the downstream side of the

runner is larger and more water will be sucked to flow towards the advancing blades, therefore the turbine performance could be improved [83] [84].

In conclusion, the tip clearance mainly has two effects on the turbine performance. Firstly, a small tip clearance can reduce the tip leakage thus reduce the reversing torque on the returning blades. Secondly, for decreasing tip clearance, the pressure drop through the inlet and outlet of the runner will be increased, which draws more water to flow through the runner and enhances the positive torque generated by the advancing blades. According to the above analysis, values of tip clearance less than 5mm are expected to further increase the turbine performance, but the manufacturing and assembling difficulties make it is challenging to fabricate a prototype. Besides, the output power of model with 5mm tip clearance is enough for the power requirement of water leakage monitoring system, so the final tip clearance of this turbine is designed as 5mm.

### **3.3.3 Design of self-adjustable vane**

As requested by the Water Supplies Department of Hong Kong, the water head loss through the turbine cannot exceed 5m water. However, according to former results, the water head losses of the proposed design scheme at higher flow velocities have exceeded 5m water. To solve this problem, a self-adjustable vane located on the downstream side of the turbine was designed and tested. As shown in Fig.3.20 is the schematic diagram of the self-adjustable vane, in which a damping device (a torsional spring in the present study) is designed to control the opening degree of the self-adjustable vane. At low flow velocities (i.e. less and equal to 1.5m/s), the damping device can hold the self-adjustable vane at its original position, but when the flow velocity is more than 1.5m/s, the water will push the self-adjustable vane to open to

some degree, so some water will flow through the space between the runner and the self-adjustable vane. With the increase of the flow velocities, the opening degree becomes larger. It is assumed that the opening degree of the self-adjustable vane at the flow velocity larger than 1.5m/s increase by  $3^\circ$  with every 0.1m/s. For example, the opening degree at 1.6m/s is  $3^\circ$  while that at 2m/s is  $15^\circ$ .

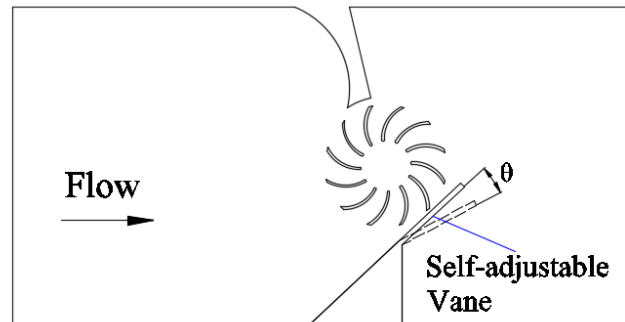


Fig.3.20 The schematic diagram of the self-adjustable vane

The comparisons of water head loss and output power of models with and without self-adjustable vane at flow velocity of 2.0m/s obtained for different TSR are indicated in Fig.3.21 and Fig.3.22. It can be observed that the water head loss reduced by about 3.5m water while the output power reduced by nearly 30W after adopting the self-adjustable vane, which means that the self-adjustable vane has a good performance in reducing the water head loss. Although the output power also reduces with the opening of self-adjustable vane, it is enough for the power requirement of water leakage monitoring system. Besides, the reduction of output power can lighten the load on controller and chargeable batteries.

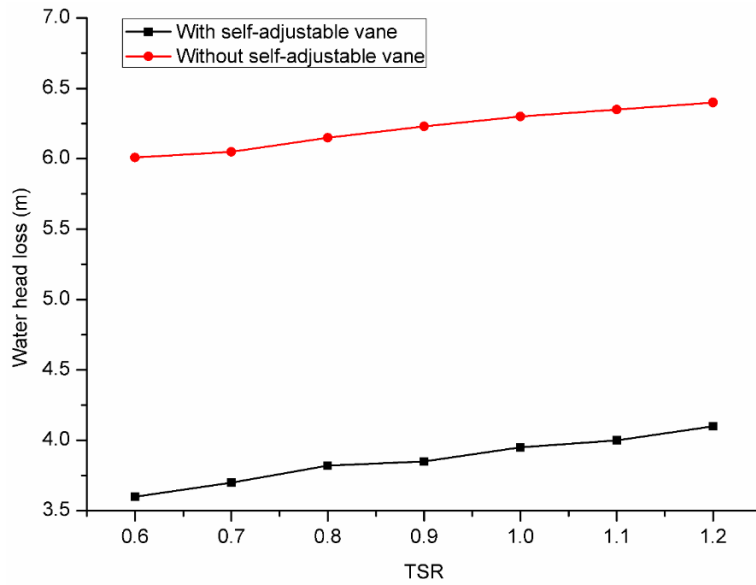


Fig.3.21 The water head loss of models with and without self-adjustable vane

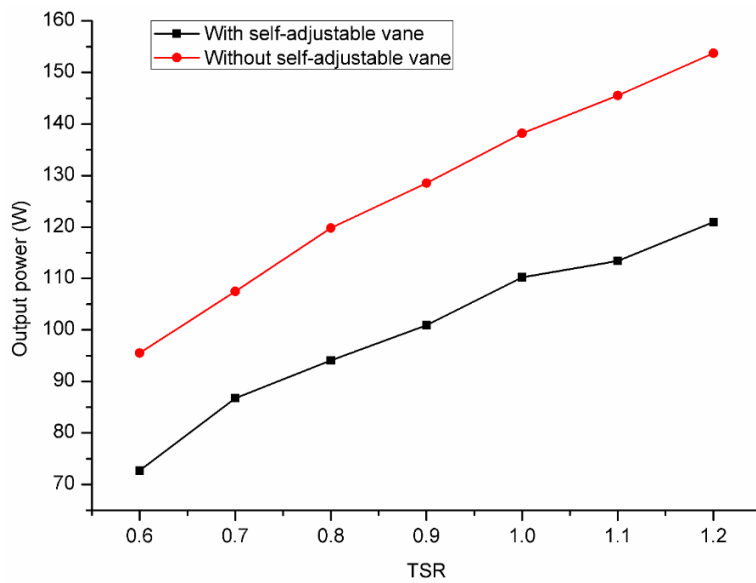


Fig.3.22 The output power of models with and without self-adjustable vane

Fig.3.23 indicates the simulated turbine performance on off-design points. Both the output power and water head loss increase with the increase of the flow velocity, but the growth becomes slow at higher flow velocities. The water head losses in the flow range from 1.2m/s to 2.0m/s are all less than 5m water, which can satisfy the requirement of the Water Supplies Department very well. Besides, it can also be

observed that the minimum and the maximum output power are about 35W and 120W, which can not only meet power demand of water leakage monitoring system, but also be within the tolerance capacity of the controller. In conclusion, the proposed self-adjustable vane can avoid too much water head loss with little influence on the output power.

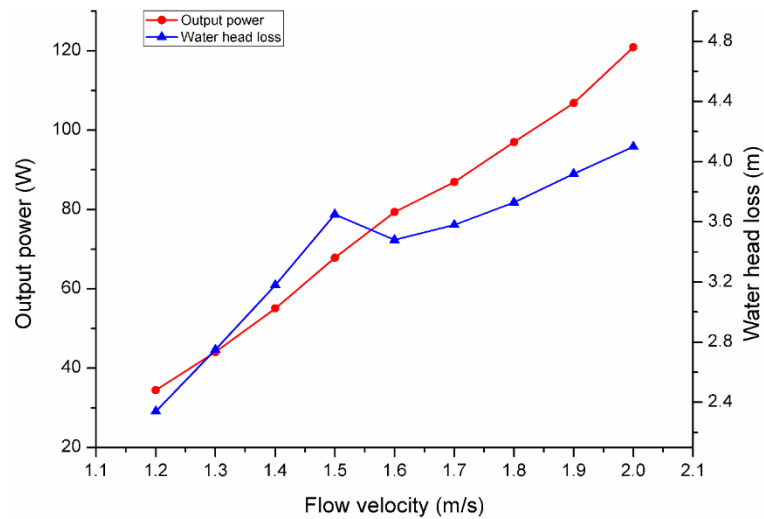


Fig.3.23 The off-design performance of turbine model with self-adjustable vane

### 3.4 Experimental results and analysis

After a series of CFD simulation, the final configuration was determined and inline cross-flow turbine prototype was fabricated, as shown in Fig.3.24. The turbine is mainly composed of turbine body, runner, runner holder, upstream block, self-adjustable vane, shaft, mechanical seal and generator. Among them, the turbine body is a DN250 pipe with a length of 460mm. The runner is made of 12 blades, which are welded to three discs, in addition, a runner holder is located on the bottom of the turbine body to hold the terminal of the runner to reduce runner deformation. The main function of the runner is to harvest hydropower and transfer the generated torque to generator through the shaft. Both the upstream block and self-adjustable vane are

manufactured by wire-electrode cutting and integrated with the turbine body by welding. The whole prototype is made of 316L stainless steel to avoid negative impacts on the water quality. Finally, the prototype was tested in the test rig to validate the simulation results and study its performance.



Fig.3.24 The inline cross-flow turbine prototype

### 3.4.1 Validation of the numerical results

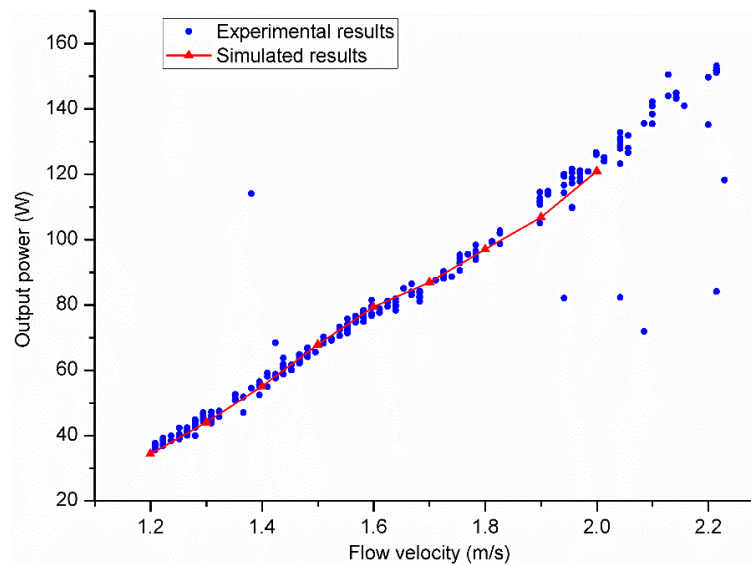


Fig.3.25 The comparison between experimental and numerical output power

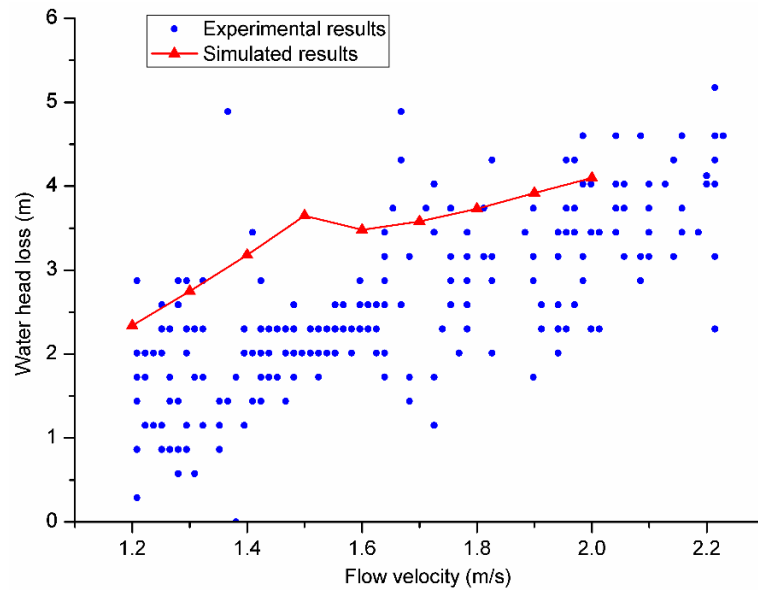


Fig.3.26 The comparison between experimental and simulation water head loss

Fig.3.25 and Fig.3.26 show the comparison between the experimental and numerical results. The turbine prototype was tested over the flow velocities varying from 1.2m/s to 2.2m/s and the experimental data was recorded to compare with the computed results. It can be observed in Fig.3.25 and Fig.3.26 that the simulated output power agrees very well with the measured values, but some difference exists between the simulated and experimental water head loss.

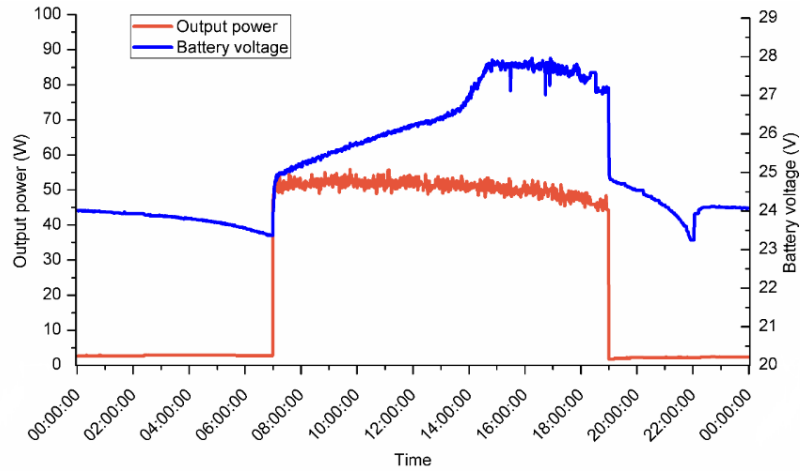
The comparison between the numerical and the experimentally measured output power and water head loss is given in Table 3.3, the error percentage is also provided in the table. The measured output power on the design point is 69.1W with 2.62m water head loss, compared to the simulated values of 67.8W and 3.65m. Most of the error percentages in terms of output power are limited in  $\pm 5\%$ . The error percentage of water head loss is relatively large and two main reasons may account for this phenomenon. Firstly, the CFD model is simplified, resulting in calculation uncertainties which are very difficult to be measured and ruled out. Secondly, the deviations can also be caused by experimental measuring errors. In the test rig, the

unstable flow caused by the turbine may result in pressure fluctuation, which has significantly negative impact on measuring accuracy. However, the error values of water head loss are all less than 1m. Hence, an acceptable agreement between numerical and experimental results was achieved.

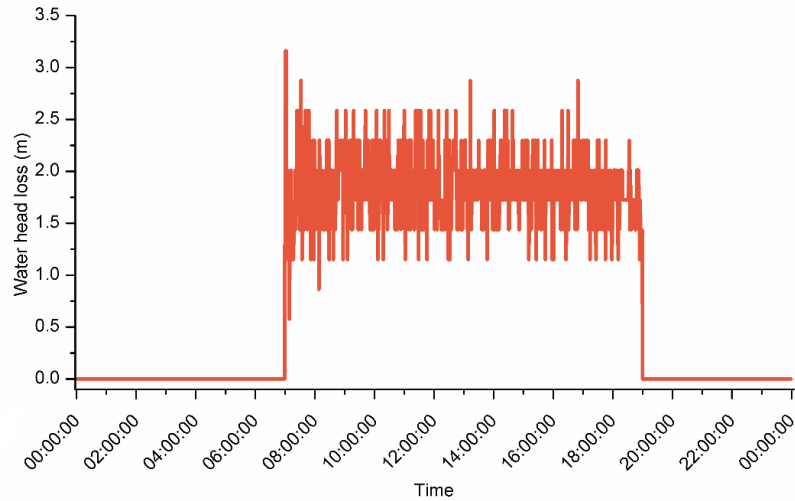
Table 3.3 Comparison between computed and measured results

Flow velocity (m/s)	Output power (W)			Water head loss (m)		
	Experimental results	Simulation results	Error (%)	Experimental results	Simulation results	Error (%)
1.2	36.8	34.4	-6.5	2.01	2.34	16.4
1.3	43.2	44.0	1.85	2.11	2.75	30.3
1.4	53.4	55.1	3.18	2.23	3.18	42.6
1.5	69.1	67.8	-1.8	2.62	3.65	39.3
1.6	76.6	79.4	3.6	2.82	3.48	23.4
1.7	87.6	86.9	-0.8	3.32	3.58	7.8
1.8	94.6	97.0	2.5	3.10	3.73	20.3
1.9	105.7	106.8	1.0	3.95	3.92	-0.76
2	124.1	121.0	-2.5	3.91	4.10	4.8

### 3.4.2 Experimental performance of the turbine



(a) Output power and battery charging voltage



(b) Water head loss

Fig.3.27 The turbine performance in one typical day

The turbine prototype was tested at a flow velocity of 1.3m/s for 12 hours a day for one month to study its performance. Fig.3.27 shows the turbine performance in one typical day. The output power keeps very stable around 50W, and the battery charging voltage increases gradually then remains steady under 28V. Although the water head loss varies significantly with the time, the maximum value is still below 3m. As described in Fig.3.28 is the statistics of daily electricity generation in one month. The

average daily electricity generation is about 600Wh, which ensures a constant power supply for almost any general monitoring system. Besides, as the tests were conducted at a flow velocity of 1.3 m/s while the actual flow velocity in the water pipe varies from 1.2m/s to 2 m/s, the turbine performance in practical application is expected to be better than the test results.

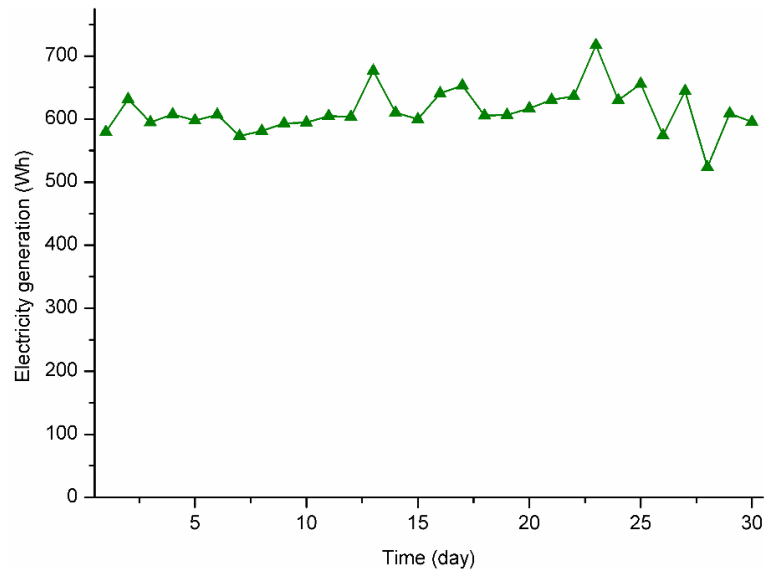


Fig.3.28 Daily electricity generation

### 3.5 Summary

This research presents the development of a novel inline vertical cross-flow turbine for hydropower generation in urban water mains by numerical and experimental methods. The flow field characteristics, output power and water head loss of the system have been analyzed to study the effects of block shape, tip clearance and self-adjustable vane on the turbine performance. As referred from the present study, the following conclusions can be obtained:

- (1) The proposed upstream and downstream blocks could act as the nozzle and diffuser of a conventional cross-flow turbine to enhance the flow velocity and pressure

difference through the runner.

(2) The configuration with an upstream concave block and a downstream plane block was suitable for the power demand of a water leakage monitoring system.

(3) A smaller tip clearance could reduce the tip leakage so that to reduce the reversing torque on the returning blades and increase the pressure drop through the runner. The turbine performance could thus be improved.

(4) The proposed self-adjustable vane achieved ideal performance in avoiding excess water head loss with little influence on the output power.

(5) The experimental results indicated that the numerical method used in the present research could predict the turbine performance with an acceptable accuracy and provide a good guidance for turbine design and improvement.

(6) The prototype test results showed that the output power at the design point was 69.1W with 2.62m water head loss. Besides, over a flow velocity range varying from 1.2m/s to 2.2m/s, the water head loss was always below 5m and the normal water supply was not affected.

(7) After a month-long test at the flow velocity of 1.3m/s, the prototype was proved very reliable with steady performance and its daily electricity generation was about 600Wh, which was sufficient for powering any general water leakage monitoring system in an urban environment.

# **CHAPTER 4 DEVELOPMENT OF THE BLOCK DESIGN METHOD AND THEORETICAL ANALYSIS ON THE CROSS-FLOW RUNNER**

In the previous chapter, a preliminary prototype of the inline cross-flow turbine was designed and tested. The experimental results indicated the feasibility of the proposed scheme of inline cross-flow turbine. However, it can also be observed that although the turbine can satisfy power demand for water monitoring system, the turbine efficiency is relatively low and there is still space for turbine performance enhancement. Based on the literature, by optimizing the shape of ducted elements and runner of cross-flow turbine, the turbine performance can be significantly improved. In this chapter, a mathematic design method for blocks in inline cross-flow turbine is presented, besides, the theoretical working principle of the runner is also introduced to provide guidance for runner parameter optimization.

## **4.1 Mathematic design method for the blocks**

### **4.1.1 Introduction and assumptions**

The blocks are vitally important components in the proposed inline turbine as they can function as the nozzle in traditional cross-flow turbine. Fig.4.1 shows the main structure of the inline cross-flow turbine. Two blocks, guide block and conversion block, are integrated to the pipe inner wall. The guide block is used to direct water flow towards the runner while the conversion block can convert part of the water head into flow kinetic energy. Fig.4.1 also indicates the main geometrical parameters

of the blocks and runner. Among them, the orientation angle of guide block  $\theta_0$  and runner inlet arc angle  $\lambda$  are two key parameters that determine the shape of conversion block.  $R_\theta$  represents the distance from runner center axis to the inner wall of conversion block at different azimuthal angle. By determining several  $R_\theta$  at different azimuthal angle, the geometrical shape of the conversion block can be obtained.

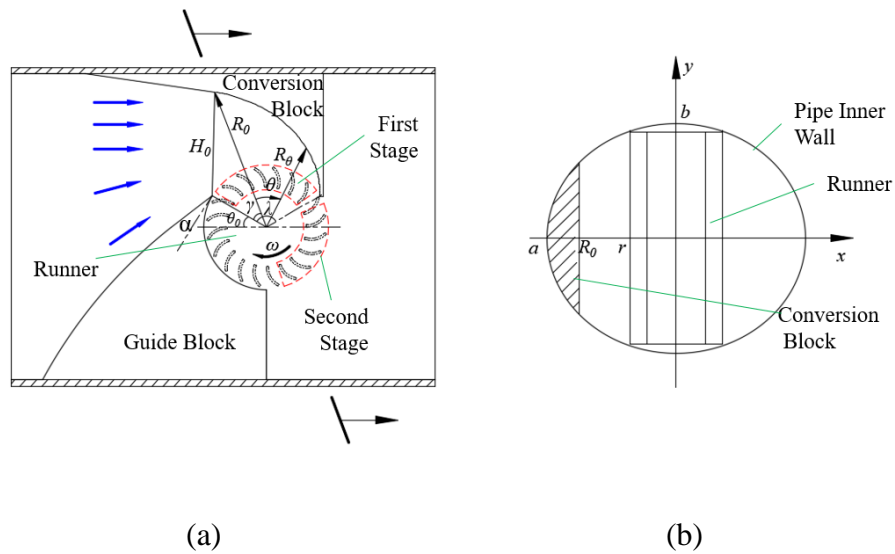


Fig.4.1 Design scheme of the inline turbine (a) Main structure of the turbine (b) Diagram of cross section at the conversion block inlet

To development a method for the block design, the following assumptions are made:

- 1) All the reduced water head through the conversion block is converted into flow kinetic energy.
- 2) The distribution of water flow rate at the runner inlet discharge area is uniform.
- 3) The flow velocity in the space between the conversion block and runner is uniform.

### 4.1.2 Design procedure

A mathematic design method is proposed for conversion block design, and the design method is developed based on the assumptions that the distribution of water flow rate at the runner inlet discharge area is uniform and all the reduced water head is converted into flow kinetic energy. The design process can be divided into two steps. The first step is to obtain the distance from runner center axis to the inlet of conversion block,  $R_0$ . Based on the first assumption, the flow rate at the inlet of conversion block is:

$$Q_{in} = \frac{\lambda - \gamma}{\lambda} Q \quad (4.1)$$

where  $Q$  is the total flow rate through the runner,  $m^3/h$ ;  $\lambda$  is runner inlet arc angle;  $\gamma$  is the orientation entry angle of the conversion block.

The orientation entry angle of the conversion block can be calculated by:

$$\gamma = \csc\left(\frac{r \cos \theta_0}{R_0}\right) - \theta_0 \quad (4.2)$$

where  $\theta_0$  is the orientation angle of the guide block;  $r$  is the runner outer radius.

According to fluid continuity, the inlet area of the conversion block  $A_{in}$  can be calculated:

$$A_{in} = \frac{Q_{in}}{V_{in}} \quad (4.3)$$

where  $V_{in}$  is the flow velocity at the inlet of conversion block.

Based on the second assumption and energy equation, the velocity at the block inlet can be determined as:

$$g\Delta H = \frac{1}{2}(V_{in}^2 - V_0^2) \quad (4.4)$$

where  $\Delta H$  is the water head reduction through the turbine, m;  $V_0$  is the water flow velocity in the pipe, m/s.

By combining Eqs.4.1-4.4, the area of conversion block inlet  $A_{in}$  can be obtained. Besides that,  $A_{in}$  can also be acquired by definite integration. Fig.4.1(b) shows the cross section of the water pipe through the inlet of the conversion block and runner central axis. The shape of the cross section is an ellipse that can be described as:

$$\frac{x^2}{a^2} + \frac{y^2}{b^2} = 1 \quad (4.5)$$

$$a = R_{pipe} / \cos\left(\frac{\pi}{2} - \theta_0 - \gamma\right) \quad (4.6)$$

$$b = R_{pipe} \quad (4.7)$$

where  $a$  is the length of long axes of the ellipse, m;  $b$  is the length of short axes of the ellipse, m;  $R_{pipe}$  is the radius of the water pipe, m.

The cross section between the block and runner is a part of the ellipse described by Eqs.4.5-4.7 and its area  $A_{in}'$  can be calculated as:

$$A'_m = 2 \int_r^{R_0} y dx \quad (4.8)$$

The definite integral can be solved by substitution method:

$$A'_m = \frac{ab}{2} (\sin 2t_2 - \sin 2t_1) - ab(t_2 - t_1) \quad (4.9)$$

$$t_1 = \csc \frac{r}{a} \quad (4.10)$$

$$t_2 = \csc \frac{R_0}{a} \quad (4.11)$$

where,  $t_1$  and  $t_2$  are the substitution parameters;  $r$  is the outer radius of the runner, m.

By combining Eqs.4.2 and 4.5-4.11, a calculation method related to  $R_0$  can be obtained for determination of the area of conversion block inlet. It is very difficult to get analytic solution of  $R_0$  but an approximate solution can be acquired based on iteration method. By giving an initial value and a range of  $R_0$ , the value of  $A'_m$  can be calculated. If the value of  $A'_m$  satisfies the followed equation, this  $R_0$  can be regarded as the required value.

$$\left| \frac{A'_m - A_m}{A_m} \right| \leq C \quad (4.12)$$

where,  $C$  is the allowable deviation, 2% is selected in this study.

The second step is to determine the interval values of  $R_0$  at different azimuthal angle, similarly, the flow rate at the cross section through runner central axis and  $R_0$

can be calculated as

$$Q_{\theta} = \frac{\lambda - \gamma - \theta}{\lambda} Q \quad (4.13)$$

It is assumed that the flow velocity in the space between the conversion block and runner is uniform, so the area of the cross section through runner central axis and  $R_{\theta}$  can be calculated:

$$A_{\theta} = \frac{Q_{\theta}}{V_{in}} \quad (4.14)$$

The elliptic equation of the cross section can be described as:

$$\frac{x^2}{a^2} + \frac{y^2}{b^2} = 1 \quad (4.15)$$

$$a = R_{pipe} \left/ \cos\left(\frac{\pi}{2} - \theta_0 - \gamma - \theta\right) \right. \quad (4.16)$$

$$b = R_{pipe} \quad (4.17)$$

The area of the cross section through runner central axis and  $R_{\theta}$  can also be calculated by definite integration:

$$A'_{\theta} = 2 \int_r^{R_{\theta}} y dx \quad (4.18)$$

By comparing  $A_{\theta}$  and  $A'_{\theta}$ , the values of  $R_{\theta}$  can be obtained and the shape of conversion block can be determined finally.

As the main function of guide block is to direct the water flow to the runner and

conversion block. Its main geometrical parameter is the attack angle  $\alpha$  which is showed in Fig.4.1. The attack angle determines the flow inlet direction and its effect on the turbine performance has been studied by several researchers [63] [85] [86]. In this study, the value of attack angle is designed as  $22^\circ$ , which is suggested as the optimum value by the references [54] [63].

#### **4.1.3 Implications for block optimization**

The block design plays an important role in performance enhancement of inline cross-flow turbines as the block converts water head into flow kinetic energy and determines the flow attack angle. The proposed mathematic design method for the blocks is a series of equations relevant to several geometrical parameters of the block. The block design method can not only provide guidance for inline cross-flow turbine design, but also indicate the main block geometrical parameters that affecting the turbine performance and offer inspirations for turbine improvement.

(1) Orientation angle of guide block  $\theta_0$ .  $\theta_0$  has effects on the shapes of both conversion block and guide block thus affects turbine performance. Firstly, with the variation of  $\theta_0$ , position of the guide block terminal will change correspondingly, which has a significant effect on the flow attack angle at the runner inlet, resulting in flow separations in blades passages on different levels [20]. Besides, the guide block with a bigger orientation angle can cover more returning blades, therefore the negative torque of water flow on the runner can be reduced. Finally, for a uniform runner inlet arc angle, position of the conversion block terminal also varies with the change of  $\theta_0$ , which has great effects on the water flow from the runner outlet.

(2) Runner inlet arc angle  $\lambda$ . The runner inlet arc angle  $\lambda$  affects the turbine

performance mainly by affecting the shape of conversion block. It is noted that the main function of the conversion block is to convert water head into flow kinetic energy, so for different  $\lambda$ , the converted water head is different and flow velocities at runner inlet also varies.

(3) It can be concluded that different block geometries can lead to different flow attack angles and velocities at runner inlet. Therefore, it is of vital importance to achieve a good matching between the blocks and the runner, otherwise shock loss may occur at the runner inlet and flow separation may exists in the blades passages, which has a negative impact on the overall performance of the inline cross-flow turbine.

## **4.2 Theoretical analysis of the cross-flow runner**

Runner is another key component for the inline cross-flow turbine as it captures torque from water flow and transmit the torque to the generator. Theoretical analysis of its working mechanism can offer inspirations for its geometrical improvement. This part starts from the derivation of turbine fundamental equations, which can be helpful to understanding the energy transformation inside the runner. In particular, the fundamental equations of cross-flow turbines are derived to obtain the expression of turbine efficiency, thus the influencing factors on the turbine performance can be analyzed.

### **4.2.1 Derivation of turbine fundamental equations**

The working mechanism of the runner can be described using Bernoulli's equation, which is actually an expression of energy conservation. For incompressible fluid and steady motion, the energy of a fluid streamline can be described as:

$$\frac{V^2}{2} + gz + \frac{p}{\rho} = C(\psi) \quad (4.19)$$

where  $\frac{V^2}{2}$  refers to kinetic energy;  $gz$  refers to potential energy;  $\frac{p}{\rho}$  refers to pressure energy;  $C(\psi)$  is the Bernoulli constant, which means total energy of the fluid streamline.

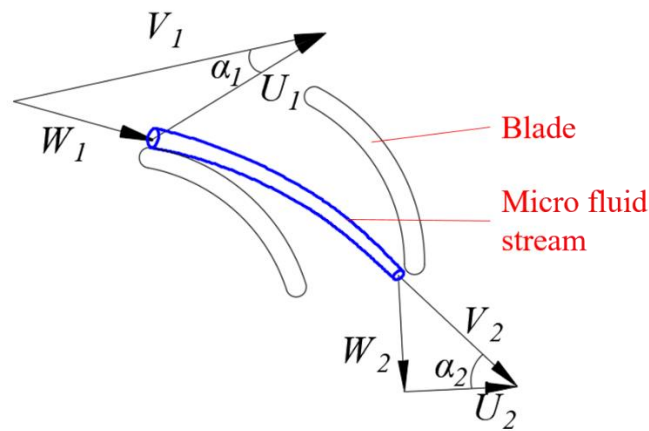


Fig.4.2 Micro fluid stream in the blades passage

To analyze the working principle of the runner, it is assumed that there is no water head loss throughout the runner. Water flow through the blades passages can be divided into a lot of micro fluid stream. As shown in Fig.4.2 is one micro fluid stream, based on Bernoulli's equation, the total energy of the micro fluid stream at blades passage inlet and outlet are:

$$e_1 = gz_1 + \frac{p_1}{\rho} + \frac{V_1^2}{2} \quad (4.20)$$

$$e_2 = gz_2 + \frac{p_2}{\rho} + \frac{V_2^2}{2} \quad (4.21)$$

The energy difference of the micro fluid stream between blades passage inlet and outlet can be regarded as the energy from micro fluid stream that captured by blades.

$$\Delta e = e_1 - e_2 = gz_1 + \frac{p_1}{\rho} + \frac{V_1^2}{2} - \left( gz_2 + \frac{p_2}{\rho} + \frac{V_2^2}{2} \right) \quad (4.22)$$

In addition, based on the Bernoulli's equation for relative motion:

$$gz_1 + \frac{p_1}{\rho} + \frac{W_1^2 - U_1^2}{2} = gz_2 + \frac{p_2}{\rho} + \frac{W_2^2 - U_2^2}{2} \quad (4.23)$$

where  $W_1$  is the relative flow velocity at the inlet of blades passage;  $W_2$  is the relative flow velocity at the outlet of blades passage;  $U_1$  and  $U_2$  are the velocities of the rotating reference system.

Combining Eqs.4.22 and 4.23:

$$\Delta e = \frac{W_2^2 - W_1^2}{2} - \frac{U_2^2 - U_1^2}{2} - \frac{V_2^2 - V_1^2}{2} \quad (4.24)$$

Based on the flow velocity triangle at the inlet of blades passage:

$$W_1^2 = V_1^2 + U_1^2 - 2V_1U_1 \cos \alpha_1 \quad (4.25)$$

Similarly, based on the flow velocity triangle at the outlet of blades passage:

$$W_2^2 = V_2^2 + U_2^2 - 2V_2U_2 \cos \alpha_2 \quad (4.26)$$

Combining Eqs.4.24-4.26, the following equation can be obtained:

$$\Delta e = V_1 U_1 \cos \alpha_1 - V_2 U_2 \cos \alpha_2 \quad (4.27)$$

Therefore, the theoretical power from the micro flow stream is:

$$dP_t = dQ\rho(V_1 U_1 \cos \alpha_1 - V_2 U_2 \cos \alpha_2) \quad (4.28)$$

For the whole flow through the blades passage, the theoretical power can be calculated by:

$$P_t = Q\rho(V_1 U_1 \cos \alpha_1 - V_2 U_2 \cos \alpha_2) \quad (4.29)$$

#### 4.2.2 Fundamental equations of cross-flow turbine

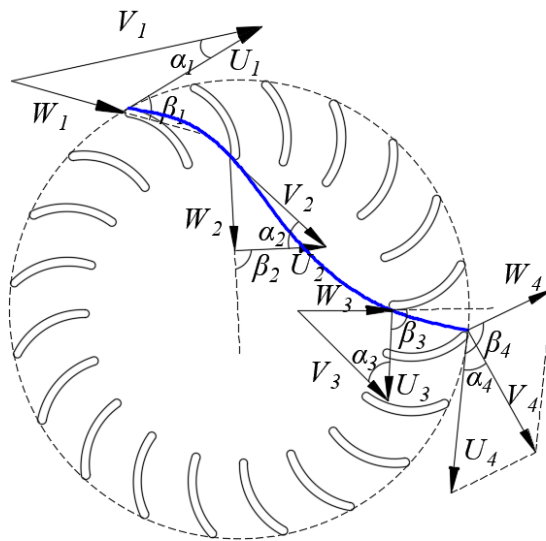


Fig.4.3 Flow streamline through the cross-flow runner

Fig.4.3 indicates the steady through the cross-flow runner. The unique characteristic of cross-flow turbine is that water flows through blades passages twice before leaving the runner. Therefore, the theoretical power of cross-flow turbine is composed of two parts: power from the first stage and the second stage. Based on

Eq.4.29, the theoretical power of cross-flow turbine can be calculated by:

$$P_{icft} = Q\rho(V_1U_1 \cos \alpha_1 - V_2U_2 \cos \alpha_2 + V_3U_3 \cos \alpha_3 - V_4U_4 \cos \alpha_4) \quad (4.30)$$

It is assumed that no energy loss in the space between the first and second stage.

Based on Fig.4.3, the following equations can be obtained:

$$V_2 = V_3 \quad (4.31)$$

$$U_2 = U_3 = \frac{D_2}{2} \omega \quad (4.32)$$

$$\alpha_2 = \alpha_3 \quad (4.33)$$

So, Eq.4.30 can be modified as:

$$P_{icft} = Q\rho U_1 (V_1 \cos \alpha_1 - V_4 \cos \alpha_4) \quad (4.34)$$

Based on the flow velocity triangles at the runner inlet and outlet:

$$V_1 \cos \alpha_1 = U_1 + W_1 \cos \beta_1 \quad (4.35)$$

$$V_4 \cos \alpha_4 = U_4 + W_4 \cos \beta_4 \quad (4.36)$$

$$\beta_4 = 180^\circ - \beta_1 \quad (4.37)$$

$$U_1 = U_4 = \frac{D_1}{2} \omega \quad (4.38)$$

Eq.4.34 can be further modified as:

$$P_{tft} = 2Q\rho U_1 (V_1 \cos \alpha_1 - U_1) \quad (4.39)$$

The input power can be calculated:

$$P_{in} = \rho g Q H_t = \rho Q V_1^2 / 2 \quad (4.40)$$

Then the theoretical efficiency can be obtained:

$$\eta_{tft} = P_{tft} / P_{in} = 4 \frac{U_1}{V_1} \cos \alpha_1 - 4 \left( \frac{U_1}{V_1} \right)^2 \quad (4.41)$$

Considering  $\frac{U_1}{V_1}$  and  $\alpha_1$  as the variables in Eq.4.41, taking a derivative with respect to the efficiency and letting the derivative equals to zero, then the following relationship can be obtained:

$$\frac{U_1}{V_1} = \frac{1}{2} \cos \alpha_1 \quad (4.42)$$

Hence the maximum turbine efficiency can be approximately calculated as:

$$\eta_{tmax} = \cos^2 \alpha_1 \quad (4.43)$$

In addition, based on the flow velocity triangle at the runner inlet which is showed in Fig.4.4, the relationship between  $U_1$  and  $V_1$  can be derived based on their geometrical relationship:

$$U_1 \sin \beta_1 = V_1 \cos(\alpha_1 + 90^\circ - \beta_1) \quad (4.44)$$

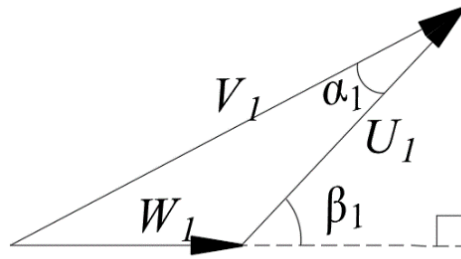


Fig.4.4 Flow velocity triangle at the runner inlet

Combing Eqs.4.42 and 4.44, the theoretical maximum efficiency of cross-flow turbine is obtained when:

$$\tan \beta_1 = 2 \tan \alpha_1 \quad (4.45)$$

The above equation reveals the relationship between flow attack and blades outer angle, and the relationship is widely used in research of many researchers.

### 4.2.3 Implications for runner optimization

The runner theoretical analysis reveals the working mechanism of the cross-flow turbine and provide a function for turbine efficiency assessment. In addition, the derivation process offers an understanding of the effects of runner geometries on the turbine performance and provide inspirations for runner improvement.

(1) Based on the obtained function about turbine efficiency, flow velocity and attack angle at the runner inlet and blades outer angle are three main parameters that affecting turbine performance. However, the flow velocity and attack angle are mainly determined by the blocks. Therefore, on the one hand, it is important to optimize the block design for turbine performance improvement. On the other hand, it is of vital importance to achieve a good matching between the blocks and the runner.

(2) The fact that attack angle can determine the turbine efficiency has been indicated by the literature review and many researchers have suggested the optimal values of attack angle based on their numerical or experimental results. However, due to the large range of operating conditions, it is still far away to have a unique optimal value for the attack angle. Hence, for different cases, the optimal attack angle should be obtained by comparing the performance of models with different attack angles using numerical or experimental methods.

(3) In the derivation process, friction and head loss through the runner are neglected. However, losses caused by friction and hydraulic shock are inevitable. For different attack angles, there are different corresponding blades outer angles and blades curvatures, resulting in different friction and shock losses. Besides, for different blades number, the area of blades passages is varying, resulting in different friction losses. Therefore, it is necessary to analyze the flow characteristics inside the runner to investigate the effects of runner geometrical parameters on turbine performance.

### 4.3 Main geometrical parameters of the blades

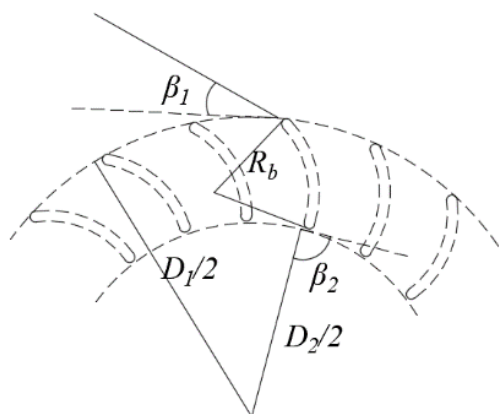


Fig.4.5 Blades geometrical parameters of the cross-flow runner

As indicated in Fig.4.5 is the blades geometry of the cross-flow turbine. The key

geometrical parameters of blades include outer blade angle  $\beta_1$ , inner blade angle  $\beta_2$  and blade radius  $R_b$ . Among them, the optimal values of  $\beta_1, \beta_2$  can be determined based on the simulations results. the blade radius  $R_b$  can be calculated by:

$$R_b = \frac{D_1^2 - D_2^2}{4D_1 \cos \beta_1} \quad (4.46)$$

It can be observed from the above equation that the blades shape can not only be affected by the blades outer angle, but also be determined by the runner inner and outer diameter. Which means after the determination of  $\beta_1$  and  $D_1$ , the runner diameter ratio  $D_2/D_1$  will also influence the blades shape. So, it is also very important to study the effects of  $D_2/D_1$  on the performance of the cross-flow turbine thus determine the optimal value finally.

#### 4.4 Summary

This chapter presents a mathematic design method for blocks in inline cross-flow turbine. Moreover, the theoretical working principle of the runner is also introduced to provide guidance for runner parameter optimization. The main works of this chapter are summarized as follows.

(1) The mathematic design method for the block design was developed based on fluid continuity and energy conservation. The proposed mathematic design method for the blocks is a series of equations relevant to several geometrical parameters of the block and it is supposed to provide design guidance for the ducted elements of inline cross-flow turbines.

(2) Based on the proposed block design method, the guide block orientation angle

and runner inlet arc angle have great impacts on the block shapes. It is necessary to study the effects of these two parameters on the turbine output power, water head loss and flow characteristics.

(3) Using Bernoulli's equation, the working mechanism of cross-flow runner was analyzed and the expression of theoretical turbine performance was obtained, which offers guidance for further research. It is suggested to determine the optimal runner parameters, including blades outer angle, runner diameter ratio and blades number, by comparing the performance of different turbine models using numerical or experimental methods.

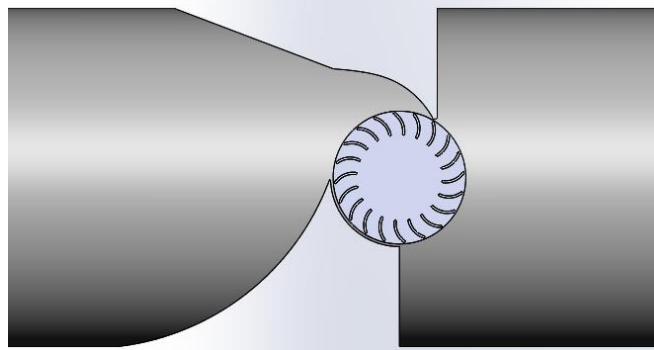
(4) Based on the analysis of this chapter, the blocks can determine the flow velocity and attack angle at the runner inlet, while the flow velocity and attack angle can influence the blades shapes and turbine efficiency, the runner design should match with the block design to achieve the best turbine performance.

# **CHAPTER 5 NUMERICAL STUDY ON THE EFFECTS OF GUIDE BLOCK ORIENTATION ANGLE ON THE PERFORMANCE OF INLINE CROSS-FLOW TURBINE**

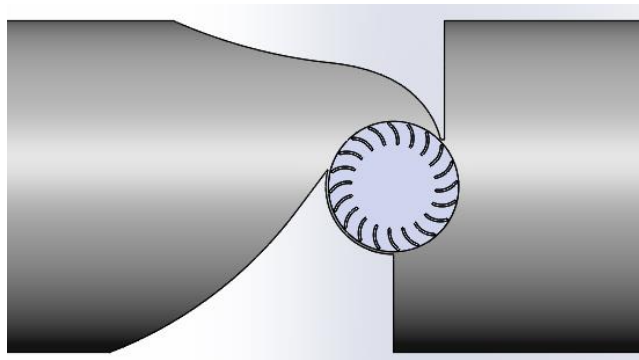
In the previous chapter, a design method for the block is proposed. The main function of the blocks is to direct water flow to the turbine and convert part of the water head into flow kinetic energy, so a better block design can lead to a higher turbine performance. As suggested in the previous chapter, the guide block orientation angle and runner inlet arc angle have great impacts on the block shapes, this chapter presents the numerical study of guide block orientation angle on the turbine performance. Specifically, numerical investigations are carried out to verify the proposed method and study the effects of different block designs on turbine performance. Three turbine models with different guide block orientation angles are built and simulated to study the impacts of guide block orientation angle on the output power, water head reduction, flow characteristics, pressure distribution and power output of each runner stage. A comparison of three models with different guide block orientation angles reveals that the model with the largest conversion block orientation angle performs best, because the blocks from this model not only function better in terms of flow separation and negative torque reduction at the first stage, but also convert more water head into kinetic energy. Numerical results show that the inline turbine can achieve its maximum efficiency of 42.4% with a power output of about 1500 W and that the water head reduction is limited within an acceptable range.

## 5.1 Physical turbine models with different guide block orientation angles

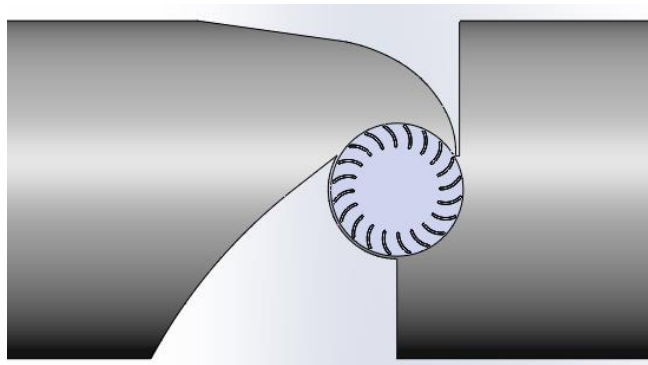
angles



(a)  $\theta_0 = 0^\circ$



(b)  $\theta_0 = 15^\circ$



(c)  $\theta_0 = 30^\circ$

Fig.5.1 Turbine models with different guide block orientation angles

Three turbine models (as shown in Fig.5.1) are obtained using the mathematic design method by varying the guide block orientation angle. The guide block orientation angles of these three models are  $0^\circ$ ,  $15^\circ$  and  $30^\circ$ , respectively. In these three models, the runner inlet arc angle keeps  $120^\circ$ . As the turbine model is symmetric, only one symmetric part is modeled.

## 5.2 Meshing and numerical setup

In this part, the three physical models were built in SolidWorks 2014 and the meshing strategy is same with that in Part 3.2, However, as the turbine model has been redesigned, it is necessary to study the effects of meshing number on computing accuracy to minimize numerical uncertainty.

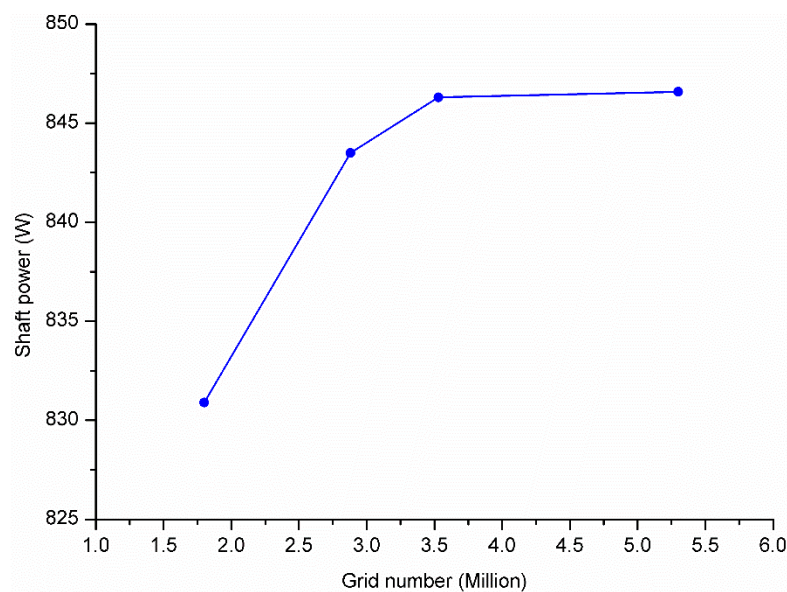


Fig.5.2 Grid independence test results

The grids were generated using ANSYS ICEM 14.5, as the geometries of the turbine body and runner were highly complex because of the curved walls and narrow tip regions, so in the meshing process, a “tetra mesh” was used to generate grids in domains far from boundaries, and a “prism mesh” was used for grid generation in

domains near boundaries, such as the pipe wall and blades. A grid independence test was conducted to measure the output shaft power at the runner rotating speed of 300 rpm. Four meshing schemes were tested with grid numbers of 1.82, 2.88, 3.77 and 5.31 million. Fig.5.2 shows the grid independence test results. Based on these results, the total grid number of 3.77 million was taken for the next study. Fig.5.3 shows the final computational mesh.

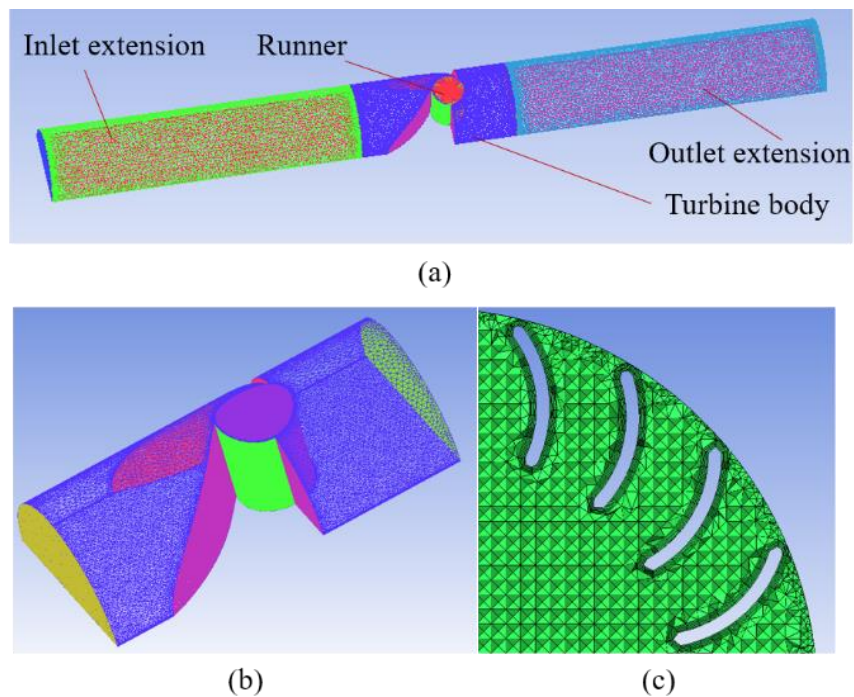


Fig.5.3 Final meshing scheme: (a) Meshing of the whole computational domain; (b) Meshing of the turbine body; (c) Zoomed view of the blades meshing

SST  $k-\omega$  model is used for CFD simulations as this model combines the standard  $k-\omega$  model and standard  $k-\varepsilon$  model and takes the effects of turbulence shear stress into consideration in the definition of turbulence viscosity and can capture the micro flow in the viscous layer. The simulations were conducted in ANSYS Fluent 14.5 using a second-order-accurate finite-volume discretization scheme, and the target RMS was set to  $10^{-5}$ . The inlet and outlet boundary conditions were determined based

on the working conditions in the water mains. Flow velocity and water head are the main parameters for turbine design, and the downstream water head on the turbine is an important issue for assessment of the influence of turbine application on the normal water supply. The inlet velocity is considered as the inlet boundary condition of the inlet face, whereas the outlet boundary condition is set as the pressure outlet. In addition, the boundary condition of the turbine wall, blocks, and blades was set as a smooth non-slip wall.

### 5.3 Data analysis

This study aims to investigate the effects of different block designs on turbine performance, and mainly uses the numerical method. In the simulation process, the water head at the inlet and outlet boundary and the torque of the runner were recorded for turbine performance assessment. The simulated performance parameters of water head loss  $\Delta H$ , output shaft power  $P_{shaft}$ , input power  $P_{in}$  and turbine efficiency  $\eta$  can be calculated by the following equations:

$$\Delta H = H_{in} - H_{out} \quad (5.1)$$

$$P_{in} = \rho g \Delta H Q \quad (5.2)$$

$$P_{shaft} = T \omega \quad (5.3)$$

$$\eta = \frac{P_{shaft}}{P_{in}} \quad (5.4)$$

where  $H_{in}$  is the water head at inlet boundary, m;  $H_{out}$  is the water head at outlet boundary, m;  $\omega$  is the rotational speed, rad/s;  $T$  is the torque of the runner, N·m;  $\rho$

is water density,  $\text{kg/m}^3$ ;  $g$  is acceleration of gravity,  $\text{m/s}^2$ ;  $Q$  is the water volume flow rate,  $\text{m}^3/\text{s}$ .

## 5.4 Results analysis and discussion

In this part, a series of simulations were conducted to understand the function of the block and the effects of different block designs on turbine performance. The simulations were conducted at different TSRs under the flow velocity of 1.5m/s. The numerical results can provide us an in-depth understanding about the influencing mechanism of guide block orientation angle on the turbine performance.

### 5.4.1 Output power and efficiency of the turbine

Fig.5.4 and Fig.5.5 indicate the output power and efficiency of the three different models. The output power and efficiency both increase as the TSR increases until they reach maximum value, then decrease. In terms of output power, the maximum value of the model with  $\theta_0 = 0^\circ$  occurred when TSR was 0.9, whereas the other two models had their maximum output power at a TSR of 1. It can also be observed that as  $\theta_0$  increases, the maximum output power also increases significantly. For example, the maximum output power of the model with  $\theta_0 = 30^\circ$  was greater by 422 W (nearly 35%) than that of the model with  $\theta_0 = 0^\circ$ . From the perspective of efficiency, the pattern of variation is similar to that for output power. However, the best efficiency of all the models was seen at a TSR of 0.7. Among the three models, the model with  $\theta_0 = 30^\circ$  had the best efficiency among the other two models, and its best efficiency was 42.4%. In conclusion, the orientation angle of the guide block does affect the turbine output power and efficiency. The reasons for this difference will be analyzed

next.

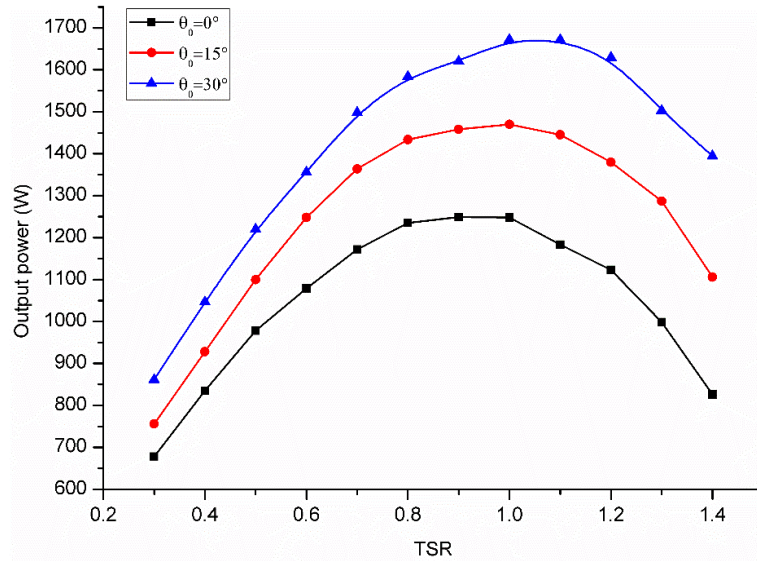


Fig.5.4 Output power of inline turbines with different blocks

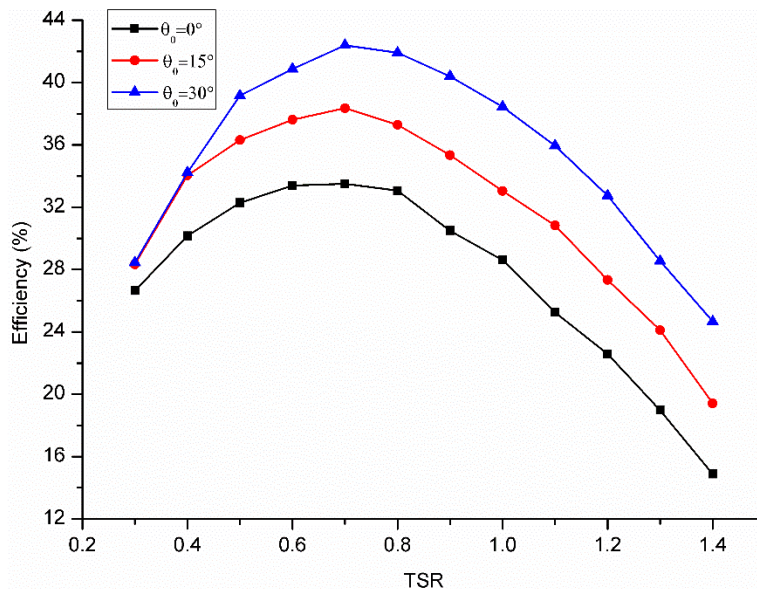
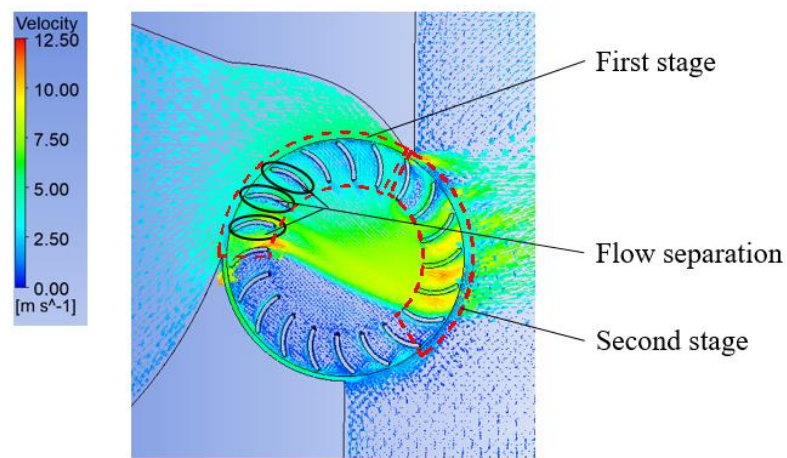


Fig.5.5 Efficiency of inline turbines with different blocks

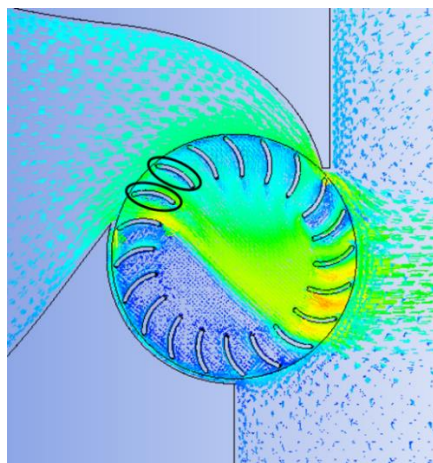
### 5.4.2 Analysis of flow characteristics

To investigate the reasons for the performance difference of the three models, their flow characteristics were analyzed because they play an important role in determining turbine performance. In this study, the flow velocity vectors in the block

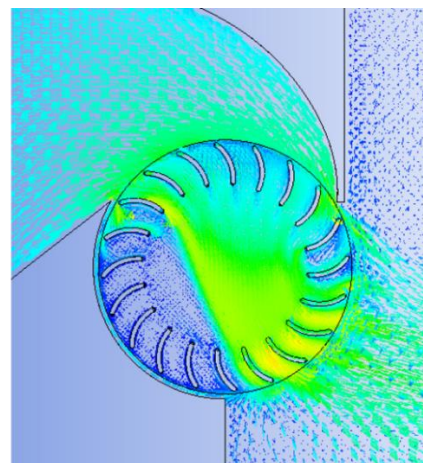
and runner domains and the flow velocity and angle at the runner inlet are emphasized. Fig.5.6 indicates the flow velocity vectors of the three models at a TSR of 0.7. In all these models, the block improves the flow velocity through the runner, which means the block increases the kinetic energy of water flow. The flow velocity in the second stage is higher than in the first stage, because the blade passages in the first stage are converging and the water flow accelerates before entering the blade passages of the second stage.



(a)  $\theta_0 = 0^\circ$



(b)  $\theta_0 = 15^\circ$



(c)  $\theta_0 = 30^\circ$

Fig.5.6 Flow velocity vectors of the three models at a TSR of 0.7

The ideal flow through the runner of a cross-flow turbine is expected to be parallel to the blade surface. However, it can be noticed that in Fig.5.6(a) and (b), flow separations occur in the first stage of the models with  $\theta_0 = 0^\circ$  and  $\theta_0 = 15^\circ$ . Flow separation is caused by a mismatch between flow attack angle and blade inlet angle and has a negative effect on turbine performance. Flow separation can not only cause hydraulic loss, but also have a negative influence on the quality of water flow in the second stage [20]. Compared to the other models, the model with  $\theta_0 = 30^\circ$  has a better flow field, and only slight flow separation occurs in the blade passages. The main reason for this phenomenon is that the guide block of the model with  $\theta_0 = 30^\circ$  covers a greater area of the runner and functions better in directing water flow, leading to a better match between the flow attack angle and blade inlet angle. It can also be observed that no flow separation occurs in the second stage of all three models, because the flow velocity at the entrance of the second stage is slightly increased due to the converging blade passages in the first stage.

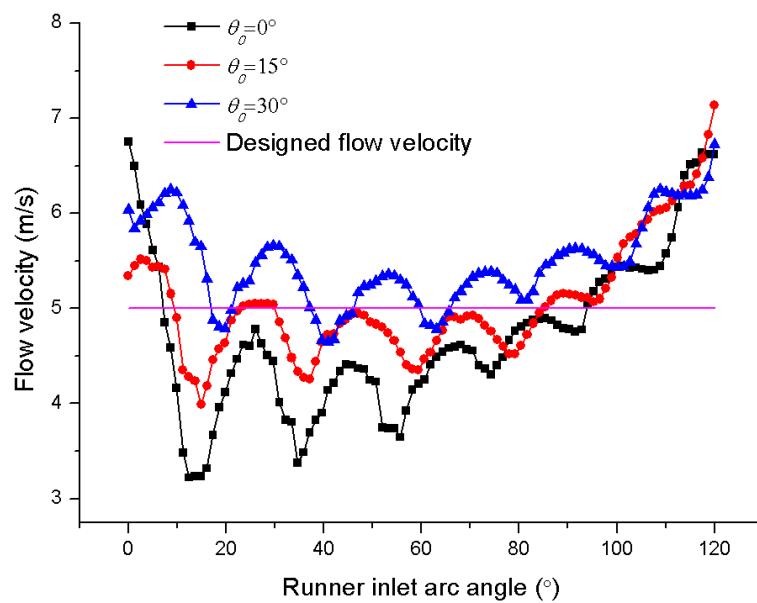


Fig.5.7 Computed and designed flow velocity along the runner inlet arc

Fig.5.7 shows the computed and designed flow velocity distribution along the runner inlet. Note that the designed flow velocity is determined based on the hypothesis that the conversion block transfers all the water head into flow kinetic energy, as expressed by Eq.4.4. It is obvious from Fig.5.7 that the computed flow velocity of all three models fluctuates sharply along the runner inlet arc. At the opening of the runner inlet, the flow velocity is relatively high, possibly because the opening of the runner inlet is also the terminal of the guide block, where jet flow is easily formed. It can be observed that in the angle range from  $20^\circ$  to  $90^\circ$  of the runner inlet arc, the flow velocity of the model with  $\theta_0 = 30^\circ$  fluctuates around the designed flow velocity, which means the conversion block can convert nearly all the reduced water head into flow kinetic energy and fulfill its intended function. The flow velocities of the models with  $\theta_0 = 15^\circ$  and  $\theta_0 = 0^\circ$  in the same runner inlet arc angle range are all less than the designed flow velocity. The reason is that the runner inlet areas covered by the conversion block in these two models are relatively small; as a result, the conversion block cannot fully achieve its function. It is interesting to note that at the terminal of the runner inlet, the flow velocities of all three models increase sharply. The main reason for this phenomenon is the tip clearance between the conversion block and runner, and leakage through the tip clearance may increase the flow velocity.

Fig.5.8 shows the computed flow inlet angle along the runner inlet and blades outer angle. A significant difference can be seen between the computed flow inlet angle and blades outer angle, especially in the angle range from  $0^\circ$  to  $40^\circ$  of the runner inlet arc. Comparing these three models, the difference in the models with  $\theta_0 = 15^\circ$  and  $\theta_0 = 0^\circ$  is greater than in the model with  $\theta_0 = 30^\circ$ , which explains the existence and variation of flow separations indicated in Fig.5.6. It can also be observed that the

difference decreases as  $\theta_0$  increases, which results from the fact that the guide block in models with greater  $\theta_0$  can cover more runner inlet area than toward the flow direction and better direct the water flow. In the angle range from  $60^\circ$  to  $120^\circ$  of the runner inlet arc, the inlet angle of all three models remains stable around  $25^\circ$ , which is much smaller than the blade inlet angle. To further enhance inline turbine performance, the blade design should be improved for a better matching with the proposed block design; this possibility will be investigated in the following chapters.

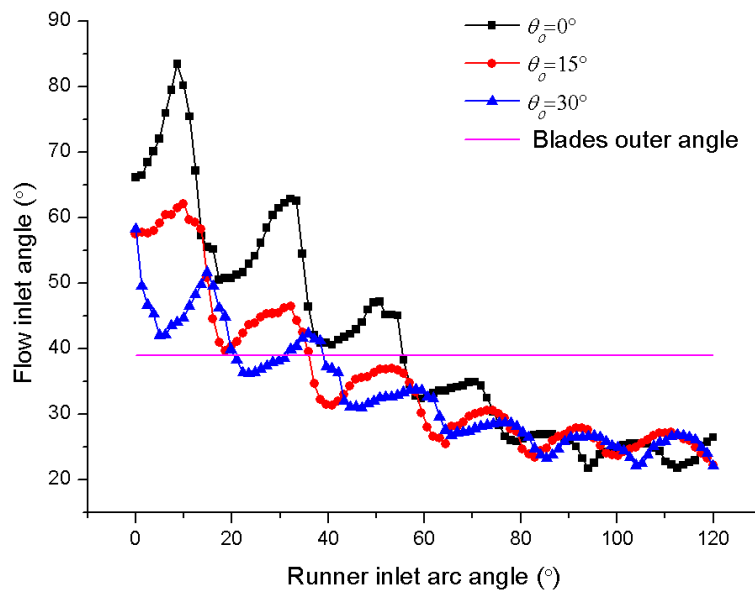
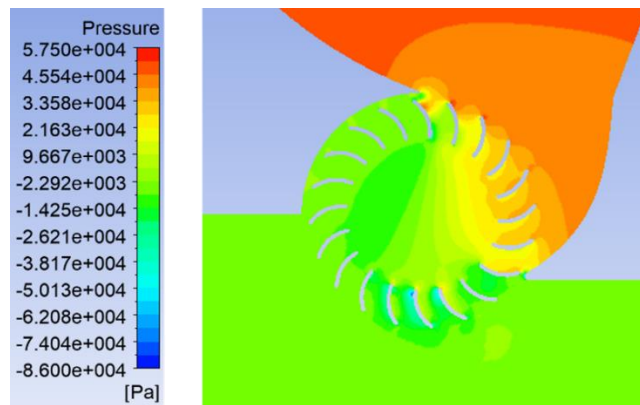


Fig.5.8 Computed flow inlet angle along the runner inlet arc

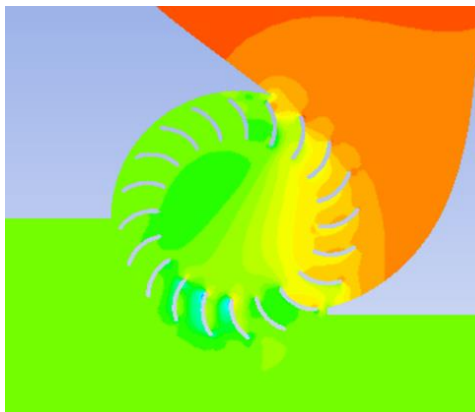
### 5.4.3 Analysis of pressure distribution

Fig.5.9 shows the pressure contours in the flow field of the conversion block and runner in the three models. In all three models, the blocks function as a convergence nozzle, while the downstream side functions as a diffuser. The water pressure at the upstream side of the runner is higher than on the downstream side, leading to a pressure difference that can draw in more water and increase the flow velocity. Usually, the runner blades rotate from the pressure side to the suction side because of the force of

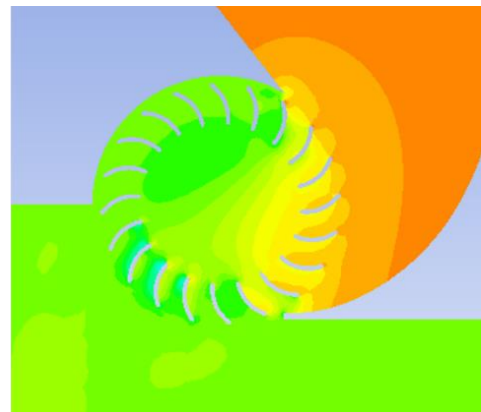
water from the pressure side. However, it can be observed that small high-pressure regions occur at the leading edge of the suction side of the first few blades at the first stage of all three models, which has a negative impact on runner torque output. A comparison of the pressure contours of three models shows that high pressure regions shrink with the increase of  $\theta_0$ , because the guide block's function of directing water flow is significantly enhanced with the increment of  $\theta_0$ . A pressure difference exists between the pressure side and suction side of the remaining blades at the first and second stage, leading to the normal torque output of the runner.



(a)  $\theta_0 = 0^\circ$



(b)  $\theta_0 = 15^\circ$



(c)  $\theta_0 = 30^\circ$

Fig.5.9 Pressure contours of the three models at a TSR of 0.7

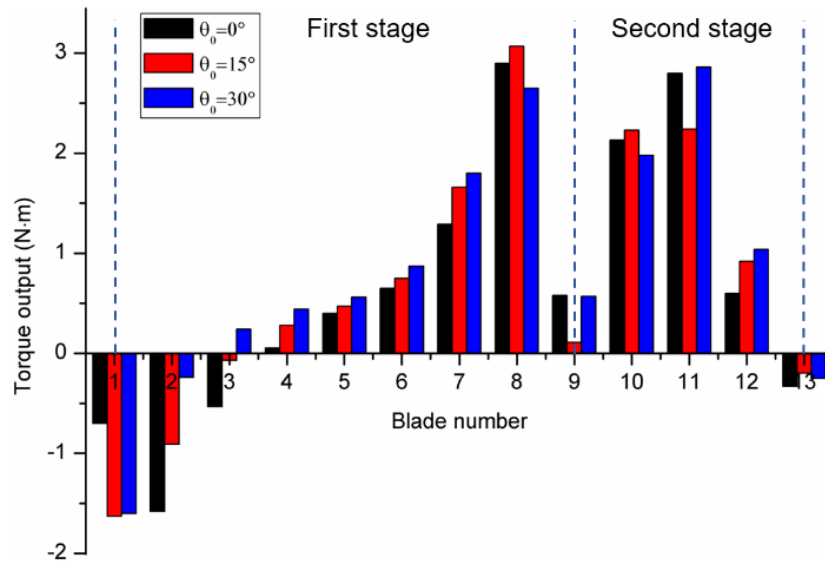


Fig.5.10 Torque output of each blade at the first and second stage

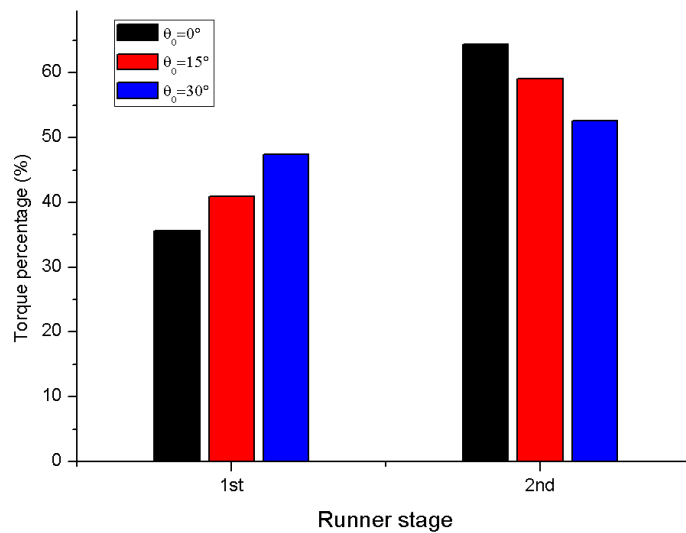


Fig.5.11 Torque output of different stages

Fig.5.10 illustrates the torque output of each blade at the first and second stage. The torque output of the first three blades at the first stage is negative or very small, which is consistent with the pressure distribution in Fig.5.9. After that, the torque extraction of the blades undergoes a significant increase. Among the three models, the model with  $\theta_0 = 30^\circ$  offers good performance in terms of blade torque extraction. Fig.5.11 compares the torque output of the first and second runner stage. It is clear that

in the three different models, the torque output at the second stage is higher than that at the first stage, mainly for the following reasons. Firstly, the flow inlet angle has a good matching with the blade inlet angle at the second stage, and no flow separation is found in the blade passages. Secondly, the water flow accelerates slightly before entering the second stage, because of the converging blade passages in the first stage. The torque output at the first runner stage increases by 12% when  $\theta_0$  increases from  $0^\circ$  to  $30^\circ$ , mainly because in models with larger  $\theta_0$ , the guide block performs better in reducing high pressure regions on the blades' suction side, thus the conversion block can convert more water head into kinetic energy.

#### **5.4.4 Water head reduction**

Water head reduction is a major consideration when applying hydro turbines in water mains, because excessive water head loss will influence normal water supply. Fig.5.12 shows the numerical water head reduction of the three models, which indicates that these three models have similar performance in water head reduction. At the best efficiency (TSR=0.7) the water head reduction of the three models is less than 5m water. The Water Supplies Department of Hong Kong has indicated that a water head reduction of 5 m is within the acceptable range. To further show the functioning of the proposed block, Fig.5.13 shows the water head reduction caused by the conversion block. It is assumed that water head loss caused by friction or shock can be ignored, so the water head reduction in the conversion block is all converted into kinetic energy. As shown in Fig.5.13, the water head reduction caused by the conversion block in the models with  $\theta_0 = 0^\circ$ ,  $\theta_0 = 15^\circ$ , and  $\theta_0 = 30^\circ$  is around 0.7, 0.85, and 1.1 m, respectively, whereas the ideal value is 1.15 m. The results further demonstrate the superior performance of the inline turbine model with  $\theta_0 = 30^\circ$ .

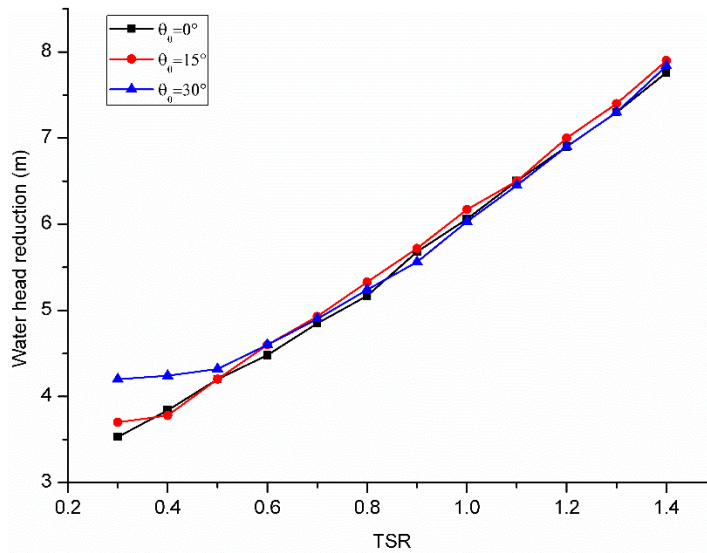


Fig.5.12 Water head reduction of the three models

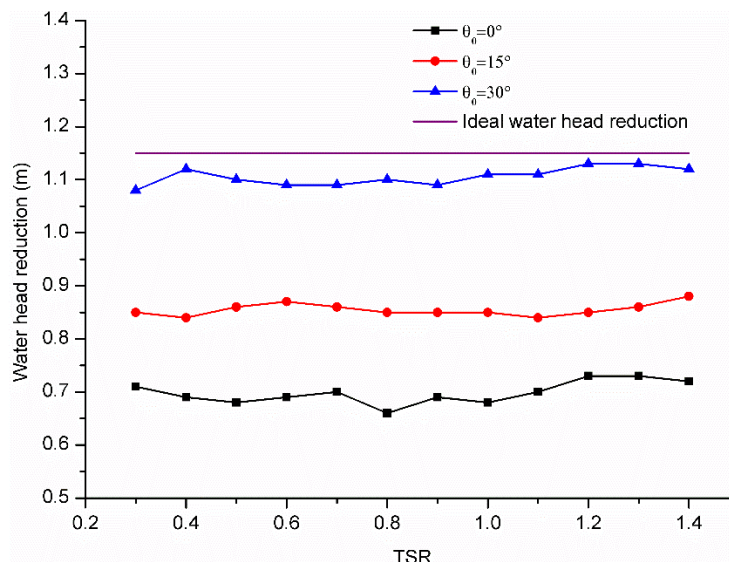


Fig.5.13 Water head reduction caused by the conversion block

## 5.5 Summary

In this chapter, three models were established using the proposed block design method. The effects of different block designs on turbine performance were studied using numerical methods. The output power, efficiency, flow field characteristics, and water head reduction were analyzed to verify the proposed method and analyze the

functions of the blocks. Based on this study, the following conclusions can be stated:

(1) The proposed design method is effective for inline cross-flow turbine design. Numerical results showed that the inline turbine could reach its maximum efficiency of 42.4% with about 1500 W power output.

(2) The blocks play an important role in performance enhancement of inline cross-flow turbines, because they convert part of the water head into kinetic energy, leading to a high flow velocity through the runner.

(3) The pressure distribution inside the inline turbine is considerably improved by improving the block design. The high-pressure regions on the suction side of the first several blades at the first stage could be reduced, and the torque output of the first stage nearly doubled after block improvement.

(4) The numerical results showed that the proposed inline turbine could be applied in water mains without affecting normal water supply because the water head reduction through the turbine was within the acceptable range.

(5) Among the models with  $\theta_0 = 0^\circ$ ,  $\theta_0 = 15^\circ$  and  $\theta_0 = 30^\circ$ , the model with  $\theta_0 = 30^\circ$  performed better than the other two. In this model, the blocks not only reduced negative torques at the runner in the first stage, but also converted more water head into kinetic energy.

(6) The research results could provide guidance for the on-site application of inline cross-flow turbines. The block shape can be determined based on different working conditions (i.e., flow rate, water head, and power demand), which will significantly contribute to the turbine's use around the world.

# **CHAPTER 6 NUMERICAL STUDY ON THE EFFECTS OF RUNNER INLET ARC ANGLE ON THE PERFORMANCE OF INLINE CROSS-FLOW TURBINE**

The guide block orientation angle and runner inlet arc angle are two key parameters that affect the shape and function of the blocks in inline cross-flow turbine. In the previous chapter, the effects of guide block orientation angle on turbine performance has been investigated and an optimal value was obtained. In this chapter, numerical study on the effects of runner inlet arc angle is performed. In particular, four models with different runner inlet arc angles are developed. The turbine's performance, function of conversion block, flow velocity characteristics, pressure distribution and blades torque output of the models are then analyzed. Results indicate that a smaller runner inlet arc can increase the flow velocity at runner inlet and pressure difference between the upstream and downstream of the runner, resulting in a higher output power but also a higher overall water head reduction through the turbine. Besides, it is found that the runner inlet arc angle has a significant influence on the power output of runner second stage. With the increase of runner inlet arc angle, the torque output at the second stage encounters a gradual decrease. To achieve a good balance between turbine efficiency and water head reduction, the suggested runner inlet arc angle is  $105^\circ$ . Numerical results show that the model with  $105^\circ$  runner inlet arc angle could produce a maximum power generation efficiency of 42.6% with about 1600W power output.

## 6.1 Physical turbine models with different runner inlet arc angles

To study the impact of different runner inlet arc angles on the turbine performance, four physical models of the inline cross-flow turbine are built using Solidworks 2014 based on the proposed design methods. Fig.6.1 shows the models studied in this research, the runner inlet arc angles of case 1-4 are  $90^\circ$ ,  $105^\circ$ ,  $120^\circ$  and  $135^\circ$ , respectively. In this part, the three physical models were discretized in Ansys ICEM 14.5 and the meshing strategy is same with that in Part 5.2.

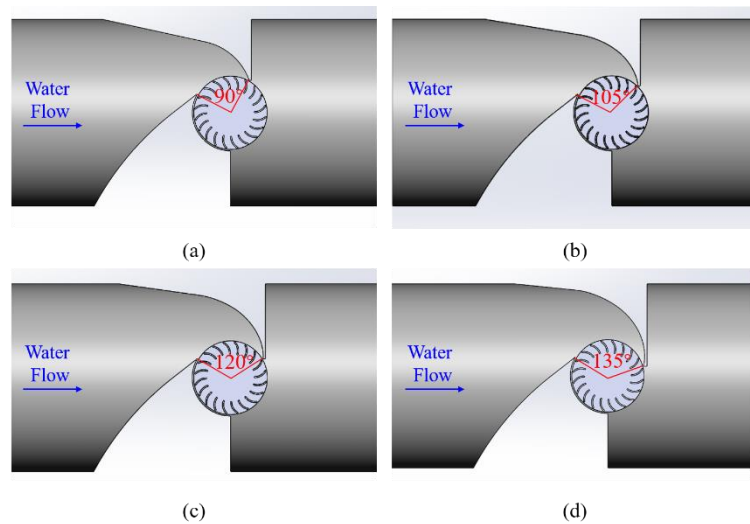


Fig.6.1 Physical models of the inline cross-flow turbine (a) Case 1:  $\lambda=90^\circ$  (b) Case 2:  $\lambda=105^\circ$  (c) Case 3:  $\lambda=120^\circ$  (d) Case 4:  $\lambda=135^\circ$

## 6.2 Results analysis and discussion

### 6.2.1 Numerical turbine performance

To fully study the effects of different runner inlet arc angles on the inline cross-flow turbine performance, the numerical models were simulated at different TSRs under the flow velocity of 1.5m/s. Fig.6.2-6.4 show the output power, water head reduction through the turbine and efficiency of the four cases, respectively. With the increase of TSR, the output power of four cases increases until reaching maximum,

then decrease. By comparing the curves in Fig.6.2, the turbine output power decreases with the increase of runner inlet arc angle. For example, when  $\lambda=90^\circ$ , the maximum output power is about 2013W, nearly 26% higher than that of the model with  $\lambda=135^\circ$ . Besides, the maximum output power of the four cases occurs when TSR equals to 1.1, 1.0, 1.0 and 0.9, respectively.

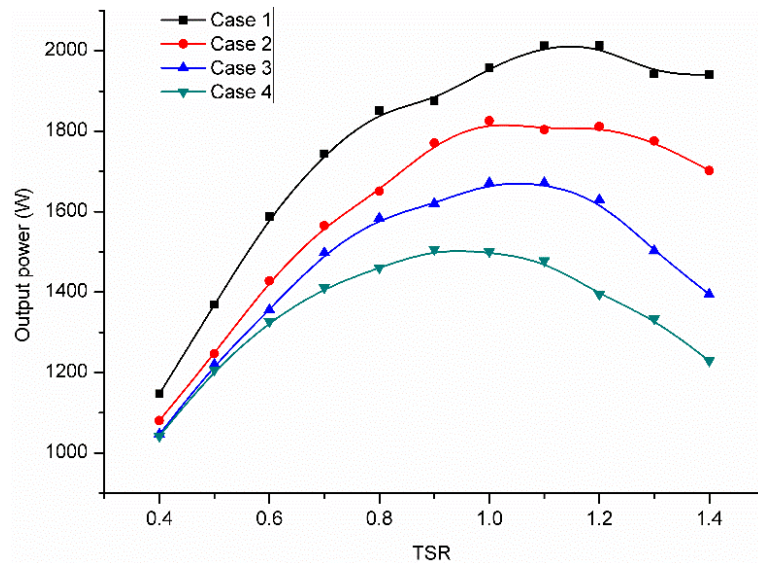


Fig.6.2 Output power of different cases

Fig.6.3 shows the water head reduction through the turbines with different runner inlet arc angle. The water head reduction of all the four cases increases gradually with the increase of TSR. However, it can be observed that, while Cases 2-4 have the similar water head reduction. In term of efficiency, the four cases have the same trend. The maximum efficiency of Case 1 occurs when TSR is 0.8 while Cases 2-4 get their maximum efficiency at TSR of 0.7. Among the four cases, the overall efficiency of Case 4 is the poorest, only around 39%, for the other cases, the efficiency difference is relatively slight. Case 2 has a better efficiency than the other three models, with the maximum value of 42.6% and the corresponding output power is about 1565W. It can be concluded that with the increase of runner inlet arc angle, the best efficiency of

inline cross-flow turbine first rises then falls. Besides, Case 2 also keeps a high efficiency in a wide range of TSR. As observed in Fig.6.3, at the best efficiency TSR, the water head reduction of Cases 2-4 is around 5m water, which satisfies the requirement of the WSD very well. In conclusion, to achieve a good balance between turbine efficiency and water head reduction, Case 2 is the best model among the four studied cases.

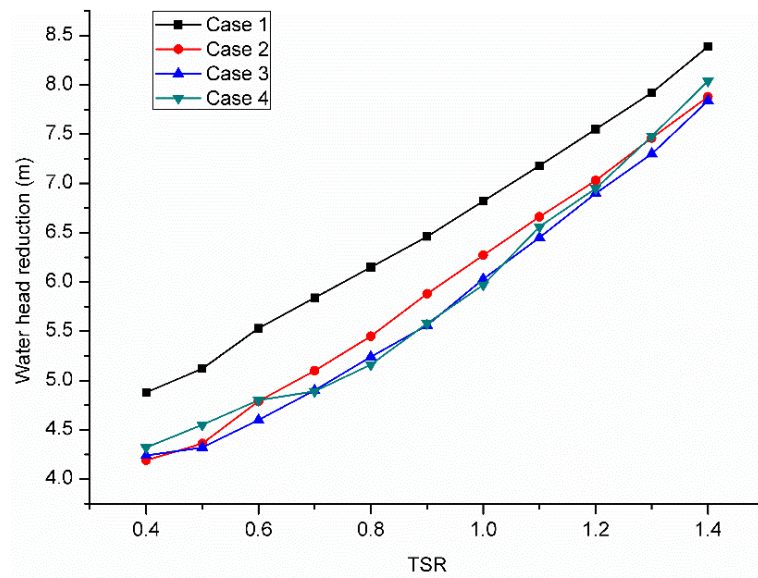


Fig.6.3 Water head reduction of different cases

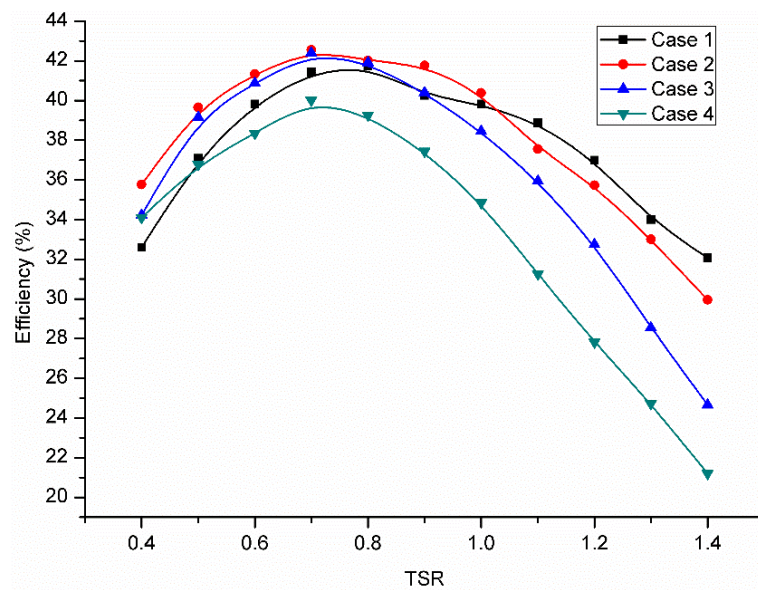


Fig.6.4 Efficiency of different cases

## 6.2.2 The function of the conversion block

As described in Chapter 2, the main function of conversion block is to convert part of the water head into kinetic energy. To analyze the effect of runner inlet arc angle on the function of conversion block, water head reduction through the conversion blocks of four cases are indicated in Fig.6.5. In the analysis, the friction and hydraulic loss are ignored, so the reduced water head through the conversion block is converted into kinetic energy completely. As shown in Fig.6.5, the overall variation trend is that the converted water head rises gradually with the increase of TSR. The case with a smaller runner inlet arc angle can convert more water head. For instance, in Case 1, the conversion block converts 1.35m water head into kinetic energy at TSR of 0.7, while in Case 4, the value is only 0.9m. The variation of converted water head with runner inlet arc angle also provides explanations for the difference of output power and water head reduction in the cases.

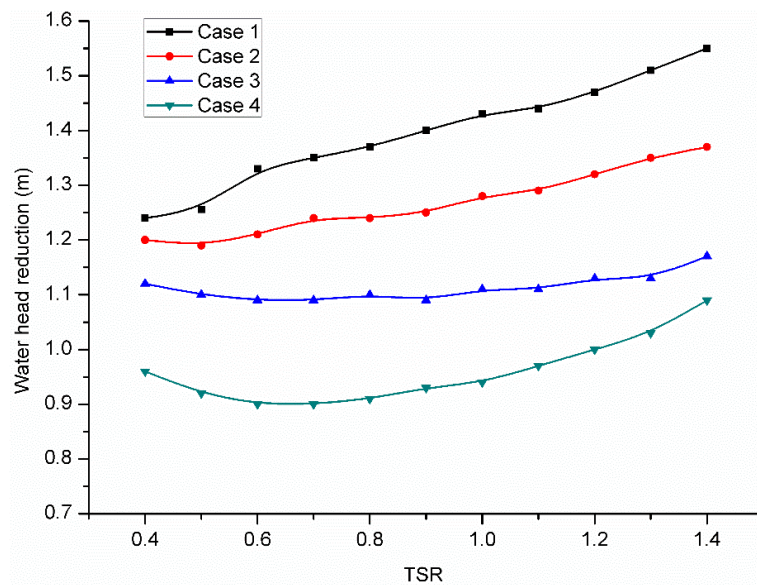


Fig.6.5 water head reduction through conversion block

### 6.2.3 Flow velocity characteristics

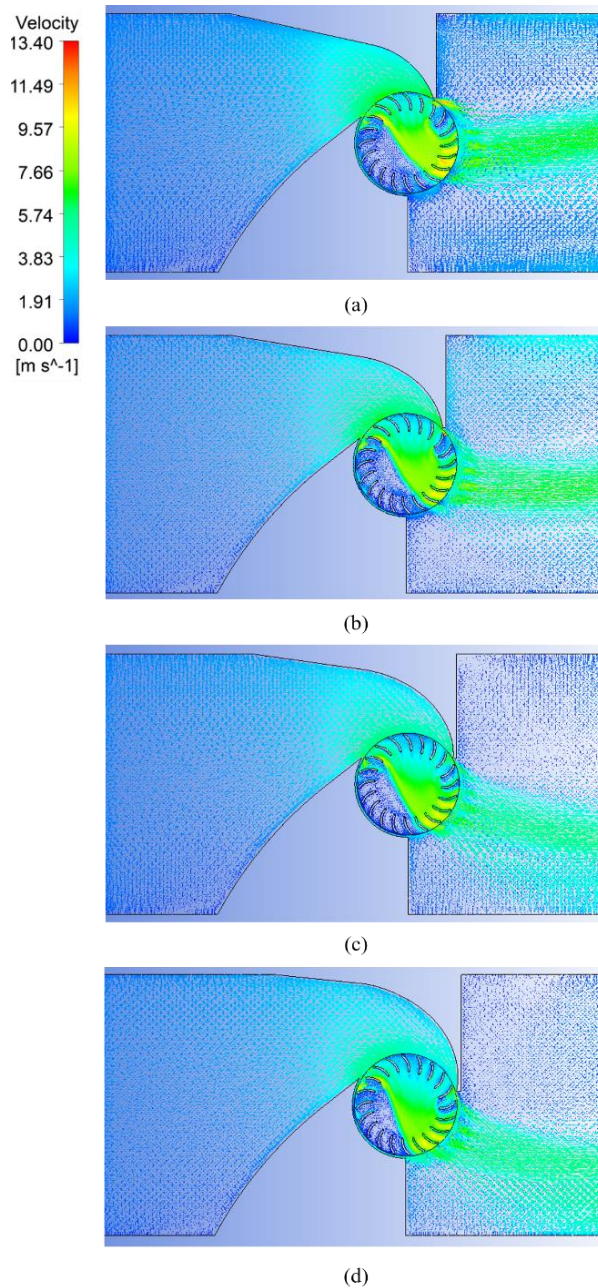


Fig.6.6 Velocity vectors showing water flow through the inline cross-flow turbine

(a) Case 1:  $\lambda=90^\circ$  (b) Case 2:  $\lambda=105^\circ$  (c) Case 3:  $\lambda=120^\circ$  (d) Case 4:  $\lambda=135^\circ$

The flow velocity characteristics through the proposed inline cross-flow turbine are studied to evaluate the influencing mechanism of runner inlet arc angle on turbine performance. As all the four cases get the best efficiency when TSR equals to 0.7 or

0.8, the flow fields at TSR of 0.7 are analyzed in this research. Fig.6.6 shows the velocity vectors distribution inside the cross-flow turbine, it can be seen clearly that the proposed blocks have a good function in directing the water flow and enhancing the flow velocity before entering the runner. It can be observed that runner inlet velocity in Case 1 is higher than the other three cases, which means the blocks in Case 1 can convert more water head into kinetic energy.

The main feature of cross-flow turbine is that the water flow passes twice through the runner and does work twice on the blades. As shown in Fig.6.6, the flow velocity in the second stage is higher than that in the first stage as the blades passage in the first stage is converging and the flow velocity is slightly accelerated after leaving the first stage. Comparing the velocity vectors of Cases 1-4, in a case with bigger runner inlet arc angle, the water flow passes through more blades, this phenomenon indicates that runner inlet arc angle has an impact on the power output of each blade and stage and this issue will be discussed in the following part.

Fig.6.7 indicates the flow velocity distribution along the runner inlet arc of the four cases. To compare the velocities of four cases, the variable of  $x$  axis in Fig.6.7 is the position of runner inlet arc. The flow velocity at the runner inlet arc of the cases fluctuates significantly in the range from 4.5-6.5m/s, but it can be observed that the mean velocity reduces slightly with the increase of runner inlet arc angle. After calculation, the mean runner inlet velocity of Case 1-4 is 6.01, 5.79, 5.36 and 5.12 m/s, respectively. The difference between runner inlet velocities also explains why the power output of Case 1 is the highest among four studied cases. As the flow velocity at runner inlet is a crucial factor in affecting the performance of cross-flow turbine, it can be concluded that the runner inlet arc angle plays an important role in influencing

the performance of inline cross-flow turbine by determining the runner inlet velocity. It is interesting to note in Fig.6.7 that the flow velocity at the end of runner inlet arc increases significantly in all the cases. The main reason for this phenomenon is the existence of tip clearance between conversion block and runner and leakage through the tip clearance may accelerate the flow velocity.

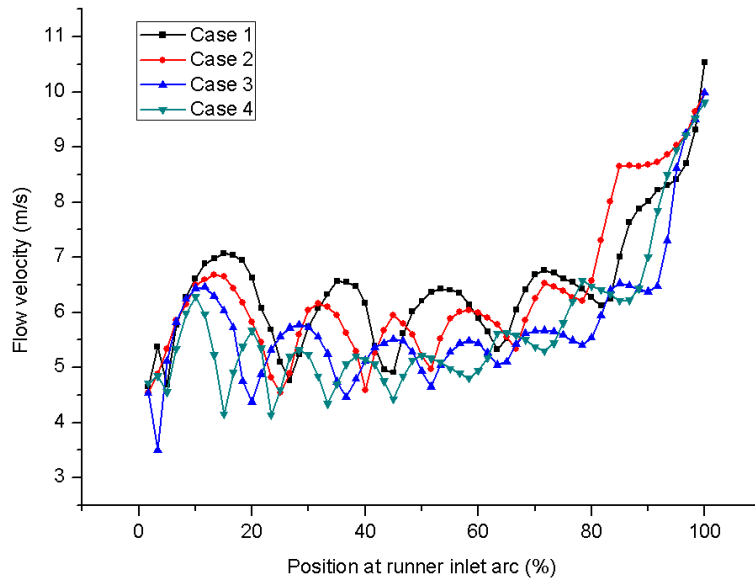


Fig.6.7 Flow velocity distribution along the runner inlet arc

#### 6.2.4 Pressure distribution

Water head variation in the cross-flow turbine is another factor that influences turbine performance. In this study, the water head distribution through the proposed turbine (as shown in Fig.6.8) is also investigated. The water head is higher on the upstream side of the runner, then reduces through and behind the runner, where pressure difference occurs. Water head through the conversion block reduces gradually, which is because that the conversion block convert part of the water head into kinetic energy. It can be observed in the blades passages at first and second stage, water head on blade pressure side is higher than that on the suction side, which caused pressure

difference. As a result, the force caused pressure difference pushes the blades to rotate from pressure side to suction side thus power is generated.

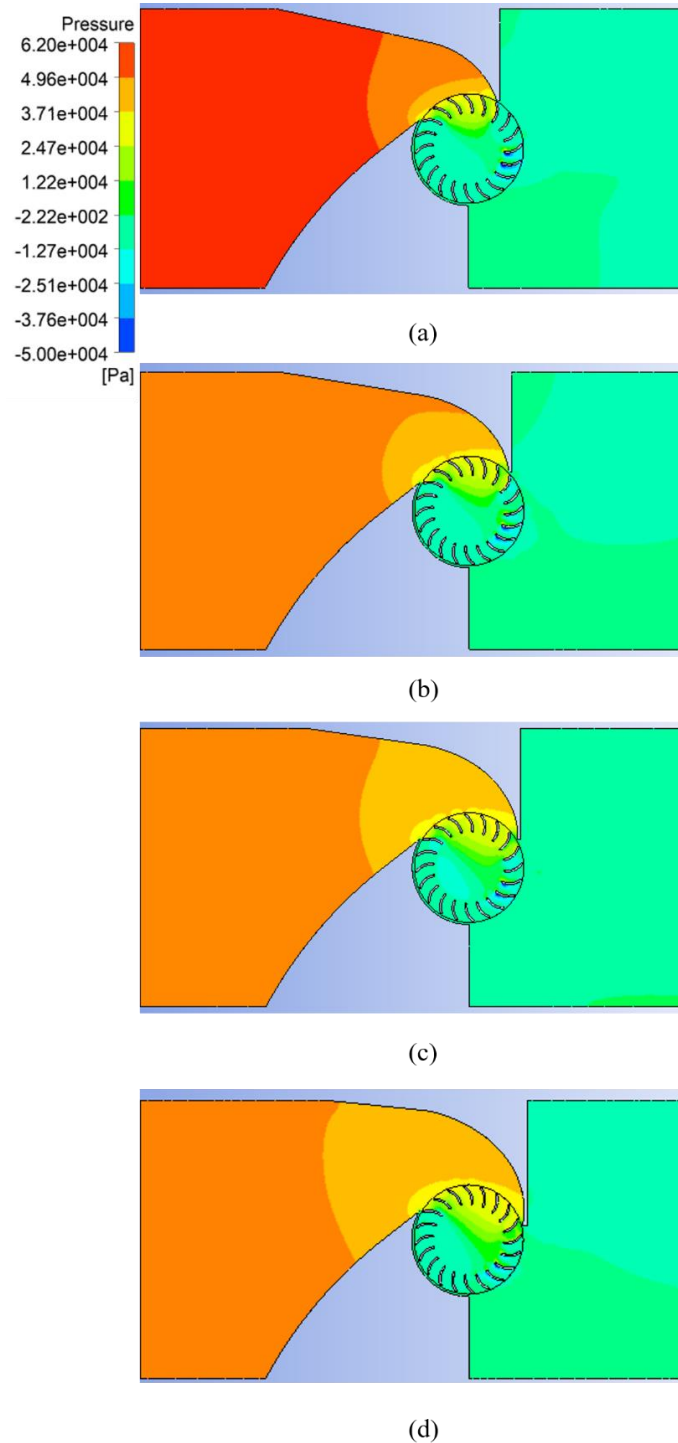


Fig.6.8 Pressure distribution through the inline cross-flow turbine: (a) Case 1:  $\lambda=90^\circ$ ;  
(b) Case 2:  $\lambda=105^\circ$ ; (c) Case 3:  $\lambda=120^\circ$ ; (d) Case 4:  $\lambda=135^\circ$

The pressure difference between runner inlet and exit is considered a significant factor in power generation as it can draw in more water and increase the flow velocity. As the downstream water head is considered the same in the four cases, the water head along runner inlet arc is a key factor in output power enhancement of the inline cross-flow turbine. From the pressure contours of the four cases, it is found that the water head at runner inlet reduces slightly with the increase of runner inlet arc angle. Fig.6.9 compares the actual variation of water head distribution at runner inlet of all the cases. The water head fluctuates sharply along the runner inlet. It is clear that the average water head at runner inlet of Case 1 is higher than that in the other cases, which corresponds well with the variation showed in Fig.6.3. In conclusion, a smaller runner inlet arc can increase the pressure difference between the upstream and downstream of the runner, resulting in a higher output power but also a higher overall water head reduction through the turbine.

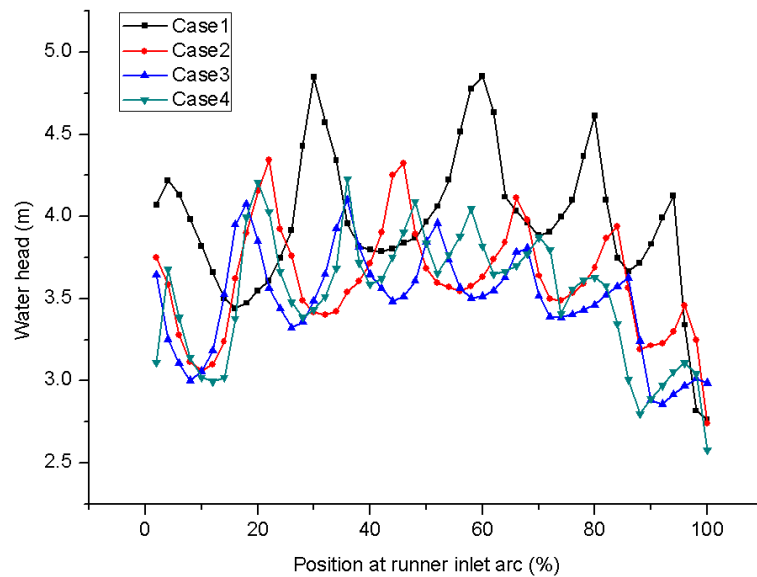


Fig.6.9 Water head distribution along the runner inlet arc

### 6.2.5 Torque of each blade and stage

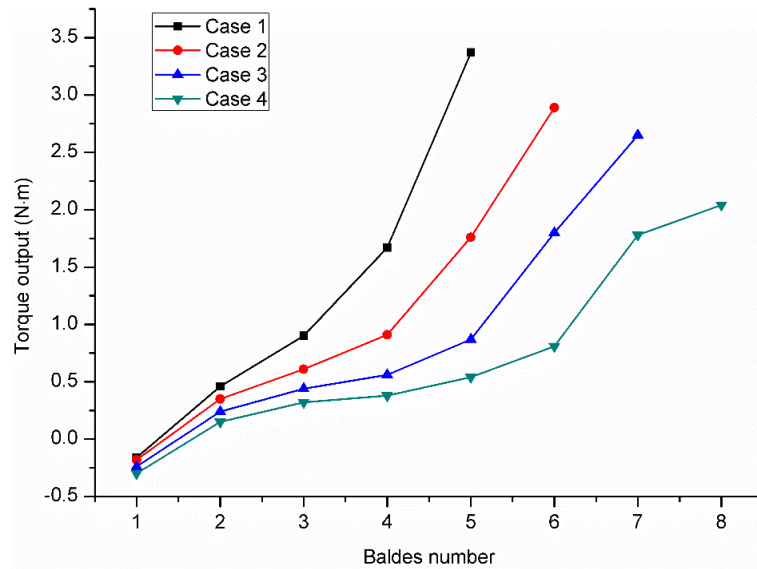


Fig.6.10 Torque output of each blade at the first runner stage

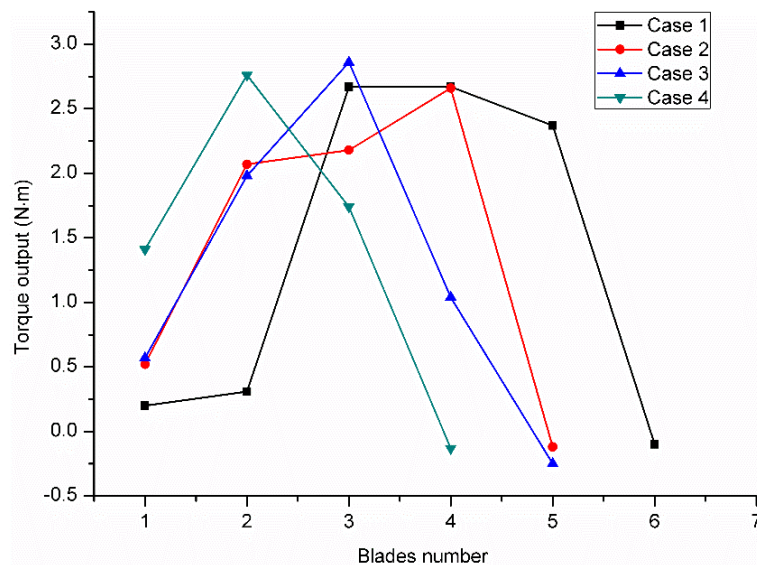


Fig.6.11 Torque output of each blade at the second runner stage

To study the effect of runner inlet arc angle on the power of each blade, blades torque output at the first and second stage is shown in Fig.6.10 and Fig.6.11, respectively. Due to the variation of inlet arc angle, the blades number at each stage in different cases is different. As can be seen in Fig.6.10, although water flow does work

on more blades in the cases with bigger runner inlet arc angle, the torque output of each blade is relatively low. The main reason that accounts for this trend is the low flow velocity and water head at runner inlet in these cases. Fig.6.11 indicates that at the second stage, more blades can generate torque in cases with smaller runner inlet arc angle. Explanation of this phenomenon is that in the cases with a bigger runner inlet arc angle, the exit area of the runner is relatively small, resulting in the number reduction of blades which output torque at the second runner stage.

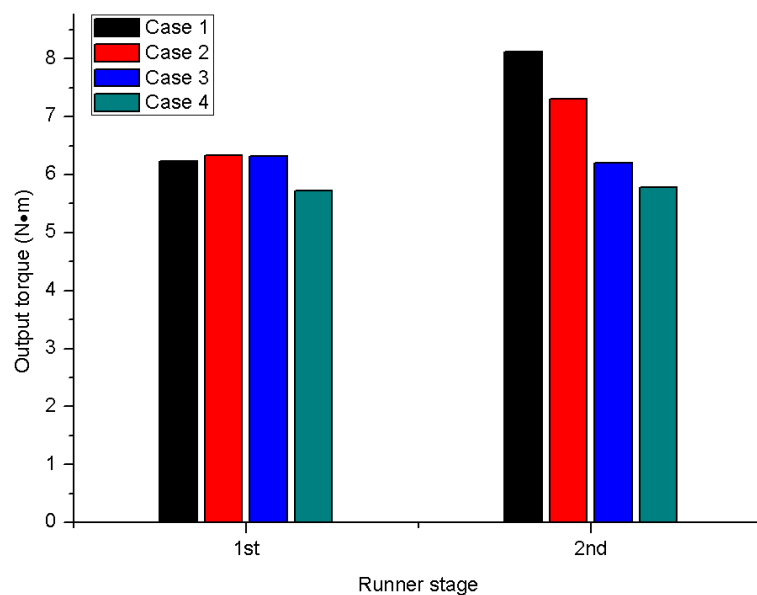


Fig.6.12 Torque output of each runner stage

Fig.6.12 summarizes the total torque output of the first and second stages. It can be observed that the effect of runner inlet arc angle on the first stage is slight. With the increase of runner inlet arc angle, the torque output at the second stage decreases gradually. For example, the torque output at the second stage in Case 1 is about 40% more than that in Case 4. The main reason for this phenomenon is that in a model with bigger runner inlet arc angle, flow velocity at the inlet of runner second stage is smaller. In addition, it can be seen that in the proposed inline cross-flow turbine, the second stage generates similar or more torque compared to the first stage, this is mainly

because of the higher flow velocity through the blades passage at the second stage.

### **6.3 Summary**

This study aimed to investigate the impact of the runner inlet arc angle on the performance of inline cross-flow turbines. With the proposed block design method, four models with different runner inlet arc angles were built and simulated to obtain an in-depth understanding about the effect and influencing mechanism of runner inlet arc angle on turbine performance. As referred from the present study, the following conclusions can be obtained:

(1) Based on the proposed block design method, the runner inlet arc angle is a key parameter in determining the shape of conversion block. Runner inlet arc angle has an important impact on the function of conversion block. A model with smaller runner inlet arc angle can convert more water head into flow kinetic energy through the conversion block.

(2) A smaller runner inlet arc angle can increase the flow velocity at runner inlet and pressure difference between the upstream and downstream of the runner, resulting in a higher output power but also a higher overall water head reduction through the turbine.

(3) The analysis about torque output of each blade and stage indicated that the runner inlet arc angle only had a slight influence on the power output of runner first stage but had a significant impact on that of runner second stage. With the increase of runner inlet arc angle, the torque output at the second stage encountered a gradual decrease.

(4) To achieve a good balance between turbine efficiency and water head

reduction, the suggested runner inlet arc angle is  $105^\circ$ . Numerical results showed that the model with  $105^\circ$  runner inlet arc angle could reach a maximum efficiency of 42.6% with about 1565W power output.

# **CHAPTER 7 INVESTIGATION OF THE EFFECTS OF RUNNER AND BLADES GEOMETRIES ON THE PERFORMANCE OF INLINE CROSS-FLOW TURBINE**

As analyzed in Chapter 4, the main function of blocks is to direct water flow toward the runner and increase the flow velocity at the runner inlet. However, as indicated in Chapter 5, mismatching exists between the flow inlet angle and blades outer angle, which may result in shock loss and flow separation. To further enhance the performance of inline cross-flow turbine, it is suggested that the blades geometry should be improved for a better matching with the proposed block design. In this chapter, the influence of blades outer angle is investigated and an optimal value is suggested for a better matching with the block design. Besides, the effects of runner diameter ratio and blades number are also studied to further enhance the performance of inline cross-flow turbine.

## **7.1 Study on effects of blades outer angle**

### **7.1.1 The optimal range of blades outer angle**

The blades outer angle  $\beta_1$  is the inlet angle of blades at runner first stage and the outlet angle of blades at runner second stage. Although many researches have suggested the optimal value of blades outer angle, as shown in the results of Chapter 5, difference exists between the flow inlet angle and blades outer angle. Therefore, it is necessary to determine the optimal blades outer angle by CFD method.

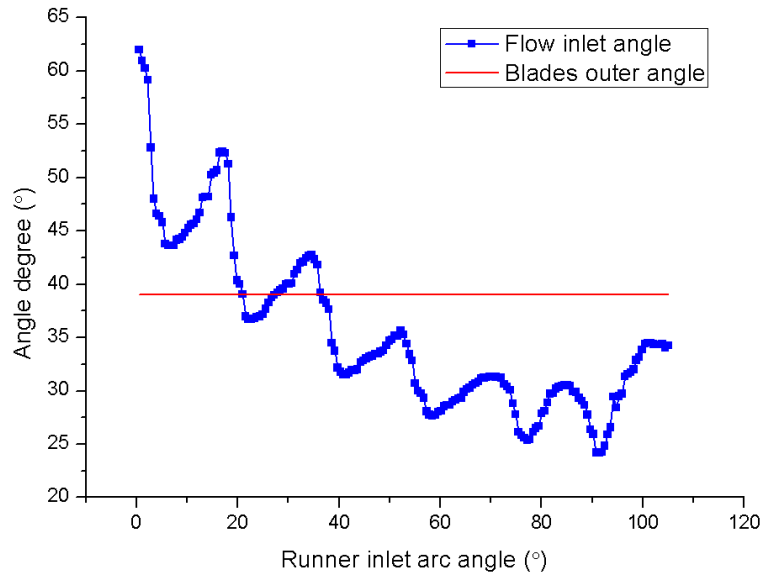


Fig.7.1 The variation of flow inlet angle along the runner inlet arc

Table 7.1 The main runner geometrical parameters with different  $\beta_1$

Blades outer angle $\beta_1$	Blades inner angle $\beta_2$	Runner diameter ratio $D_2/D_1$	Blades radius $R_b$	Blades number $N_b$
26°	90°	0.68	14.9mm	20
28°	90°	0.68	15.2mm	20
30°	90°	0.68	15.5mm	20
32°	90°	0.68	15.8mm	20

In Chapters 5 and 6, the optimal shape of the blocks has been determined by CFD method, the results indicated that the optimal guide block orientation angle and runner inlet arc angle are 30° and 105°, respectively. Fig.7.1 indicates the variation of flow inlet angle along the runner inlet arc in the turbine model with the optimal block shape. It can be observed that the flow inlet angle reduces when runner inlet arc angle

increases from  $0^\circ$  to  $50^\circ$  and fluctuates from  $26^\circ$  to  $32^\circ$  in the runner inlet arc angle range from  $50^\circ$  to  $105^\circ$ . To achieve a good matching between the flow inlet angle and blades outer angle, the optimal value of blades outer angle may occur in the range from  $26^\circ$  to  $32^\circ$ . In this part of research, computations were performed when  $\beta_I$  equals to  $26^\circ$ ,  $28^\circ$ ,  $30^\circ$  and  $32^\circ$ . The block geometries are selected as the optimal values which are suggested in the former parts and the main geometrical parameters of the runner are indicated in Table 7.1.

### 7.1.2 Turbine performance

All the simulations were conducted under the flow velocity of 1.5m/s at different TSRs. Fig.7.2 indicates the influence of  $\beta_I$  on turbine output power. It could be observed that the output power of turbines with  $\beta_I$  equals to  $28^\circ$  and  $30^\circ$  are better than the other models. The maximum turbine output power, 2200W, occurs when  $\beta_I=30^\circ$  at TSR equals to 1.2. It can also be noticed that when the TSR is lower (less than 0.8), the power deviation between each model is smaller. When the TSR is higher, the variation becomes more obvious. As can be seen in Fig.7.3 is the effects of  $\beta_I$  on water head reduction. With the increase of blades outer angle, water head reduction through the turbine decreases. When the blades outer angle is  $26^\circ$ , the water head reduction is higher than the other three models. The main reason for this phenomenon is that in the model with  $\beta_I$  equals to  $26^\circ$ , mismatching between flow inlet angle and blades outer angle is severe, resulting in more hydraulic loss than other models. The effects of blades outer angle on turbine efficiency is shown in Fig.7.4. When  $\beta_I$  increases from  $26^\circ$  to  $30^\circ$ , the maximum turbine efficiency increases significantly from 45.9% to 49.6%, keeping increase  $\beta_I$  from  $30^\circ$  to  $32^\circ$ , the turbine efficiency decreases slightly from 49.6% to 48.5%. Therefore, the turbine obtains its best efficiency when  $\beta_I=30^\circ$ ,

where the TSR is 0.8. The variation of turbine output power and efficiency with the change of blades outer angle proves that a good matching between flow inlet angle and blades outer angle can significantly improve the turbine performance. To obtain a better turbine efficiency, the blades outer angle of the inline cross-flow turbine is suggested as  $30^\circ$ .

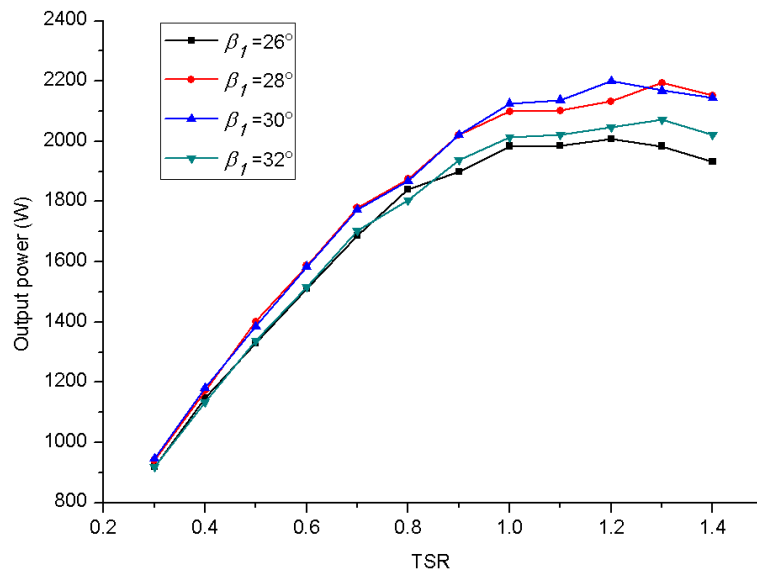


Fig.7.2 The influence of blades outer angle on turbine output power

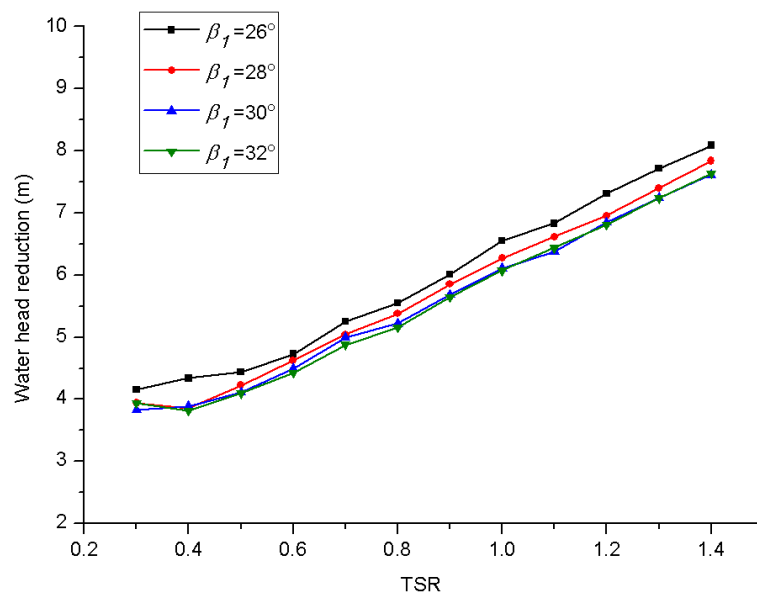


Fig.7.3 The influence of blades outer angle on water head reduction

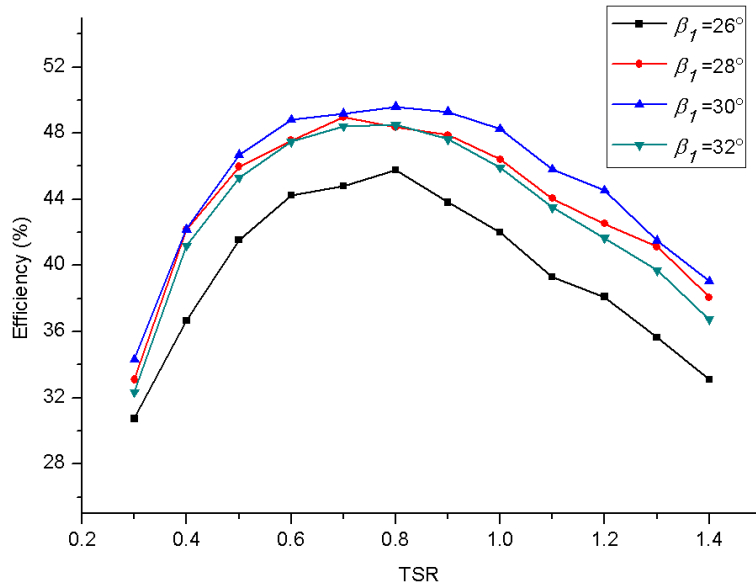


Fig.7.4 The influence of blades outer angle on turbine efficiency

### 7.1.3 Torque output of each runner stage

The influence of blades outer angle on torque output of each blade is shown in Fig.7.5. It can be observed that at runner first stage, the output torque of each blade increases gradually with the increase of runner inlet arc angle due to the function of conversion block, while the blade torque at second runner stage increases first then decreases. When blades outer angle is  $30^\circ$ , the blade output torque at first runner stage is improved comparing to other models, which means the flow inlet angle matches well with the blades outer angle. For the other three models, the performance of the first runner stage is similar.

To study the influence of blades outer angle on the performance of each runner stage, the percentage of total torque output at each runner stage is recorded and shown in Fig.7.6. It can be observed that for all the four studied cases, each runner stage can generate nearly 50% of the total output torque, but slight difference exists between different models due to the different blades outer angles. It can be seen that the highest

torque output of the first runner stage occurs when blades outer angle equals to  $30^\circ$ , this is mainly because that a good matching between the flow inlet angle and the blades outer angle is achieved in this case, leading to less hydraulic loss and better performance at the first runner stage.

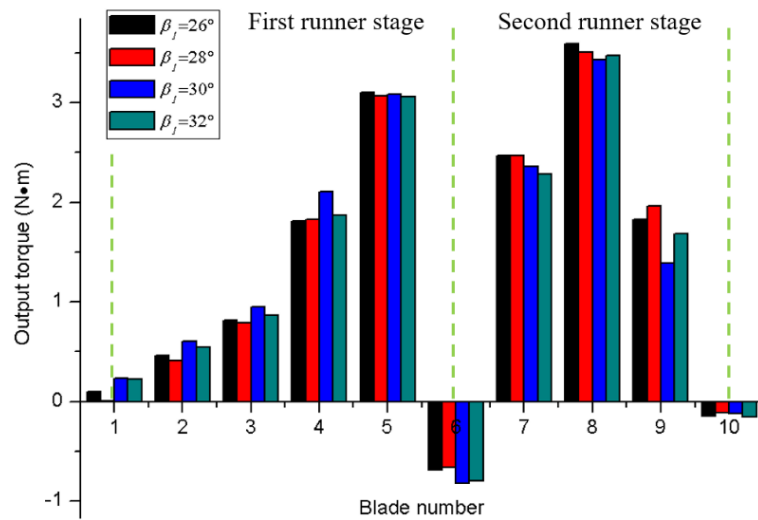


Fig.7.5 The influence of blades outer angle on torque output of each blade

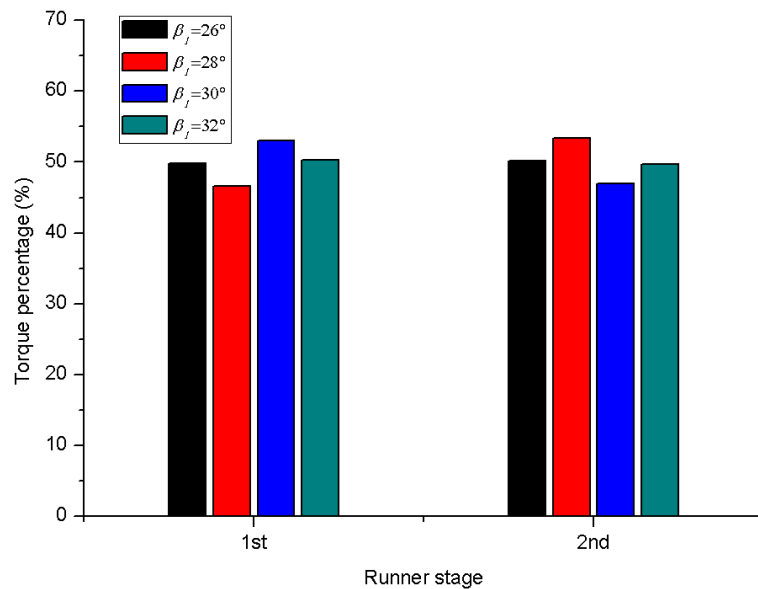


Fig.7.6 The influence of blades outer angle on torque output of each runner stage

## 7.2 Study on effects of runner diameter ratio

The ratio between runner inner and outer diameter ( $D_2/D_1$ ) can have an influence on the blades radius and further affect the curvature and length of each blade [20]. For different runner diameter ratios, the blades passage and length are different, resulting in different hydraulic loss and friction loss. Besides, the variation of runner diameter ratio also has an influence on the torque capture from water flow due to the different blades length. Based on the literature review, the suggested value of runner diameter ratio is 0.68 in the previous researches. However, as there has no relevant research about inline cross-flow turbine, it is necessary to determine the optimal  $D_2/D_1$  for this special application. To investigate the effects of runner diameter ratio on the performance of inline cross-flow turbine, three models with  $D_2/D_1$  equals to 0.64, 0.68 and 0.72, respectively, are established and simulated. In the simulation process, the block parameters are selected as the optimal values which suggested in the former parts and the main geometrical parameters of the runner are indicated in Table 7.2.

Table 7.2 The main runner geometrical parameters with different  $D_2/D_1$

Runner diameter ratio $D_2/D_1$	Blades outer angle $\beta_1$	Blades inner angle $\beta_2$	Blades radius $R_b$	Blades number $N_b$
0.64	30°	90°	16.7mm	20
0.68	30°	90°	15.5mm	20
0.72	30°	90°	13.6mm	20

### 7.2.1 Turbine performance

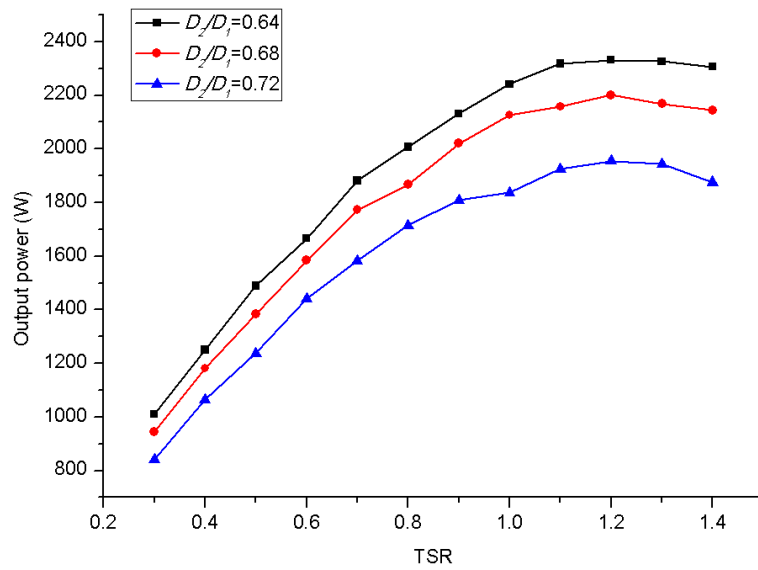


Fig.7.7 The influence of runner diameter ratio on turbine output power

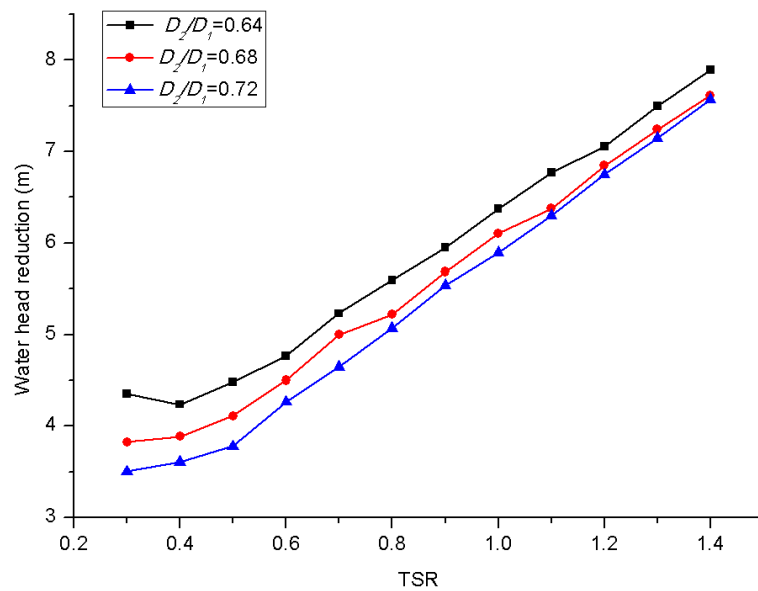


Fig.7.8 The influence of runner diameter ratio on water head reduction

All the simulations were conducted under the flow velocity of 1.5m/s at different TSRs. Fig.7.7-7.9 indicate the influence of runner diameter ratio on the turbine output power, water head reduction and efficiency, respectively. It can be seen in Fig.7.7 that when  $D_2/D_1$  increases from 0.68 to 0.72, the turbine output power reduces significantly, besides, the water head reduction through the turbine also experiences a slight

reduction. The main reason for the variation of turbine output power and water head reduction is that when  $D_2/D_1$  increases from 0.68 to 0.72, the blade length becomes short. Therefore, the blades have less opportunities to capture the torque from water flow and less water head is converted into runner kinetic energy. The turbine efficiency decreases when  $D_2/D_1$  becomes 0.72, specially, the maximum turbine efficiency declines from 49.6% to 47.2% when  $D_2/D_1$  increases from 0.68 to 0.72. It is worth noting that both the output power and water head reduction experience obvious increase when the runner diameter ratio decreases from 0.68 to 0.64. The increase of output power may result from the blade length increase and curvature reduction while the higher water head reduction is because more water head is converted into flow kinetic energy. The maximum turbine efficiencies when  $D_2/D_1$  equal to 0.68 and 0.64 are 49.6% and 49.8%, respectively. When the TSR is lower than 0.8, the efficiency of turbine with  $D_2/D_1=0.68$  is higher than that of turbine with  $D_2/D_1=0.64$ . Taking the water head reduction and turbine efficiency into account together, the suggested value of runner diameter ratio in this research is 0.68.

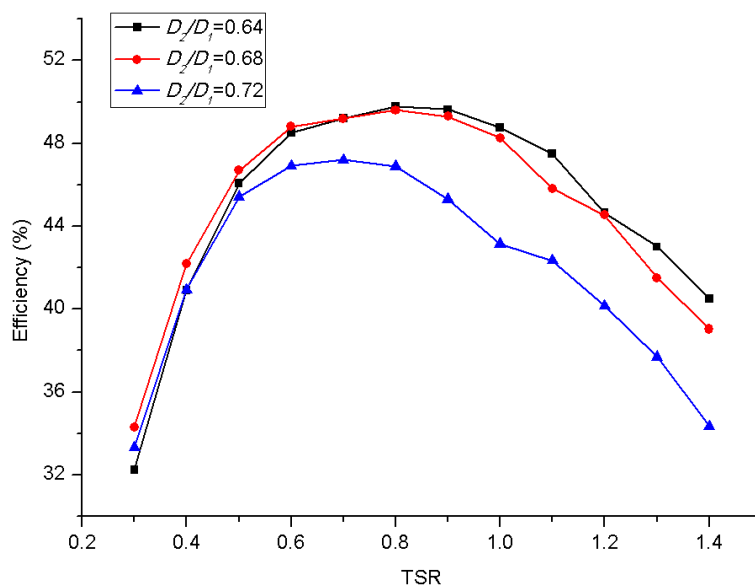


Fig.7.9 The influence of runner diameter ratio on turbine efficiency

## 7.2.2 Torque output of each runner stage

Fig.7.10 and Fig.7.11 indicate the influence of runner diameter ratio on torque output of each blade. When  $D_2/D_1=0.64$ , the torque output at the first stage is the highest, while the lowest torque output at the first stage occurs when  $D_2/D_1=0.72$ . The main reason for this phenomenon is the bigger blade length and smaller blade curvature when  $D_2/D_1=0.64$ . On the contrary, when  $D_2/D_1=0.72$ , the torque output of first runner stage is the smallest due to the smaller blade length and bigger blade curvature. As can be seen in Fig.7.10 that when  $D_2/D_1=0.64$ , the torque output of the second stage is also the highest. Fig.7.11 indicates that influence of runner diameter ratio on torque output of each runner stage. The torque percentage of each runner stage is similar when  $D_2/D_1$  equals to 0.64 and 0.68, and the first runner stage generates more torque than the second runner stage in these two models. As the torque output of first runner stage is small when  $D_2/D_1=0.72$ , torque percentage of the second runner stage is much higher than that of the first runner stage in this model.

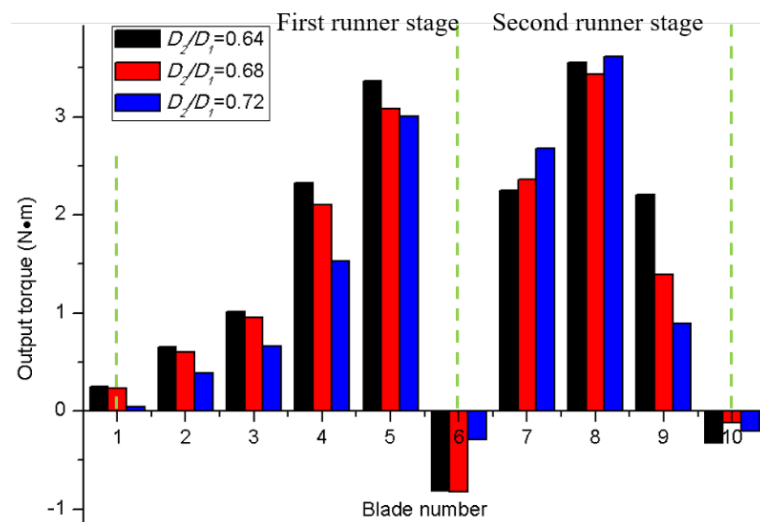


Fig.7.10 The influence of runner diameter ratio on torque output of each blade

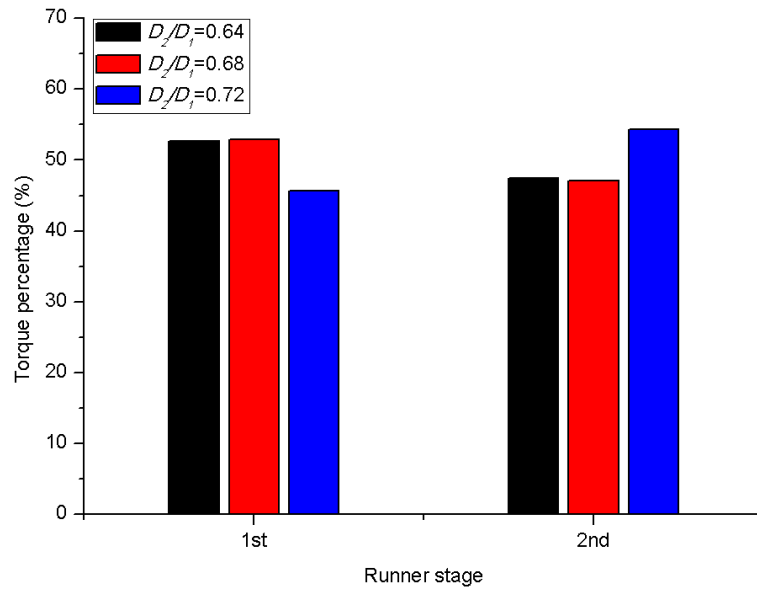


Fig.7.11 The influence of runner diameter ratio on torque output of each runner stage

### 7.3 Study on effects of blades number

#### 7.3.1 Turbine performance

Blades number ( $N_b$ ) is another parameter that may influence the turbine performance by affecting the flow separations in blades passages and power extraction of each runner stage. In this study, three turbine models with blades number of 20, 24 and 28 were built and simulated. As shown in Fig.7.12-7.14 are the influences of blades numbers on turbine output power, water head reduction and efficiency, respectively. It can be seen that when the blades number increases from 20 to 24, the turbine output power rises significantly and the maximum output power reaches 2285W. However, if blades number continues to increase, the variation of output power is very slight. In terms of water head reduction, the difference between the investigated three models is very slight. Water head reductions of all the three models increase with the increment of TSR, but the model with more blades consumes more water head, this is mainly because that a runner with more blades has more

opportunities to convert the water head into its kinetic energy.

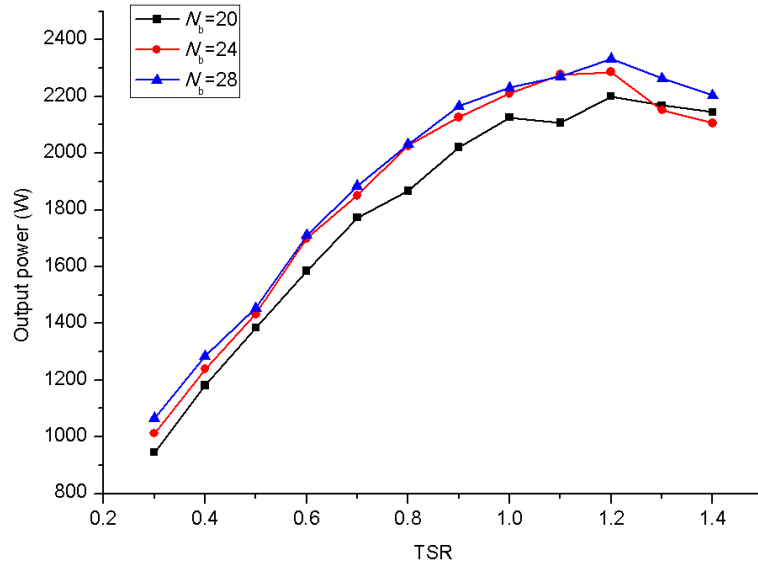


Fig.7.12 The influence of blades number on turbine output power

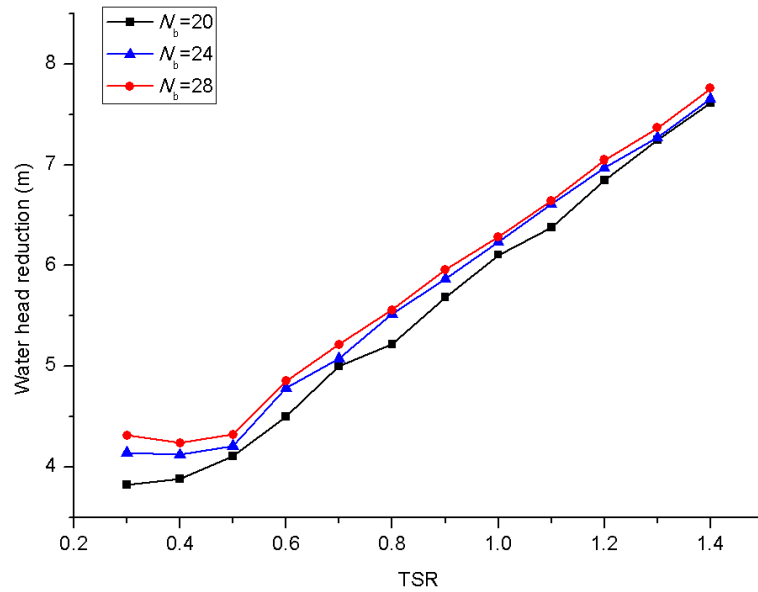


Fig.7.13 The influence of blades number on turbine water head reduction

Based on Fig.7.14, the three models have similar efficiency when TSR is smaller than 0.7, however, turbine efficiency is much lower than the other two models when blades number equals to 20 at higher TSRs. For all the three models, the turbine efficiency increases with the increment of TSR until reaching the maximum efficiency,

after that, the turbine efficiency decreases. The best efficiency TSRs for the models are 0.8. The recorded maximum efficiency is 50.9% when  $N_b = 24$ . In conclusion, the optimal blades number for the inline cross-flow turbine is 24. However, it is suggested to determine the blades number according to the mechanical processing level.

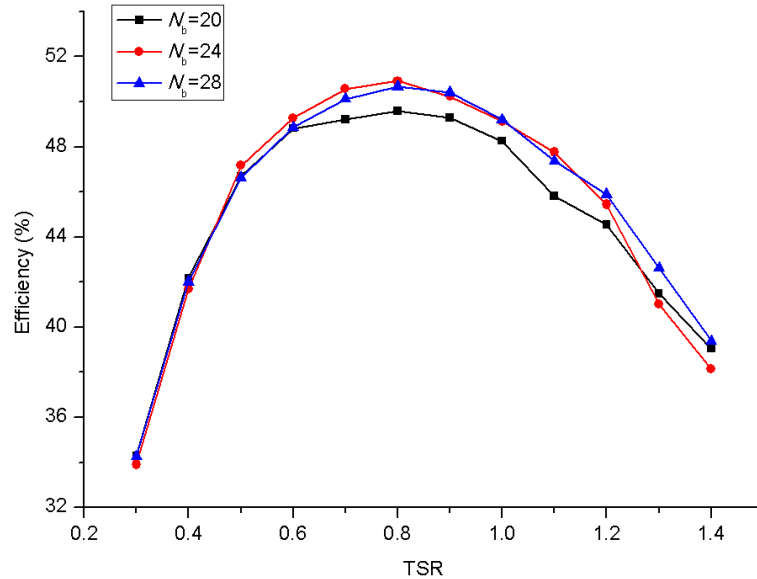


Fig.7.14 The influence of blades number on turbine efficiency

### 7.3.2 Torque output of each runner stage

The torque output of each runner stage is shown in Fig.7.15. It can be observed that with the increase of blades number, torque output from the second runner stage experiences an obvious increase. This is mainly because that when the blades number increases, the opportunity of extracting power at the second stage is improved as the blades inlet angles varies significantly at the second stage [20]. However, a large blades number causes shrink of blades passages, resulting in turbine efficiency reduction. Besides, the friction loss will also increase with the growth of blades number.

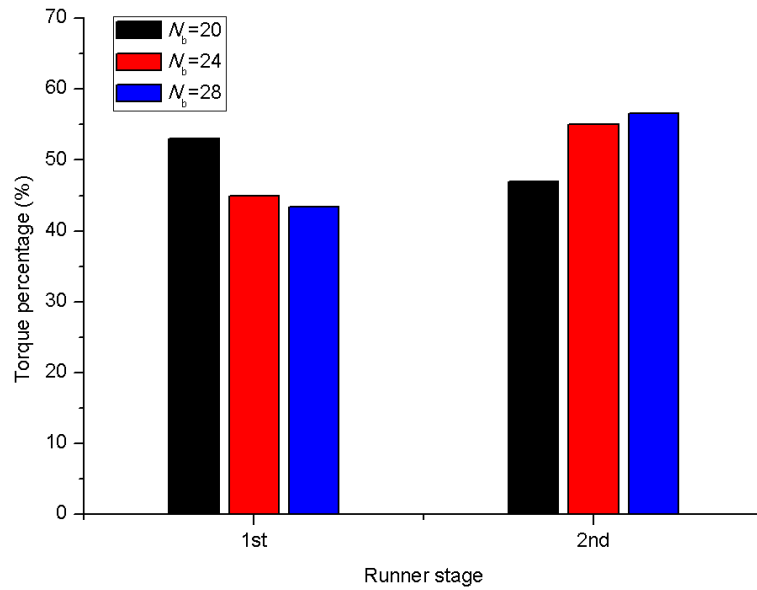


Fig.7.15 The influence of blades number on torque output of each runner stage

## 7.4 Summary

In this chapter, the influence of runner and blades geometrical parameters, including blades outer angle, runner diameter ratio and blades number, on the performance of inline cross-flow turbine was studied by numerical methods. This part of research not only provides an in-depth understanding about influencing mechanism of runner and blades geometry on turbine performance, but also suggests the optimal geometrical parameters of the runner and blades. Based on the present study, the following conclusions can be obtained:

(1) A good matching between flow inlet angle and outer blade angle can significantly improve the turbine performance. Specially, the maximum turbine efficiency increased significantly from 45.9% to 49.6% when adjusting the outer blade angle from  $26^\circ$  to  $30^\circ$ . Besides, a suitable outer blade angle could enhance the torque output of runner first stage. To achieve a balance between turbine efficiency and water head reduction, the outer blade angle of the inline cross-flow turbine was suggested as

30°.

(2) Numerical study indicated that a smaller runner diameter ratio may lead to higher output power, but the water head reduction was also higher. The runner diameter ratio affected the turbine performance mainly by influencing the performance of the first runner stage. Based on the results, the suggested runner diameter ratio was 0.68.

(3) Investigation of the blades number indicated that when the blades number increased from 20 to 24, the turbine output power rose significantly and the maximum output power reached 2285W. However, if blades number continued to increase, the variation of output power was very slight. The variation of water head reduction with blades number increase was very slight. The optimal blades number was suggested 24 and the recorded maximum efficiency was 50.9% when the TSR was 0.8.

# **CHAPTER 8 DEVELOPMENT OF A MAGNETIC DRIVEN BIDIRECTIONAL INLINE CROSS-FLOW TURBINE: A CASE STUDY**

In the previous parts of the thesis, a block design method for the inline cross-flow turbine has been proposed. With the proposed theoretical method, the block shape can be designed based on the expected working conditions. In addition, the optimal values of runner main geometrical parameters, including blades outer angle, runner diameter ratio and blades number, are determined using CFD simulation. The proposed method and the suggested optimal geometrical parameters can provide guidance for the inline cross-flow turbine design. In this chapter, a micro inline cross-flow turbine that can operate under bidirectional flow is designed for DN150 water pipes. In addition, magnetic coupling is adopted in the turbine for sealing and torque transmission. Finally, a turbine prototype is manufactured and tested to investigate its performance.

## **8.1 Design process**

The water flow inside urban water pipes is very complex and bidirectional flow may occur in water pipes. For example, as shown in Fig.1.2, there are two service reservoirs that can supply water to the indicated region. When switching the service reservoir from one to another one, the water flow inside pipes that between the two service reservoirs will change. Besides, bidirectional flow may occur under the operations of cutline valves by regional staff or under pipe bursting and drain off for maintenance. Therefore, the inline hydro turbine should be capable to generate electricity with bidirectional water flow.

The design requirements are as following:

1. The design flow velocity is 1.5m/s.
2. The maximum water head reduction cannot exceed 5m at the design flow velocity.
3. The turbine should be used in DN150 water pipes.
4. The application of the turbine cannot cause water pollution.

### 8.1.1 Design of the blocks

Fig.8.1 shows the cross-sectional view of the turbine and indicate the working principle of the proposed bidirectional turbine. To apply in bidirectional flow, the shape of blocks integrated to pipe inner wall is specially designed. Each block consists of a plane surface and a curved surface. The function of the plane surface is to direct the water flow while the curved surface can force the water to flow towards the runner gradually. With the developed blocks, the inline turbine could operate under bidirectional water flow without changing the runner rotation direction.

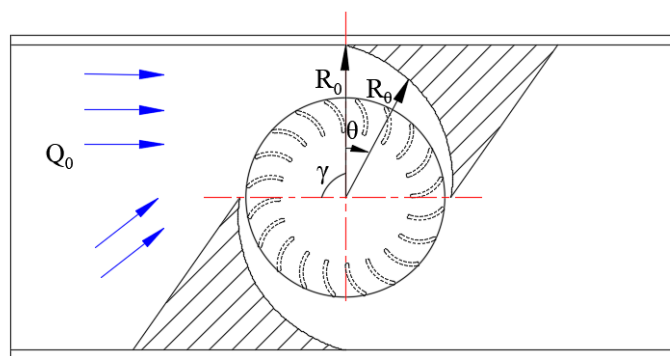


Fig.8.1 Block shape of the bidirectional cross-flow turbine

The shape of the blocks is different from the optimal shape which is obtained by numerical methods in Chapters 5 and 6. To make the inline cross-flow to operate under

bidirectional flow, the orientation angle of guide block is  $0^\circ$ . The inlet of the conversion block (the curved surface in this case study) is tangential to the pipe inner wall as the space inside DN150 pipe is very limited. Therefore, the orientation entry angle of the conversion block is  $90^\circ$ . The detailed shape of the block is designed using the theoretical design method proposed in Chapter 4.

### 8.1.2 Geometries of the runner

Table 8.1 The main geometrical parameters of runner and blade

Geometrical Parameters	Symbol	Values
Blade outer angle	$\beta_1$	$30^\circ$
Blade inner angle	$\beta_2$	$90^\circ$
Outer diameter	$D_1$	98mm
Inner diameter	$D_2$	66mm
Runner diameter ratio	$D_2/D_1$	0.68
Runner length	$L$	215mm
Blades radius	$R_b$	15.5mm
Blades number	$N_b$	12

As shown in Fig.8.2 is the physical model of the runner and blade. The runner length  $L$  is determined based on the pipe diameter. Besides, the runner inner diameter  $D_2$ , runner diameter ratio  $D_2/D_1$ , the blade outer angles  $\beta_1$  and inner angle  $\beta_2$  are determined based on numerical results presented in Chapter 7. Due to the difficulty in

manufacturing, the blades number is selected as 12 in this case study. The blades are fixed to two discs to enhance runner strength. The detailed geometrical parameters of runner and blade are shown in Table 8.1.

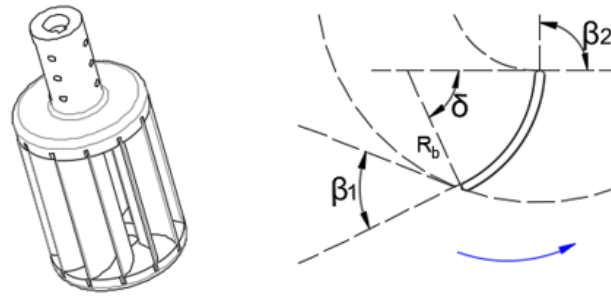


Fig.8.2 Physical model of the runner and blade

### 8.1.3 Application of magnetic coupling

According to working principle of hydro turbines, the runner harvests torque from water flow then transmit it to the generator. However, mechanical loss in mechanical transmission parts, such as mechanical sealing, shaft and bearings, causes significant efficiency loss in transmission process. In traditional micro turbines, mechanical seals are often used in the space between turbine body and shaft to avoid leakage. However, the mechanical seals achieve sealing by tight fit of two different seal parts, the friction caused by sliding of two surfaces against each another may result in a significant mechanical loss, furthermore, the mechanical seals would eventually wear out and fail. To avoid this problem, magnetic coupling is used in this case study to reduce mechanical loss of the turbine.

A magnetic coupling is a coupling that transfers torque from one shaft, but using a magnetic field rather than a physical mechanical connection. Fig.8.3 shows the structure and working principle of a magnetic coupling, which consists of external

coupling half, internal coupling half and a containment shroud. The external coupling half and internal coupling half are made of permanent magnet and they are separated by the containment shroud, which means that they do not connect to each other. As the magnetic coupling transfers torque by magnetic force, there is no friction between the external coupling half and internal coupling half.

Magnetic shaft couplings are often used for liquid pumps and propeller systems, since a static, physical barrier can be placed between the two shafts to separate the fluid from the motor operating in air. However, the application of magnetic coupling in hydraulic turbines is still seldom, in this project, a specially designed magnetic coupling (Fig.8.4) was designed and manufactured. The internal coupling half is covered by 316L stainless steel shell while the containment shroud is made of 316L stainless steel to avoid bad effects on the water quality. As the external coupling half does not contact with water, it is made of carbon steel to reduce costs.

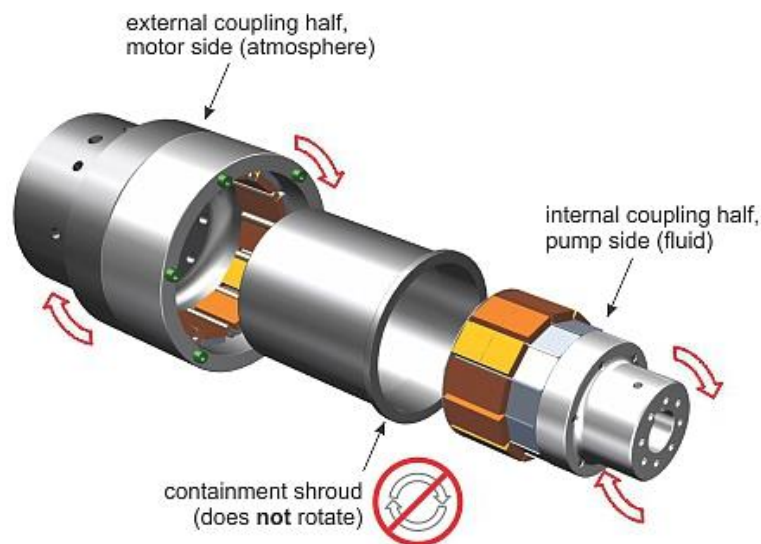


Fig.8.3 Structure and working principle of magnetic coupling [87]

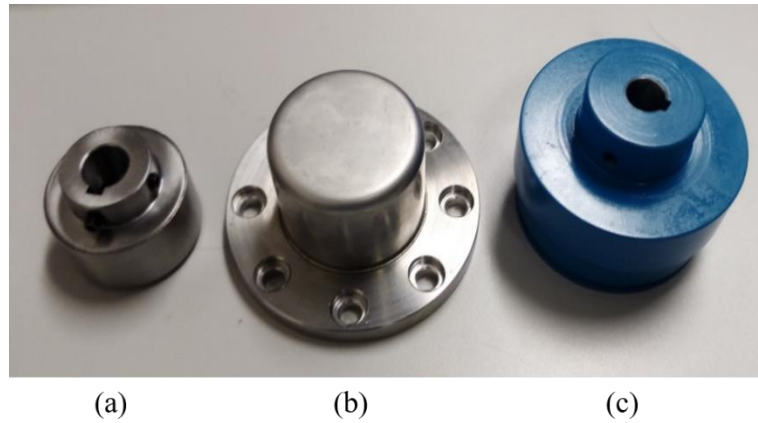


Fig.8.4 The prototype of magnetic coupling: (a) Internal coupling half; (b) Containment shroud (c) External coupling half

#### 8.1.4 Mechanical structure of the turbine

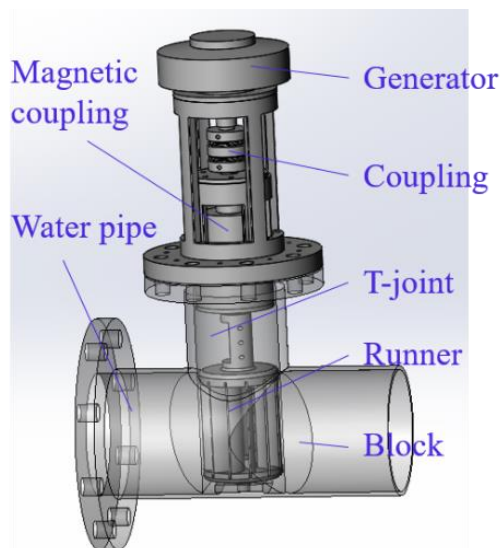


Fig.8.5 The structure of bidirectional inline cross-flow turbine

In order to install the magnetic coupling to the micro Francis turbine, a magnetic coupling assembly was designed. Fig.8.5 shows the mechanical structure of the magnetic coupling assembly. The runner connects to the magnetic coupling internal half through a shaft, after that, the external half of magnetic coupling transmits torque to the generator through a shaft and a mechanical coupling. In this assembly, all parts

that contact with water are made of 316L stainless steel to avoid water quality deterioration.

## 8.2 Prototype and experimental setup

Fig.8.6 indicates the prototype of the bidirectional inline cross-flow turbine. The runner is made of 12 blades, which are welded to two discs. In addition, a runner holder is located on the bottom of the turbine body to hold the terminal of the runner to reduce runner deformation.



Fig.8.6 Prototype of the bidirectional turbine

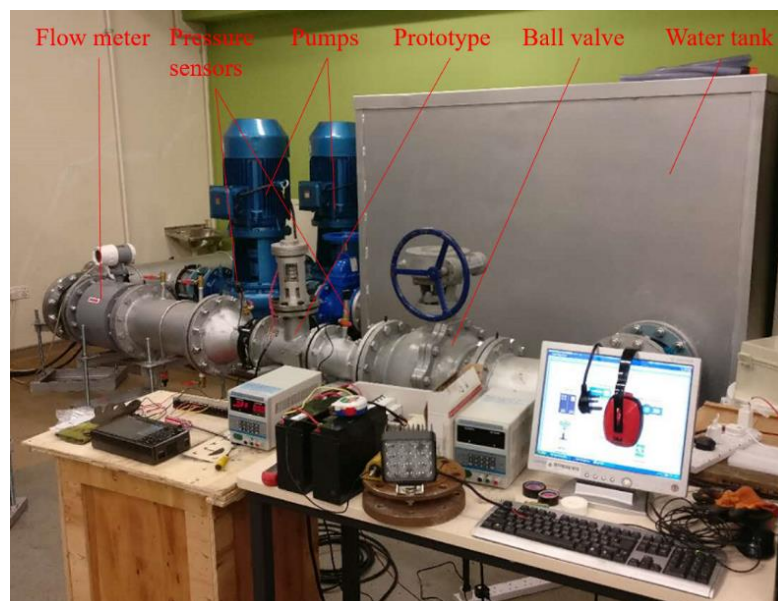


Fig.8.7 Hydraulic test rig for the bidirectional turbine

The prototype is tested in the hydraulic test rig built by the Renewable Energy Research Group of the Hong Kong Polytechnic University. Fig.8.7 shows the hydraulic test rig which is composed of two centrifugal pumps, a water tank, flow meter, pressure sensors, ball valves and the monitoring computer. The centrifugal pumps are controlled by a frequency converter controller. By adjusting the frequency converter controller and the opening degree of the ball valve, the flow velocity can be adjusted from 1.0 to 3.0m/s and the maximum water head can reach 40m water. The pressure sensors and electromagnetic flow meter are used to detect water head and flow velocity, respectively. To study the turbine performance at different rotation speed, a set of dynamic torque meter system (as shown in Fig.8.8) is used to measure the torque and power output. The dynamic torque meter system is composed of a dynamic torque meter, an electronic brake and a brake controller. By adjusting the brake controller, current on the electronic brake varies and the brake force will also change. Therefore, the torque and rotation speed of the shaft changes and the turbine performance under different rotation speed can be measured by the dynamic torque meter.

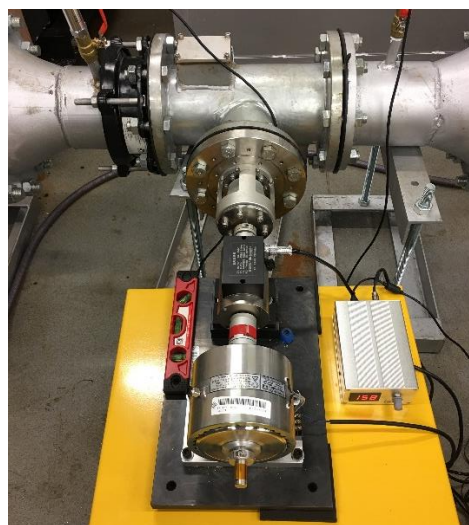


Fig.8.8 Dynamic torque meter system for the bidirectional turbine

## 8.3 Results and discussion

### 8.3.1 Turbine performance at different rotation speed

By using the dynamic torque meter system, turbine performance under different rotation speeds and work load can be obtained, which is helpful for the generator selection. As the design flow velocity in this study is 1.5m/s, in the experimental process, the flow velocity was kept around 1.5m/s.

The turbine performance curves are shown in Fig.8.9 and Fig.8.10. It can be observed from Fig.8.9 that with the increase of runner rotation speed, the turbine output power increases until reaching the maximum value, then decreases significantly, while the water head reduction increases gradually. As shown in Fig.8.10, the turbine efficiency encounters a same trend with the output power. The maximum output power and efficiency are 190W and 17.4%, respectively. And both the maximum output power and efficiency are recorded when runner rotation speed is 600rpm. Although the water head reduction is more than 5m at higher rotation speed (more than 800rpm), at the best efficiency rotation speed, the water head reduction is about 4.7m, which can meet the design requirement about water head reduction.

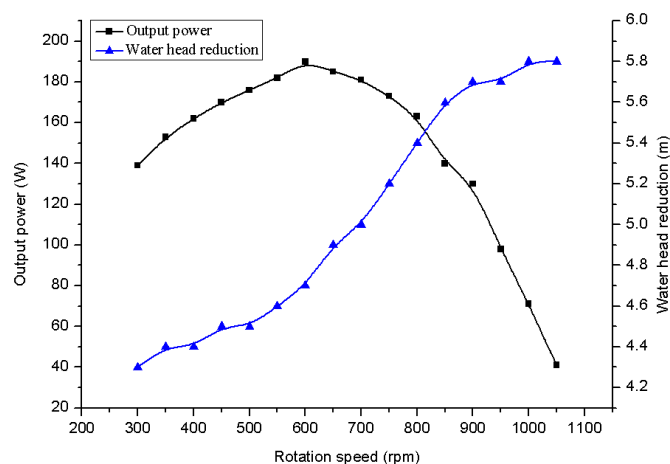


Fig.8.9 Turbine power and water head reduction under different rotation speed

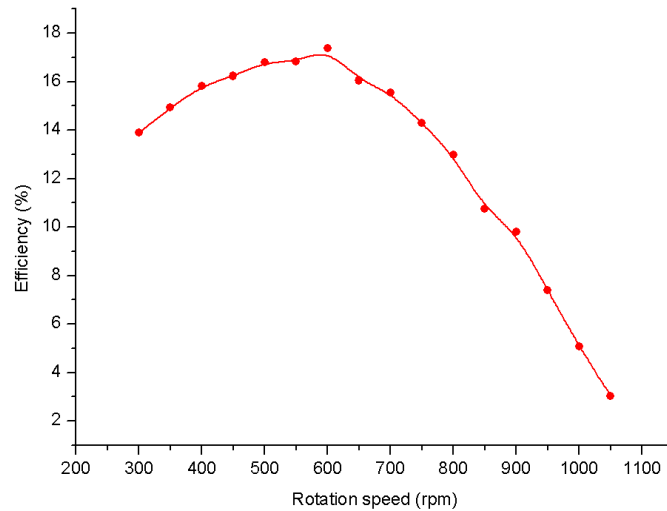


Fig.8.10 Turbine efficiency under different rotation speed

Compared to the simulated results shown in Chapters 5-7, the turbine performance in this case study is not as good as the numerical results. There are four main reasons for the difference. Firstly, in the numerical studies shown in previous parts, the turbine models are all developed for DN250 pipes while in this case study, the bidirectional turbine is designed for DN150 pipes. The runner length and friction losses DN150 inline turbine is very different from that in DN250 inline turbine. Secondly, to make the turbine able to operate under bidirectional flow, the block shape is much different from the numerical models. In the case study, the block is designed tangential to the pipe inner wall and the orientation angle of guide block is  $0^\circ$ . Thirdly, according to the simulation results, the optimal blades number is 24. However, due to the limited processing space in the runner, it is very different to manufacture 24 blades for the prototype and the blades number is selected as 12 in this case study. Finally, the physical models in numerical simulations are simplified. However, in the real product, water leakage exists in the space between runner terminal and pipe inner wall and friction losses occur when water flows through the blocks and blades. But the overall turbine performance is acceptable for this case study.

### 8.3.2 Effects of the distance between block and runner on turbine performance

As mentioned above, the experimental results of the turbine performance under different rotation speeds can provide guidance for generator selection. In the following research, a 24V three-phase permanent magnet alternating generator with low starting torque is selected to study the real turbine capacity. The rated power and rotation speed of the generator is 200W and 500 rpm, respectively. To study the effects of distance between block and runner (represented by  $S$ ) on turbine performance, the blocks are manufactured adjustable, so the distance between block and runner can be changed. In this research, a series of lab tests were performed under the  $S$  values of 10mm, 25mm and 40mm. Besides, the controller mentioned in Chapter 3 is used for power management and data collection and the monitored water head, flow velocity, turbine rotation speed, charging voltage and current can be recorded in the computer.

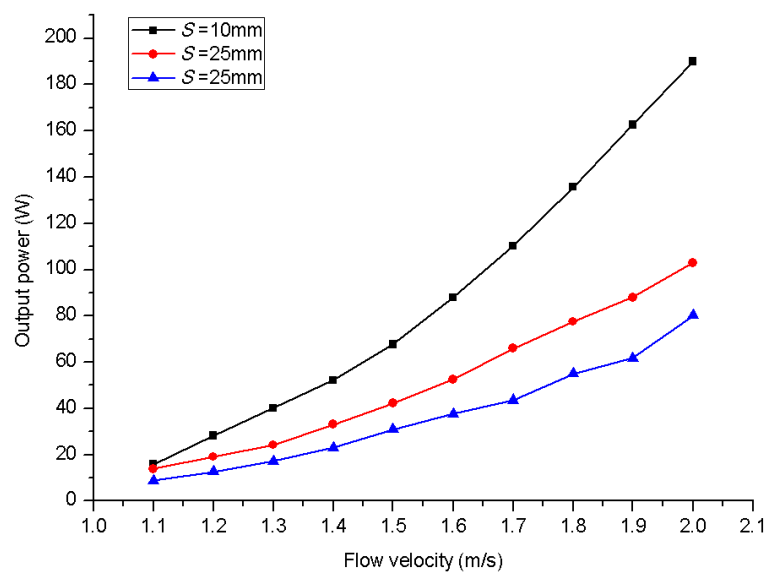


Fig.8.11 Output power of the bidirectional turbine

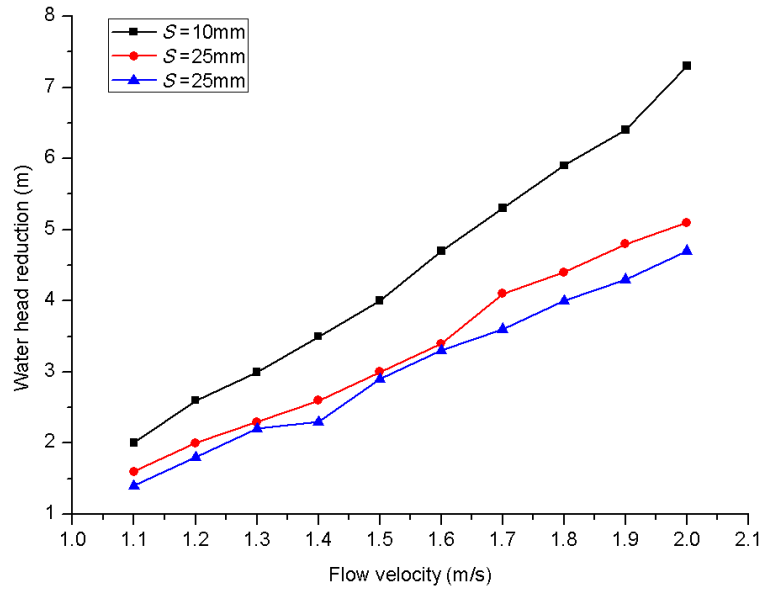


Fig.8.12 Water head reduction of the bidirectional turbine

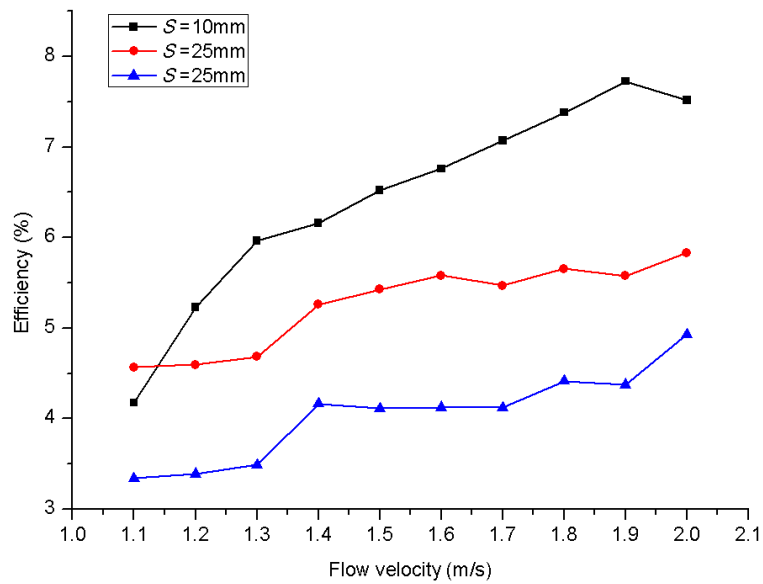


Fig.8.13 Efficiency of the bidirectional turbine

After a series of lab tests, the performance of the proposed bidirectional inline turbine under different distances between block and runner is obtained and the performance curves are shown in Fig.8.11-8.13. It can be observed that the distance between block and runner has significant effects on the output power and water head reduction. for a smaller  $S$  can not only lead to a higher output power, but also result in

a higher water head reduction. This is because that when  $S$  is smaller, the blocks can function well and more water head is converted into flow kinetic energy, thus both the output power and water head reduction is higher. Besides, when the distance between block and runner becomes bigger, more water leaks without flowing through the runner, resulting in a lower output power and water head reduction.

When  $S$  equals to 10mm, the output power and water head reduction increase quicker with the increment of flow velocity than other two cases. This is also because of the function of blocks. For the case with  $S=10\text{mm}$ , at 1.5m/s, which is the design flow velocity in this project, the output power is 67W while the water head reduction is 4m water. When the flow velocity increases to 2m/s, the output power reaches 190W with 7m water head reduced. When  $S$  equals to 25mm and 40mm, the water head reduction can keep under 5m in the flow velocity range from 1.1-2.0m, and the maximum output power are 103W and 80W, respectively. It is suggested to select the optimal value of  $S$  according to the real working conditions, including the power demand, water head reduction limitation, flow velocity, etc.

It can also be observed from Fig.8.13 that compared the experimental results shown in Section 8.3.1, the turbine efficiency with a generator is much lower than the turbine efficiency measured by dynamic torque meter. For example, the maximum turbine efficiency with a generator is only about 8% when  $S$  equals to 10mm, nearly 1/2 lower than the turbine efficiency measured in Section 8.3.1. There are two main reasons for this phenomenon. On the one hand, the conversion loss exists in generator when the mechanical energy is converted into electricity. Based on the data of generator supplier, the maximum generator efficiency is only 80%. On the other hand, the generator is not suitable for the turbine. Although the generator is selected based

on the rated rotation speed and power, but it is likely that the generator cannot operate under the best working conditions. Therefore, it is suggested to select more generators and perform more lab tests to select the optimal generator for the project.

## **8.4 Summary**

In this chapter, a magnetic driven bidirectional inline turbine was developed as bidirectional flow may occur in the water supply pipes. In the proposed turbine, the block shape was specially designed to satisfy the working condition of bidirectional flow. Besides, a magnetic coupling which transmitted torque using magnetic field was adopted to avoid leakage and reduce mechanical loss. After that, lab tests were conducted to investigate the performance of the developed bidirectional turbine. As referred from the present study, the following conclusions can be obtained:

(1) The proposed block design method can be helpful for inline cross-flow turbine design based on the working conditions. In this chapter, the inline cross-flow turbine could operate under bidirectional flow by improving the block shape. Specially, each block consisted of a plane surface and a curved surface, so the block could function as guide block as well as conversion block. With the developed blocks, the inline turbine could operate under bidirectional water flow without changing the runner rotation direction.

(2) It is feasible to adopt magnetic coupling in micro cross-flow turbine for sealing and transmission. By using the magnetic coupling to replace the mechanical seal, the risk of sealing failure can be significantly reduced and the water supply security can be ensured.

(3) The turbine performance under different rotation speed was first tested using

dynamic torque meter system. The maximum output power and efficiency were recorded 190W and 17.4%, respectively, when runner rotation speed was 600rpm. at the best efficiency rotation speed, the water head reduction was about 4.7m, which could meet the design requirement about water head reduction.

(4) A 24V three-phase permanent magnet alternating generator with low starting torque was selected to study the real turbine capacity, and the effects of distance between block and runner on turbine performance was studied. For the case with  $S=10\text{mm}$ , at 1.5m/s, which is the design flow velocity in this project, the output power was 67W while the water head reduction was 4m water. When the flow velocity increased to 2m/s, the output power reached 190W with 7m water head reduced. When  $S$  equaled to 25mm and 40mm, the water head reduction could keep under 5m in the flow velocity range from 1.1-2.0m, and the maximum output power were 103W and 80W, respectively.

## **CHAPTER 9 CONCLUSIONS AND RECOMMENDATIONS FOR FUTURE WORK**

This research investigated a micro hydropower technology that can be used in urban water mains to supply power for water monitoring devices. Firstly, an inline cross-flow turbine was newly developed by numerical and experimental methods to study the feasibility of micro hydropower harvesting from water pipes. Then a mathematic block design method was proposed and theoretical analysis on the working principle of cross-flow runner was conducted to obtain guidance for performance improvement of the developed turbine. After that, effects of geometrical parameters of block and runner on the turbine performance were investigated using CFD simulation and the optimal geometrical parameters were determined based on the numerical results. Finally, a case study about the development of a magnetic driven bidirectional inline cross-flow turbine was performed and the turbine performance was studied by lab tests.

In this chapter, the key findings from this research are summarized and the main academic contribution are presented. Lastly, the limitations are discussed and the recommendations for future work are presented.

### **9.1 Experimental study on the preliminary turbine prototype**

In this study, a novel inline cross-flow turbine for hydropower generation in urban water mains was newly designed and manufactured. The numerical and experimental results indicated that by integrating two blocks to the pipe inner wall, the turbine performance could be enhanced because the blocks functioned as the nozzle and

diffuser of a conventional cross-flow turbine to enhance the flow velocity and pressure difference through the runner. Besides, the research also revealed that the self-adjustable vane could achieve ideal performance in avoiding excess water head loss with little influence on the output power.

The prototype test results showed that the turbine output power at the design point was 69.1W with 2.62m water head reduced. Besides, over a flow velocity range varying from 1.2m/s to 2.2m/s, the water head loss was always below 5m, so the normal water supply would not be affected. After a month-long test at the flow velocity of 1.3m/s, the prototype was proved very reliable with steady performance and its daily electricity generation was about 600Wh, which was sufficient for powering any general water leakage monitoring system in an urban environment.

## **9.2 Theoretical analysis on the inline cross-flow turbine**

A mathematic design method for the block design was developed based on fluid continuity and energy conservation. Besides, the working mechanism of cross-flow runner was analyzed and the expression of theoretical turbine performance was obtained using Bernoulli's equation. Based on the proposed block design method and theoretical analysis on the runner, the guide block orientation angle, runner inlet arc angle, blades outer angle and runner diameter ratio are the key parameters that affect turbine performance. The analysis results could provide guidance for inline cross-flow turbine design and performance improvement.

The analysis also revealed that the blocks could determine the flow velocity and inlet angle at the runner inlet, and the flow velocity and inlet angle could influence the blades shapes and turbine efficiency. Therefore, the runner design should match with the block design to achieve the best turbine performance.

### **9.3 Effects of block geometries on the turbine performance**

Numerical study on the effects of guide block orientation angle on turbine performance showed that the blocks could convert part of the water head into kinetic energy, leading to a high flow velocity through the runner. Besides, the pressure distribution inside the inline turbine was considerably improved by adjusting the orientation angle of guide block. The high-pressure regions on the suction side of the first several blades at the first stage could be reduced, and the torque output of the first stage nearly doubled after block improvement. As indicated in the numerical research, the inline turbine could reach its maximum efficiency of 42.4% with about 1500 W power output by adjusting the block design and the suggested orientation angle of guide block is 30°.

Investigations of the impact of runner inlet arc angle on the turbine performance indicated that a smaller runner inlet arc angle could increase the flow velocity at runner inlet and pressure difference between the upstream and downstream of the runner, resulting in a higher output power but also a higher overall water head reduction through the turbine. Besides, the runner inlet arc angle had a significant influence on the power output of runner second stage. To achieve a good balance between turbine efficiency and water head reduction, the suggested runner inlet arc angle is 105° and the corresponding maximum turbine efficiency is 42.6% with about 1565W power output.

### **9.4 Effects of runner geometries on the turbine performance**

Numerical study on the impact of blades outer angle on the turbine performance showed that a good matching between flow inlet angle and blades outer angle could

significantly improve the turbine performance. Based on the results, the optimal blade outer angle in this research was suggested as  $30^\circ$ . By improving the blades outer angle, the maximum turbine efficiency increased significantly from 42.6% to 49.6%.

Investigation was performed to study the effects of runner diameter ratio on the turbine performance. The results indicated that runner diameter ratio had an obvious impact on the torque output of runner first stage. A smaller runner diameter ratio would lead to higher output power, but the water head reduction was also higher. Based on the results, the suggested runner diameter ratio was 0.68.

Numerical study on the blades number indicated that when the blades number increased from 20 to 24, the turbine output power rose significantly and the maximum output power reached 2285W. However, if blades number continued to increase, the variation of output power was very slight. The variation of water head reduction with blades number increase was very slight. The optimal blades number was suggested 24 and the recorded maximum efficiency was 50.9%.

## **9.5 Case study about the development of bidirectional inline cross-flow turbine**

Based on the block design method and the optimal geometrical parameters suggested in the research, a magnetic driven bidirectional inline turbine was developed. Firstly, a block profile which consisted of a plane surface and a curved surface was designed to ensure the inline turbine could operate under bidirectional water flow without changing the runner rotation direction. Besides, a magnetic coupling was used to replace the mechanical seal for sealing and transmission, which significantly reduced the risk of sealing failure and ensures water supply security.

The turbine performance under different rotation speeds was tested using dynamic torque meter system. When runner rotation speed was 600rpm, the bidirectional turbine reached its best efficiency 17.4% with 190W output power and 4.7m water head reduction, which could meet the design requirements in this case study. The case study indicated that the research presented in this thesis could provide an effective method for the design of inline cross-flow turbine design under different working conditions.

## **9.6 Limitations and recommendations for future work**

This thesis tried to develop a micro hydropower technology that can harvest hydropower from water supply pipes and supply power to water monitoring system. However, due to the limitation of time and availability of data, there are still aspects not covered. Therefore, further detailed investigations need to be done in future works.

Firstly, the proposed mathematic design method for the block is simplified, and it is developed based on several assumptions. In future studies, a more complex block design method which considers more parameters will be developed. With the newly developed method, the block shape will be more reasonable and the turbine performance will be significantly improved. In further research, a database can be established and a software package could be built, in this way, the block shapes can be generated automatically after inputting parameters including pipe diameter, power demand, flow velocity and water head reduction, etc.

Secondly, in this research, the design flow velocity is set as uniform. However, in the water supply pipes, water flow velocity fluctuates over time the variation of user demand. The variation of flow velocity will result in unstable output power and voltage, which possesses a challenge for the controller. In the future studies, it is expected to

solve this problem by adding adjustable device in the turbine or improving the control strategy of the controller.

Thirdly, based on the research presented in Chapter 8, the current used generator is not suitable for the current project. In the future works, the generator will be replaced by more efficient one to fully convert the harvested hydropower into electricity.

Finally, in current design, the torque generated by the runner must be transferred through the shaft, magnetic coupling, bearings to the generator, resulting in unavoidable mechanical loss and relatively huge size of the turbine. Based on the successful application of magnetic coupling, it is possible to develop a generator integrated turbine. In this turbine, the internal half of the magnetic coupling can operate as the rotor of generator, and the stator is fixed to the turbine body directly. Between the rotor and stator, a stainless shroud is used for sealing. As the shroud is made of stainless steel, its effects on magnetic field is slight. The generator integrated turbine will be more compact than the former turbine, thus less space is needed for installation. Besides, due to the reduction of transmission components, the reliability can be improved.

## REFERENCES

- [1] Venkatesh, G., Chan, A., & Brattebø, H. (2014). Understanding the water-energy-carbon nexus in urban water utilities: Comparison of four city case studies and the relevant influencing factors. *Energy*, 75, 153-166.
- [2] <https://www.wsd.gov.hk/en/home/index.html>
- [3] Mehajabin, N., Razzaque, M. A., Hassan, M. M., Almogren, A., & Alamri, A. (2016). Energy-sustainable relay node deployment in wireless sensor networks. *Computer Networks*, 104, 108-121.
- [4] Valera, A. C., Soh, W. S., & Tan, H. P. (2017). Enabling sustainable bulk transfer in environmentally-powered wireless sensor networks. *Ad Hoc Networks*, 54, 85-98.
- [5] Rosenbloom, D., & Meadowcroft, J. (2014). Harnessing the Sun: Reviewing the potential of solar photovoltaics in Canada. *Renewable and Sustainable Energy Reviews*, 40, 488-496.
- [6] Dondi, D., Bertacchini, A., Brunelli, D., Larcher, L., & Benini, L. (2008). Modeling and optimization of a solar energy harvester system for self-powered wireless sensor networks. *IEEE Transactions on industrial electronics*, 55(7), 2759-2766.
- [7] Weimer, M. A., Paing, T. S., & Zane, R. A. (2006, June). Remote area wind energy harvesting for low-power autonomous sensors. In *Power Electronics Specialists Conference, 2006. PESC'06. 37th IEEE* (pp. 1-5). IEEE.

- [8] Akhtar, F., & Rehmani, M. H. (2015). Energy replenishment using renewable and traditional energy resources for sustainable wireless sensor networks: A review. *Renewable and Sustainable Energy Reviews*, 45, 769-784.
- [9] Jiyun, D., Hongxing, Y., Zhicheng, S., & Xiaodong, G. (2018). Development of an inline vertical cross-flow turbine for hydropower harvesting in urban water supply pipes. *Renewable Energy*, 127, 386-397.
- [10] Kaunda, C. S., Kimambo, C. Z., & Nielsen, T. K. (2014). A technical discussion on micro hydropower technology and its turbines. *Renewable and Sustainable Energy Reviews*, 35, 445-459.
- [11] Elbatran, A. H., Yaakob, O. B., Ahmed, Y. M., & Shabara, H. M. (2015). Operation, performance and economic analysis of low head micro-hydropower turbines for rural and remote areas: a review. *Renewable and Sustainable Energy Reviews*, 43, 40-50.
- [12] Twidell, J., & Weir, T. (2015). *Renewable energy resources*. Routledge.
- [13] Alexander, K. V., Giddens, E. P., & Fuller, A. M. (2009). Radial-and mixed-flow turbines for low head microhydro systems. *Renewable Energy*, 34(7), 1885-1894.
- [14] Davis, S. (2003). *Microhydro: Clean Power from Water* (Vol. 13). New Society Publishers.
- [15] Židonis, A., & Aggidis, G. A. (2015). State of the art in numerical modelling of Pelton turbines. *Renewable and Sustainable Energy Reviews*, 45, 135-144.

- [16] Anagnostopoulos, J. S., & Papantonis, D. E. (2007). Flow modeling and runner design optimization in Turgo water turbines. *World Academy of Science, Engineering and Technology*, 28, 206-211.
- [17] TamarHydro, Turgo Hydro Turbines. Available (<http://tamarhydro.com.au/products/turgo-hydro-turbines/>) (accessed 21.03.2018).
- [18] Williamson, S. J., Stark, B. H., & Booker, J. D. (2013). Performance of a low-head pico-hydro Turgo turbine. *Applied Energy*, 102, 1114-1126.
- [19] Ossberger Limited. Ossberger-turbine information. Ossberger Limited, Weissenburg/ Bavaria Germany. Available (<http://www.ossberger.de/cms/pt/hydro/ossberger-turbine/>) (accessed 21.03.2018).
- [20] Adhikari, R. (2016). *Design improvement of crossflow hydro turbine* (Doctoral dissertation, University of Calgary).
- [21] River Engineering & Restoration at OSU. Types of turbine. Available (<http://rivers.bee.oregonstate.edu/turbine-sizing>) (accessed 21.03.2018).
- [22] Okot, D. K. (2013). Review of small hydropower technology. *Renewable and Sustainable Energy Reviews*, 26, 515-520.
- [23] European Small Hydropower Association. Guide on how to develop a small hydropower plant. In: Penche C editor. Guideline book. Brussels, Belgium: ESHA. Available [http://www.canyonhydro.com/images/Part\\_2\\_ESHA\\_Guide\\_on\\_how\\_to\\_develop\\_a\\_](http://www.canyonhydro.com/images/Part_2_ESHA_Guide_on_how_to_develop_a_)

small\_hydropower\_plant.pdf ; 2004 (accessed 22.03.2018).

[24] Mechanical Booster. Francis Turbine Working Principle, Main Parts, Diagram and Application. Available <<http://www.mechanicalbooster.com/2018/01/francis-turbine.html>> (accessed 22.03.2018).

[25] Chica, E., Agudelo, S., & Sierra, N. (2013). Lost wax casting process of the runner of a propeller turbine for small hydroelectric power plants. *Renewable energy*, 60, 739-745.

[26] PumpWorld. Pump as turbine: description. PumpWorld. Available <<http://www.worldpumps.com/view/5086/pumps-as-turbines-in-the-water-industry/>>; (accessed 23.08.2018).

[27] Thoma, D., & Kittredge, C. P. (1931). Centrifugal pumps operated under abnormal conditions. *Power*, 73, 881-884.

[28] Jain, S. V., & Patel, R. N. (2014). Investigations on pump running in turbine mode: A review of the state-of-the-art. *Renewable and Sustainable Energy Reviews*, 30, 841-868.

[29] Agostinelli A, Shafer L. (2013). Centrifugal pumps as hydraulic turbines. *Power Fluids*, 7(3), 5–7.

[30] Williamson, S. J., Stark, B. H., & Booker, J. D. (2014). Low head pico hydro turbine selection using a multi-criteria analysis. *Renewable Energy*, 61, 43-50.

[31] Ghosh, T. K., & Prelas, M. A. (2011). *Energy resources and systems: volume 2:*

*renewable resources (Vol. 2)*. Springer Science & Business Media.

[32] Fraenkel, P., Paish, O., Bokalders, V., & Harvey, A. P. (1991). *Micro-Hydro Power: a guide for development workers*. ITDG Publ.

[33] Paish, O. (2002). Micro-hydropower: status and prospects. Proceedings of the Institution of Mechanical Engineers, Part A: *Journal of Power and Energy*, 216(1), 31-40.

[34] Vilanova, M. R. N., & Balestieri, J. A. P. (2014). Energy and hydraulic efficiency in conventional water supply systems. *Renewable and Sustainable Energy Reviews*, 30, 701-714.

[35] Tanaka Hydropower Co., Ltd, Products, Available < <http://www.tanakahydro.jp/products/> > (accessed 22.03.2018)

[36] Du, J., Yang, H., Shen, Z., & Chen, J. (2017). Micro hydro power generation from water supply system in high rise buildings using pump as turbines. *Energy*, 137, 431-440.

[37] Hitachi Industrial Equipment Systems, Co., Ltd, Products, Available < <http://www.hitachi-ies.co.jp/solution/kankyo/enkaishu/index.htm> > (accessed 22.03.2018).

[38] SINFONIA, Civil Infrastructure, Available < <http://www.sinfo-t.jp/eng/social.html> > (accessed 22.03.2018).

[39] Sammartano, V., Sinagra, M., Filianoti, P., & Tucciarelli, T. (2017). A Banki–Michell turbine for in-line water supply systems. *Journal of Hydraulic Research*, 55(5),

686-694.

[40] Coelho, B., & Andrade-Campos, A. (2014). Efficiency achievement in water supply systems-A review. *Renewable and Sustainable Energy Reviews*, 30, 59-84.

[41] Ramos, H. M., Mello, M., & De, P. K. (2010). Clean power in water supply systems as a sustainable solution: from planning to practical implementation. *Water science and technology: water supply*, 10(1), 39-49.

[42] Pérez García, J., Cortés Marco, A., & Nevado Santos, S. (2010). Use of centrifugal pumps operating as turbines for energy recovery in water distribution networks. Two case study. In *Advanced Materials Research* (Vol. 107, pp. 87-92). Trans Tech Publications.

[43] Williams, A. A. (1996). Pumps as turbines for low cost micro hydro power. *Renewable Energy*, 9(1-4), 1227-1234.

[44] Fontana, N., Giugni, M., & Portolano, D. (2011). Losses reduction and energy production in water-distribution networks. *Journal of Water Resources Planning and Management*, 138(3), 237-244.

[45] Fecarotta, O., Carravetta, A., & Ramos, H. M. (2011). CFD and comparisons for a pump as turbine: Mesh reliability and performance concerns. *International Journal of Energy & Environment*, 2(1).

- [46] Carravetta, A., del Giudice, G., Fecarotta, O., & Ramos, H. M. (2013). PAT design strategy for energy recovery in water distribution networks by electrical regulation. *Energies*, 6(1), 411-424.
- [47] Carravetta, A., Fecarotta, O., Sinagra, M., & Tucciarelli, T. (2013). Cost-benefit analysis for hydropower production in water distribution networks by a pump as turbine. *Journal of Water Resources Planning and Management*, 140(6), 04014002.
- [48] Alatorre-Frenk, C. (1994). *Cost minimisation in micro-hydro systems using pumps-as-turbines* (Doctoral dissertation, University of Warwick).
- [49] Inhabitat. Portland is now powered by water pipes and flushing toilets. Available <<https://inhabitat.com/portlands-water-pipes-are-the-newest-source-of-clean-energy/>> (accessed 25.03.2018).
- [50] Fast Company. Portland's New Pipes Harvest Power from Drinking Water. Available <<https://www.fastcompany.com/3041300/portlands-new-pipes-harvest-power-from-drinking-water>> (accessed 25.03.2018).
- [51] Chen, J., Yang, H. X., Liu, C. P., Lau, C. H., & Lo, M. (2013). A novel vertical axis water turbine for power generation from water pipelines. *Energy*, 54, 184-193.
- [52] Hoffmann, D., Willmann, A., Göpfert, R., Becker, P., Folkmer, B., & Manoli, Y. (2013). Energy harvesting from fluid flow in water pipelines for smart metering applications. In *Journal of Physics: Conference Series* (Vol. 476, No. 1, p. 012104). IOP Publishing.

- [53] Hao, W. S., & Garcia, R. (2014). Development of a digital and battery-free smart flowmeter. *Energies*, 7(6), 3695-3709.
- [54] Michell, A. G. M. (1904). *U.S. Patent No. 760,898*. Washington, DC: U.S. Patent and Trademark Office.
- [55] Sammartano, V., Aricò, C., Carravetta, A., Fecarotta, O., & Tucciarelli, T. (2013). Banki-Michell optimal design by computational fluid dynamics testing and hydrodynamic analysis. *Energies*, 6(5), 2362-2385.
- [56] Adhikari, R. C., & Wood, D. H. (2017). A new nozzle design methodology for high efficiency crossflow hydro turbines. *Energy for Sustainable Development*, 41, 139-148.
- [57] Acharya, N., Kim, C. G., Thapa, B., & Lee, Y. H. (2015). Numerical analysis and performance enhancement of a cross-flow hydro turbine. *Renewable energy*, 80, 819-826.
- [58] Elbatran, A. H., Ahmed, Y. M., & Shehata, A. S. (2017). Performance study of ducted nozzle Savonius water turbine, comparison with conventional Savonius turbine. *Energy*, 134, 566-584.
- [59] Prasad, D. D., Ahmed, M. R., & Lee, Y. H. (2014). Flow and performance characteristics of a direct drive turbine for wave power generation. *Ocean Engineering*, 81, 39-49.
- [60] Elbatran, A. H., Yaakob, O. B., Ahmed, Y. M., & Jalal, M. R. (2015). Novel

approach of bidirectional diffuser-augmented channels system for enhancing hydrokinetic power generation in channels. *Renewable Energy*, 83, 809-819.

[61] FUKUTOMI, J., NAKASE, Y., & Watanabe, T. (1985). A numerical method of free jet from a cross-flow turbine nozzle. *Bulletin of JSME*, 28(241), 1436-1440.

[62] Fiuzat, A. A., & Akerkar, B. P. (1991). Power outputs of two stages of cross-flow turbine. *Journal of energy engineering*, 117(2), 57-70.

[63] Chen, Z., Singh, P. M., & Choi, Y. D. (2014). Effect of Guide Nozzle Shape on the Performance Improvement of a Very Low Head Cross-flow Turbine. *The KSFM Journal of Fluid Machinery*, 17(5), 19-26.

[64] Khosrowpanah, S., Fiuzat, A. A., & Albertson, M. L. (1988). Experimental study of cross-flow turbine. *Journal of Hydraulic Engineering*, 114(3), 299-314.

[65] Mockmore, C. A., & Merryfield, F. (1949). The Banki water turbine.

[66] Katayama, Y., Iio, S., Veerapun, S., & Uchiyama, T. (2015). Investigation of blade angle of an open cross-flow runner. *International Journal of Turbo & Jet-Engines*, 32(1), 65-72.

[67] Desai, V. R. (1993). *A parametric study of the cross-flow turbine performance* (Doctoral dissertation, Clemson University).

[68] Totapally, H. G., & Aziz, N. M. (1994). Refinement of cross-flow turbine design parameters. *Journal of energy engineering*, 120(3), 133-147.

[69] Choi, Y. D., Lim, J. I., Kim, Y. T., & Lee, Y. H. (2008). Performance and internal

flow characteristics of a cross-flow hydro turbine by the shapes of nozzle and runner blade. *Journal of fluid science and technology*, 3(3), 398-409.

[70] Adhikari, R., & Wood, D. (2018). The Design of High Efficiency Crossflow Hydro Turbines: A Review and Extension. *Energies*, 11(2), 267.

[71] Akerkar, B. P. (1989). *A study of the performance of the cross flow turbine* (Doctoral dissertation, Clemson University).

[72] Aziz, N. M., & Desai, V. R. (1991). An Experimental Study of the Effect of Some Design Parameters in Cross-Flow Turbine Efficiency. *Engineering Report, Department of Civil Engineering, Clemson University*.

[73] Pereira, N. H., & Borges, J. E. (2016). Prediction of the Cross-Flow Turbine Efficiency with Experimental Verification. *Journal of Hydraulic Engineering*, 143(1), 04016075.

[74] Sammartano, V., Morreale, G., Sinagra, M., Collura, A., & Tucciarelli, T. (2014). Experimental study of cross-flow micro-turbines for aqueduct energy recovery. *Procedia Engineering*, 89, 540-547.

[75] Hothersall, R. (1985). A review of the cross-flow turbine. In *Waterpower'85* (pp. 914-923). ASCE.

[76] Kim, K. P., Ahmed, M. R., & Lee, Y. H. (2012). Efficiency improvement of a tidal current turbine utilizing a larger area of channel. *Renewable energy*, 48, 557-564.

[77] De Andrade, J., Curiel, C., Kenyery, F., Aguillón, O., Vásquez, A., & Asuaje, M.

(2011). Numerical investigation of the internal flow in a Banki turbine. *International Journal of Rotating Machinery*, 2011.

[78] Popescu, D., Popescu, C., & Dragomirescu, A. (2017). Flow control in Banki turbines. *Energy Procedia*, 136, 424-429.

[79] Dragomirescu, A., & Schiaua, M. (2017). Experimental and numerical investigation of a Bánki turbine operating far away from design point. *Energy Procedia*, 112, 43-50.

[80] Gourdain, N. (2015). Prediction of the unsteady turbulent flow in an axial compressor stage. Part 1: Comparison of unsteady RANS and LES with experiments. *Computers & Fluids*, 106, 119-129.

[81] Coroneo, M., Montante, G., Paglianti, A., & Magelli, F. (2011). CFD prediction of fluid flow and mixing in stirred tanks: Numerical issues about the RANS simulations. *Computers & Chemical Engineering*, 35(10), 1959-1968.

[82] Moffat, R. J. (1988). Describing the uncertainties in experimental results. *Experimental thermal and fluid science*, 1(1), 3-17.

[83] Kirke, B. (2006). Developments in ducted water current turbines. *Tidal paper*, (25-04).

[84] Ponta, F., & Dutt, G. S. (2000). An improved vertical-axis water-current turbine incorporating a channelling device. *Renewable energy*, 20(2), 223-241.

[85] Aziz, N. M., & Totapally, H. G. S. (1994). Design Parameter refinement for

improved Cross-Flow turbine performance. *Engineering Report*.

[86] Aziz, N. M., & Desai, V. R. (1993). A laboratory study to improve the efficiency of cross-flow turbines. *Engineering Report*.

[87] Permanent Magnetic Couplings, Available <https://www.jbj.co.uk/magnetic-couplings.html>.